UNIVERSITÉ DE GENÈVE FACULTÉ DES SCIENCES

Département de Chimie Minérale, Analytique et Appliquée

Professeur Michal Borkovec

Interaction forces between surfaces coated with highly branched polyelectrolytes

THÈSE

présentée à la Faculté des Sciences de l'Université de Genève

pour obtenir le grade de Docteur ès sciences, mention interdisciplinaire

par

Ramón Pericet-Cámara

de

Córdoba (Espagne)

Thèse Nº 3738

GENÈVE

Atelier de reproduction de la section de Physique

2006

La Faculté des sciences, sur le préavis de Messieurs M. BORKOVEC, professeur ordinaire et directeur de thèse (Département de chimie minérale, analytique et appliquée), C. PIGUET, professeur ordinaire (Département de chimie minérale, analytique et appliquée), et M. TEXTOR, professeur (Eidgenössische Technische Hochshule Zürich – Department of Materials – Laboratory for Surface Science and Technology – Zürich, Switzerland), autorise l'impression de la présente thèse, sans exprimer d'opinion sur les propositions qui y sont énoncées.

Genève, le 15 mai 2006

Thèse - 3738 -

Le Doyen, Pierre SPIERER

Contents

Résumé

Le contrôle de certaines propriétés colloïdales comme l'agrégation, la déposition ou la rhéologie, est essentiel pour l'élaboration de nombreux produits chimiques, comme les peintures, colles, cosmétiques ou additifs alimentaires, ainsi que d'autres processus industriels et environmentaux comme la séparation des minéraux, l'élaboration du papier ou le traitement des eaux usées. Dans ces processus, il est important de contrôler la stabilité colloïdale des suspensions. L'interaction entre les surfaces impliquées dans ces systèmes détermine les propriétés colloïdales mentionnées. Normalement, l'emploi de polymères tensioactifs ou simplement la manipulation du pH ou de la force ionique de la solution nous permet de contrôler ces interactions.

Les surfaces des solides en contact avec l'eau sont généralement chargées. Ainsi les forces électrostatiques à longue portée dominent typiquement les interactions entre ces surfaces en solution aqueuse. D'après la théorie de Derjaguin, Landau, Verwey et Overbeek (DLVO), la stabilité d'une dispersion colloïdale dépend de l'équilibre entre les forces électrostatiques et de van der Waals. Des expériences de mesures de forces directes confirment l'importance des forces électrostatiques et de dispersion dans les systèmes réels.

La présence de polyelectrolytes de charge opposée ont une influence importante dans l'agrégation des systèmes colloïdaux. Ceci est dû à la possibilité de neutralisation ou inversion de la charge des particules colloïdales après l'adsorption des polyelectrolytes sur leur surface. Par contre, certains phénomènes observés dans ces systèmes n'ont pas pu être expliqués par la théorie DLVO. Par exemple, l'agrégation de particules colloïdales en présence de polyelectrolytes est parfois plus rapide que celle mesuré en absence de polymères chargées. Ces résultats peuvent être expliqués par l'hétérogénéité de la surface suite à l'adsorption de polyelectrolytes à haute densité de charge. Dans ce cas, la surface est composée d'une distribution de patchs hautement chargés, qui localement laissent des zones libres et de charge opposée. Si ces zones sont suffisamment

étendues, l'adsorption d'éléments de charge contraire reste favorable au-delà du point de neutralisation de la charge. Ainsi, cela peut provoquer l'agrégation avec une autre particule recouverte de polyelectrolytes. Lorsque la répulsion entre les polyelectrolyte adsorbées est prédominante sur l'attraction locale des aires de charge opposée, l'agrégation des particules colloïdales est évitée.

La mesure des forces directes d'interactions des systèmes colloïdaux a été toujours un challenge. Avec le développement du microscope à force atomique (AFM) dans les années 1980, cet instrument s'est distingué par son énorme résolution et sensibilité pour des forces en dessous du piconewton. Cette technique a été utilisée pour obtenir des images topographiques avec une résolution inférieure à l'Angstrom. Elle a aussi été employée pour mesurer quantitativement des forces entre des surfaces. Cette méthode est idéale pour étudier les interactions à courtes et longues distances ainsi que l'adhérence entre une grande variété de surfaces solides, y compris celles avec des polymères adsorbées, comme présenté dans ce travail de recherche.

Le but de cette thèse est d'élaborer des surfaces avec une distribution de charge souhaitée au moyen de l'adsorption de polyelectrolytes, et de mesurer ensuite les forces entre ces surfaces. L'étude de la topographie des surfaces avec couche de polymères adsorbés est effectuée au moyen de la microscopie à force atomique en mode *tapping*. En mode *tapping*, la pointe de l'AFM oscille à sa fréquence de résonance avec une amplitude constante donnée. La pointe est amenée au contact intermittent avec la surface pendant qu'un module de balayage piézoélectrique déplace la surface horizontalement. L'interaction de la surface d'échantillon avec la pointe change l'oscillation de celle-ci. Le module de balayage est déplacé verticalement à l'aide d'un signal du type *feedback* pour maintenir l'oscillation à amplitude constante (amplitude *setpoint*). Ce signal et celui de la position horizontale du module de balayage sont utilisés pour produire une image topographique de la surface. Afin de garder de faibles forces de cisaillement, l'amplitude *setpoint* est ajustée typiquement à 90-95 % de l'oscillation libre. Ce mode permet d'obtenir des images d'échantillons comportant des éléments faiblement adsorbés, tels que des particules, des

polymères ou d'autres matériaux mous. En plus de l'acquisition d'images topographiques, il est possible d'enregistrer des changements de l'angle de phase de la fréquence de résonance de la pointe pour produire une deuxième image, une technique qui s'appelle *phase imaging*. Le changement de phase de l'oscillation dépend de l'énergie de dissipation de l'échantillon, qui peut être liée à ses propriétés mécaniques, à savoir l'adhérence, la rigidité ou la viscoélasticité. Ce mode est idéal pour obtenir des images des surfaces contenant différents matériaux. On peut obtenir des images de polymères adsorbés sur des particules colloïdales de silice, qui sont connues pour avoir une haute rugosité. Bien que les propriétés de ces images soient surtout qualitatives, elles sont souvent plus contrastées que des images topographiques, et sont de ce fait complémentaires.

Les interactions entre de surfaces recouvertes de polyelectrolytes adsorbés peuvent également être étudiées avec la technique de la sonde colloïdale. Une amélioration significative de la description des couches adsorbées a été réalisée avec le développement de cette technique. En collant une particule micrométrique à l'extrémité d'une pointe d'AFM, les restrictions dues à la nature de la pointe ont été surmontées, et il a été possible d'avoir une géométrie bien définie entre la sonde et l'échantillon et une résolution de force encore plus élevée. La technique de sonde colloïdale peut être employée avec beaucoup de matériaux, à condition qu'il soit microscopiquement plat. De plus, cette technique peut permettre de calculer localement les forces d'interaction. En mesure de forces directes, l'échantillon ou le support de la pointe est déplacé verticalement par un dispositif piézoélectrique ou par le module de balayage lui-même, alors que les autres composants demeurent en place. Le débattement du support (cantilever) de la pointe est enregistré pendant le mouvement vertical du piezo, généralement par la technique du levier optique. Dans cette technique, la photodiode agit comme un détecteur de position, enregistrant le débattement du support au moyen d'un rayon laser réfléchi sur la partie supérieure du support de la pointe. La conversion du débattement du support en force est faite en utilisant la loi de Hooke $F = kY$, où k est la constante de ressort du support, Y est son débattement, et F est la force de déflexion résultée. L'analyse quantitative des mesures de forces directes exige une

connaissance précise de la constante de ressort du support de la pointe afin d'établir la corrélation entre débattement et force. Malheureusement, bien que la dimension et la nature d'un support suffisent pour établir la constante de ressort, il est difficile d'obtenir des valeurs constantes d'un ressort à l'autre, et on note souvent des variations considérables. En conséquence, le calibrage des supports de pointe est une étape importante dans des mesures des forces directes. On note plusieurs méthodes dans la littérature. Nous utilisons la méthode *Hutter-Bechoeffer* et la méthode *Sader*. La méthode *Hutter-Bechoeffer* analyse les fluctuations du support de la pointe dans l'air pour obtenir la constante de ressort. La méthode de *Sader* emploie la réponse en fréquence du support, ses dimensions géométriques, et les propriétés du milieu environnant.

Les forces électrostatiques entre surfaces de colloïdes sont typiquement obtenues à partir de la résolution de l'équation de Poisson-Boltzmann dans la couche diffuse

$$\frac{d^2\psi}{dx^2} = -\frac{e}{\varepsilon\varepsilon_0}\sum_i z_i c_i \exp\left(-\frac{z_i e\psi}{k_B T}\right)$$

où ψ est le potentiel électrostatique, $\varepsilon\varepsilon_0$ la constante diélectrique de l'eau, e la charge élémentaire, k_B la constante de Boltzmann, T la température, z_i et c_i sont la valence et la concentration au bulk de l'ion i. La résolution de cette équation exige de choisir des conditions aux limites, et normalement soit la condition de charge de surface constante (CC) ou bien celle du potentiel de surface constant (CP) est utilisée pour décrire des systèmes réels. Par contre, des mesures de forces directes expérimentales montrent qu'aucune de ces conditions n'est couramment une bonne approximation. Les forces mesurées se trouvent typiquement entre les deux cas, une situation qui est appelée *régulation de charge*. L'origine de cette situation est due aux réactions de dissociation des groupes ionisables à la surface, dont l'équilibre chimique est modifié lorsque les surfaces se situent à courtes distances. A cette thèse, une nouvelle approche pour résoudre l'équation de Poisson-Boltzmann est proposée, et appelée condition de régulation constante de charge (CR). L'approximation CR fournit une description précise des forces d'interaction des surfaces ionisables à travers d'une solution d'électrolyte au niveau de Poisson-

Boltzmann. L'approximation consiste à linéariser le rapport charge-potentiel de la surface autour du potentiel de la surface isolée, et de résoudre exactement l'équation de PB pour la couche diffuse. Cette approximation élimine la nécessité de considérer les surfaces en interaction simultanément avec les équilibres d'adsorption chimique des espèces chargées sur chaque surface. En fait, aucun modèle mathématique pour l'ionisation de la surface n'est nécessaire, et la réponse chimique de la surface est exprimée en fonction de deux paramètres, à savoir, le *potentiel de couche diffuse* et le *paramètre de régulation de charge p*. Ces paramètres se rapportent à une surface isolée et peuvent également être obtenus à partir des modèles classiques d'équilibre de la surface, ou en explorant les interfaces par des techniques expérimentales (par exemple, mesures électrocinétiques). Les limites classiques du CP correspondent à $p = 0$ et cela correspond en CC à $p = 1$. Dans le cas général, le paramètre de régulation p assume typiquement des valeurs dans cet intervalle. Ce paramètre peut être lié à deux capacités de charge: à la capacité de la couche diffuse et à la capacité de la couche intérieure. Quand la charge de la couche intérieure reste constante, la capacité de la couche intérieure est plus grande que la capacité de la couche diffuse, et la surface se comporte comme CC ($p = 1$). Quand la charge de la couche intérieure peut être facilement réglée par l'adsorption de l'espèce chargée, la capacité intérieure est petite, et la surface se comporte comme CP ($p = 0$). La capacité de la couche diffuse augmente avec l'augmentation du potentiel extérieur et avec l'augmentation de la force ionique. Par conséquent, le paramètre de régulation montrera une dépendance semblable. L'approximation de CR représente une généralisation normale de la théorie linéaire de Carnie et Chan. Cette théorie est basée sur l'équation linéaire de Debye-Hückel dont la validité est plutôt limitée dans la pratique. En traitant l'équation de PB exactement et en linéarisant le rapport de charge-potentiel autour du potentiel de la surface isolée, nous conservons la simplicité de l'approche de Carnie et Chan mais nous pouvons développer sensiblement sa gamme de validité. Sur la base de notre expérience jusqu'ici, l'approximation est excellente dans la plupart des situations pratiques même à de petites séparations, dans des systèmes symétriques aussi bien que dans

des asymétriques. Plusieurs exemples ont été présentés ici avec succès. Dans certains cas, cependant, l'approximation de CR devient moins bonne à de petites distances de séparation. Un cas important concerne une surface proche de la neutralité, sur laquelle seulement quelques ions adsorbés déterminent la charge. Dans cette situation, la courbe de la charge de la couche intérieure approche asymptotiquement 0 pour des potentiels élevés, et l'approximation de CR donne des résultats moins bons près du contact. Néanmoins, nous suspectons que ces situations sont probablement d'importance mineure dans la pratique, et pour cette raison nous pensons que l'approximation de CR fournira un cadre utile pour discuter des interactions électrostatiques entre surfaces chargées.

Les forces d'interaction ont été étudiées entre couches pré-adsorbées de poly(éthylène imine) (PEI) hautement branchée de masse moléculaire différente en utilisant la technique de sonde colloïdale. Cette technique est basée sur la microscopie à force atomique (AFM). Le PEI est un polyelectrolyte faible, branché, cationique, qui s'adsorbent fortement sur des surfaces négativement chargées, ce qui provoque leur inversion de charge. Le PEI a gagné en importance dans la conception de multicouches planes ou sphériques. Les multicouches de polyelectrolytes sont préparés en alternant l'adsorption de deux polyelectrolytes à charge opposée sur un substrat approprié, dans lequel le PEI est souvent employé comme couche précurseur. Pendant l'approche des surfaces couvertes de PEI, les forces à longues distances de séparation entre les surfaces sont répulsives du au recouvrement des couches diffuses jusqu'aux distances de quelques nanomètres. Sur ces courbes, on observe la régulation de la charge de surface. La dépendance avec la force ionique des potentiels de couche diffuse observés peut être caractérisée par une charge extérieure de 2.3 mC/m^2. Les forces demeurent répulsives jusqu'au contact, probablement en raison des interactions électro-stériques entre les couches de PEI. Ces forces électro-stériques se manifestent à quelques nanomètres et semblent être superposées à la force provenant du recouvrement des couches diffuses. Pendant l'éloignement des surfaces, des forces attractives erratiques sont observées et dues aux événements d'adhérence moléculaires pontage ou *bridging*. La fréquence des événements d'adhérence

moléculaires augmente avec l'augmentation de la force ionique. La réponse de la force des trains d'adsorption du PEI est dominée par des profils d'extension caoutchoutique. On observe des forces d'adhérence fortes pour le PEI de faible masse moléculaire aux distances courtes directement après séparation. Cependant, pour le PEI de plus grande masse moléculaire, des forces d'adhérence plus faibles à de plus grandes distances sont plus communes. Le travail de l'adhérence a été estimé en intégrant les profils de force de rétraction, et on a démontré qu'il augmentait avec la force ionique.

Les dendrimères sont des polymères globulaires fortement branchés, qui ont attiré un intérêt croissant dans les deux dernières décades. Séquentiellement synthétisé à partir d'un noyau moléculaire, chaque séquence de réaction complète a pour résultat une nouvelle génération, qui a une masse moléculaire, un diamètre, et un nombre de groupes terminaux à la surface du dendrimère bien définie. L'intérêt croissant pour ces molécules est également dû à leur capacité de représenter certaines propriétés des protéines ou des micelles, et en raison de leurs applications dans l'identification moléculaire, des processus d'auto-assemblage, ou en catalyse. Parmi les premières structures dendritiques synthétisées, il y a eu les poly(amido amine) (PAMAM) dendrimères. Cette classe intensivement caractérisée parmi celle des macromolécules hydrosolubles peut être considérée comme un système modèle approprié pour des protéines ou des polyélectrolytes branchés. Ces molécules sont moins bien définies dans beaucoup d'aspects. En particulier, les différentes caractéristiques moléculaires telles que la taille, la charge, et la fonctionnalité peuvent être contrôlées pour des dendrimères de PAMAM de façon indépendante, en tenant compte d'une étude systématique de leur influence sur le comportement des processus d'adsorption.

A cette thèse, l'adsorption des dendrimères de PAMAM de génération G8 et G10, sur une surface de mica est étudiée par AFM en fonction de la concentration ionique et du pH. Les mesures initiales de l'adsorption des dendrimères sont conformes à un processus de diffusion-limitée, alors que le taux de recouvrement sature aux temps longs. Le taux de recouvrement maximum et les fonctions de corrélation correspondantes de paire ont été déterminés pour différentes

concentrations ioniques. Les tendances observées de taux de recouvrement peuvent être décrites par le modèle de sphère dure efficace correspondant à un processus d'adsorption séquentiel aléatoire (RSA). En particulier, à faible concentration ionique, le taux de recouvrement expérimentalement observé est plus important que celui prévue par le modèle de RSA. On a observé des différences semblables mais plus faibles pour les particules colloïdales. Nous suspectons que cette plus importante différence provient en partie du fait que la charge de la surface de mica joue un rôle dans le processus d'adsorption de dendrimères. Les mesures du taux de recouvrement maximum en fonction du pH suggèrent également que le modèle a besoin d'amélioration. Néanmoins, les tendances principales de l'adsorption de dendrimère de PAMAM se sont avérées compatibles avec le modèle de RSA. Cette étude prouve que des surfaces avec une densité bien définie des dendrimères avec différents taux de recouvrement s'étendant de 0,05 jusqu'à 0,4 peuvent être préparées en choisissant une génération appropriée de dendrimère, concentration ionique de l'électrolyte de fond, et valeur de pH. Ces dendrimères, bien que déposés de manière aléatoire, montrent qu'il existe des distances de séparation caractéristiques entre ces derniers à l'échelle du nanomètre. De cette façon, des nanostructures de surfaces peut être obtenues, à de plus petites échelles de longueur que des approches semblables utilisant des particules colloïdales.

Les propriétés d'adsorption des dendrimères poly(amidoamine) (PAMAM) sur des surfaces de silice sont étudiées. Des mesures de forces directes entre des substrats de silice en présence de PAMAM adsorbés sont analysées. L'adsorption des générations 8 et 10 de dendrimères PAMAM est étudiée à l'aide d'images topographiques des dendrimères déposé sur des surfaces planes et des sphères colloïdales. Le comportement de l'adsorption pour différentes forces ioniques est bien conforme au modèle d'adsorption séquentiel aléatoire (RSA). De plus, des mesures de forces directes sont réalisées entre les surfaces de silice en présence de dendrimères de PAMAM adsorbés. De cette façon, la masse adsorbée et la distribution de surface des dendrimères sur les plans de silice et la sphère colloïdale sont connues a priori. Les mesures avec la technique de la sonde

colloïdale démontrent que les interactions à longues distances sont purement électrostatiques. Les potentiels de couche diffuse sont obtenus à partir de l'optimisation des courbes de force au modèle de régulation constante, et ils diminuent avec la force ionique du milieu. En addition, les potentiels expérimentaux augmentent pour une force ionique fixe quand le recouvrement avec les dendrimères augmente. La densité de charge de surface est obtenue pour toutes les conditions d'adsorption de dendrimère et on montre qu'elle augmente avec le taux de recouvrement de la surface. On observe que la densité de charge augmente pour un même recouvrement pour les générations mineures de PAMAM. Nous avons réussi à obtenir des valeurs de la charge efficace des différents dendrimères de PAMAM adsorbés à partir des mesures des forces directes. Cette charge s'est avérée de loin inférieure à la densité des emplacements ionisés, et elle augmente quand la taille du dendrimère augmente. Ces tendances de variation de la charge efficace sont conformes avec celle prévue théoriquement, et à celle obtenue à partir des mesures de mobilité électrophorétiques. Une analyse qualitative des interactions à courtes distances a été fournie. On démontre que l'orientation des surfaces qui s'approchent peut expliquer la dispersion des potentiels de couche diffuse optimisés pour certaines positions.

En résumé, des interactions entre surfaces avec des polyelectrolytes adsorbées ont été étudiées avec la technique de la sonde colloïdale. L'étude du comportement d'adsorption des polyelectrolytes hautement branchés nous a permit de relier la distribution de la charge à la surface selon les divers états d'adsorption. En choisissant différents polyelectrolytes, il a été possible d'étudier les forces entre des couches homogènement chargées, ainsi que des surfaces composées de pièces rapportées de charge où la taille et la distance entre elles pourraient être accordées. Les résultats des mesures de force nous ont permis non seulement de connaître la dépendance de l'hétérogénéité de la charge de la surface, mais également quelques propriétés des différentes polymères adsorbées.

Nous considérons que les résultats de ce travail auront un impact dans beaucoup de secteurs scientifiques et technologiques. Les distributions

hétérogènes de charge sont présentes dans beaucoup de systèmes naturels, tels que les membranes cellulaires, ou des dispositifs technologiques, comme les puces électroniques. Des examens des systèmes modèles réglables à l'échelle du nanomètre ont été réalisés ici pour la première fois. L'élaboration des nanomodèles au moyen de l'adsorption contrôlé des dendrimères PAMAM peut être appliquée dans la nanolithographie ou dans la fonctionalisation des surfaces. Cependant, plus d'efforts doivent être fait, par exemple, dans l'élaboration des systèmes modèles de réseau réguliers de charge, où les études théoriques sont plus efficaces. La possibilité de réaliser des mesures des forces directes entre les surfaces hétérogènement chargées avec une distribution régulière demeure un challenge. Il est souhaitable aussi d'améliorer l'étude des interactions locales d'une manière quantitative. Le développement des expériences avec un positionnement des surfaces plus fin pourrait être réalisé en réalisant des images de volume de force au moyen de microscopie à force atomique.

List of publications

«Atomic Force Microscopy Study of the Adsorption and Electrostatic Self-Organization of Poly(amidoamine) Dendrimers on Mica»

Pericet-Cámara, R.; Papastavrou, G.; Borkovec, M. *Langmuir* 2004, 20, 3264-3270

«Interaction between Charged Surfaces on the Poisson-Boltzmann Level: The Constant Regulation Approximation»

Pericet-Cámara, R.; Papastavrou, G.; Behrens, S. H.; Borkovec, M. *Journal of Physical Chemistry B* 2004, *108*, 19467-19475.

«Interaction Forces and Molecular Adhesion between Pre-adsorbed Poly(ethylene imine) Layers»

Pericet-Cámara, R.; Papastravrou, G.; Behrens, S. H.; Helm, C. A.; Borkovec, M. *Journal of Colloid and Interface Science* 2006, 296, 496-506

So blind is the curiosity by which mortals are possessed, that they often conduct their minds along unexplored routes, having no reason to hope for success, but merely being willing to risk the experiment of finding whether the truth they seek lies there.

Le Discours de la Méthode (1637). René Descartes

Chapter 1

Surface forces

1.1 Introduction

The control of certain properties of colloidal dispersions such as aggregation, deposition or rheology, is essential for many chemical products like paints, glues, cosmetics or food additives, as well as in other industrial and environmental processes like mineral separation, papermaking or wastewater treatment[1]. In some of these processes, the aggregation of the suspended colloidal particles is attempted. In other cases, it is desirable to obtain stable particle dispersions or emulsions. The interaction forces between the surfaces involved in these systems usually determine the above-mentioned colloidal properties.

Surfaces of solids in contact with water are charged, and therefore, electrostatic forces, originating from the overlap of the electric double layers, typically dominate the long-range interactions between such surfaces. About fifty years ago, Derjaguin and Landau[2], and Verwey and Overbeek[3], proposed that the stability of a colloidal dispersion is determined by the balance between electrostatic and van der Waals forces, nowadays referred to as the DLVO theory. Direct force measurements repeatedly confirmed the relevance of electrostatic and dispersion forces in real systems[4]. In many situations, the DLVO theory provides a quantitative description of the interaction forces down to separations of a few nanometers.

Many studies have addressed the influence of adsorbed polymers to the interaction of colloids[5]. There is much interest in this topic due to its application in various industrial and environmental processes. Therefore, one could witness a remarkable progress in the understanding of this process through the investigation of polymer adsorption to interfaces, forces between polymer-covered surfaces,

and the role of polymers in particle aggregation. While polymer-mediated forces, such as steric or depletion interactions, dominate uncharged systems, the most important forces in charged systems are of electrostatic origin. For example, this observation applies to depletion-type interactions occurring in mixtures of particles and polyelectrolytes with equal sign of charge, as well as to aggregation phenomena in suspensions of charged particles induced by polyelectrolytes of opposite charge. While many processes involving neutral polymers are now understood[6, 7], more effort has to be done for polyelectrolytes. The main difficulty appears from the ubiquity of dissolved ions and surface charges. In this case, the polymer-induced forces are acting in competition with the electrostatic forces. A clear example of this behavior can be found in colloidal dispersions with the presence of polyelectrolytes. In these systems, polyelectrolytes act like giant counterions, adsorbing to colloidal particle surfaces, and controlling the suspension stability. If the net charge of a surface is neutralized by the adsorption of polyelectrolytes, the long-range double layer force disappears. Thus, the attractive van der Waals forces dominate, and the stability of the system will be reduced. When only small amounts of the polyelectrolyte are added to the system, reciprocal adsorption of polyelectrolyte molecules on neighboring particles or "bridging" may also act as a secondary mechanism for promoting interparticle attraction. On the other hand, in cases where the adsorbed amount of polyelectrolytes is higher, charge reversal of the underlying surfaces may occur, and result in electrostatic restabilization of a particle suspension. Further, if the polyelectrolyte adsorbed layer is of appreciable thickness, an additional steric barrier to coagulation may also exist leading to "electrosteric" stabilization[8].

Direct force measurement between surfaces was a long-standing experimental challenge and it was first possible in the late 1970's with the invention of the surface force apparatus. With the development of the atomic force microscope (AFM) in the mid 1980's, an instrument became available that was distinguished by its force resolution down to the piconewton range. This technique has been used to image topographically surfaces with Angstrom resolution. Since the pioneering work of Butt and Senden[9, 10], it is further used to quantitatively

measure surface forces. This method is ideally suited to study the short and long range interactions as well as the adhesion behavior between a large variety of solid surfaces, including those bearing deposited polyelectrolytes, and it has been used extensively throughout this work.

1.2 Forces between surfaces

The basic interactions that take place between surfaces are of the same nature than the ones acting between atoms and molecules, namely electrostatic, van der Waals or solvation forces. Indeed, forces between macroscopic objects result from a complex interplay between many interacting atoms or molecules both in the particles or surfaces and in the media separating them. However, they can manifest themselves in quite different ways and lead to qualitatively new features when acting between particles or surfaces. When we consider long-range interactions between particles and surfaces in liquids, we find that the three most important forces are the van der Waals, electrostatic and, in the presence of polymers, steric forces. At shorter distances of a few nanometers, solvation and other types of forces often dominate. In the case of mineral surfaces with adsorbed branched polyamines in aqueous solutions, as considered in this thesis, electrostatic interactions, polymer-origin steric forces, and van der Waals forces will dominate. The origin of these interactions will be described next in more detail.

a) Van der Waals forces

Van der Waals forces between macroscopic bodies have three contributions: the relative orientation of permanent dipole moments (Debye interactions), the induced dipole moment of a non-polar element by a permanent dipole (Keesom interactions), and the formation of dipole moments due to temporary charge fluctuations in non-polar elements (London interactions). The latter is the most important contribution to the van der Waals interactions, and it depends strongly on the polarizability of the molecules. The possibility of obtaining van der Waals

forces in macroscopic structures comes from the fact that these interactions can be considered as pairwise additive to a good approximation, and it is possible to obtain the forces by integration over the volume of two bodies close to each other. The expressions obtained are inversely proportional to a power *n* of the separation distance *D*, directly proportional to a dimensionless constant *B* (*n* and *B* depend on the shape of the interacting bodies), and to the Hamaker constant *H*

$$W(D) = -\frac{H \cdot B}{D^n} \tag{1.1}$$

The Hamaker constant plays a central role in the description of the van der Waals forces between surfaces summarizing the contributions of the Debye, Keesom, and London interactions. It has the dimension of energy, and it depends on the strength of the interaction, which at the same time is dependent on the quantum polarizability of the atoms. Another important condition for the Hamaker constant between two bodies is the medium in which they interact. This is because the dispersion interaction takes place between all the constituents of the system. Indeed, for certain cases, the van der Waals force between two surfaces across a medium can even be repulsive. This effect may be found for the case of a thin liquid film wetting a solid surface in air, explaining the effect of liquid helium climbing the walls of its container[4, 11, 12].

b) Electrostatic forces

Situations were only van der Waals forces are predominant are limited to some simple situations such as interactions in vacuum or to non-polar wetting films on surfaces. However, in aqueous systems, and due to the presence of free charges in solution, electrostatic interactions must be taken into account. Indeed, long-range electrostatic forces determine many properties of the dispersions. Most surfaces submerged in a dielectric medium, such as water, are usually charged. Thus, the electrostatic repulsion between similarly charged surfaces may prevent them from coalescence. One may find the origin of the charge on the surfaces in the presence of ionizable chemical groups in aqueous solution, such as amine groups that become protonated at low pH conditions

$$-NH_2 + H^+ \rightleftharpoons -NH_3^+ \tag{1.2}$$

As well, ions present in solution may bind onto previously uncharged surfaces, or they may also adsorb on oppositely charged groups. The presence of a charged surface creates in its vicinity a cloud of counterions that keeps the net charge of the system neutral. Some of those counterions are bound to the surface, forming the Stern layer. The remaining ions form an extended atmosphere close to the surface due to thermal motion that is called diffuse layer[4]. The electrostatic interaction between two charged surfaces in solution is actually of entropic origin, due to the overlapping of the approaching diffuse electric double layers. Indeed, the system has an overall neutral charge, and the electrostatic energy profile between the plates takes part only in the arrangement of the ions in the diffuse layer.

In Figure 1-1, a schematic representation of the Stern model for an isolated charged surface in solution is shown. Charged surfaces in solution are usually characterized by its surface charge density σ and diffuse layer potential ψ_d. It is important to determine the relationship between these two parameters, and the distribution of ions in the solution, to further evaluate the electrostatic interactions between surfaces[13]. For this, the Poisson-Boltzmann equation needs to be solved in the diffuse layer region

$$\frac{d^2\psi}{dx^2} = -\frac{e}{\varepsilon\varepsilon_0}\sum_i z_i c_i \exp\left(-\frac{z_i e\psi}{k_B T}\right) \qquad \text{for several ions } i = 1,\ldots, N \qquad (1.3)$$

where ψ is the electrostatic potential profile, $\varepsilon\varepsilon_0$ is the water dielectric constant, e the elementary charge, k_B is the Boltzmann constant, T is the temperature, z_i is the valency of the ion i, and c_i is the concentration of the ion species i in bulk where $\psi = 0$.

The solution of this equation is the electrostatic potential profile from the charged surface. The effect of the fixed charges on the surface enters the equation through the boundary conditions of the calculation. The Poisson-Boltzmann equation is often difficult to solve analytically, and in many situations, it has to be done numerically. In order to describe the surface interactions exposed in this work, a solution scheme of the Poisson-Boltzmann equation will be proposed in

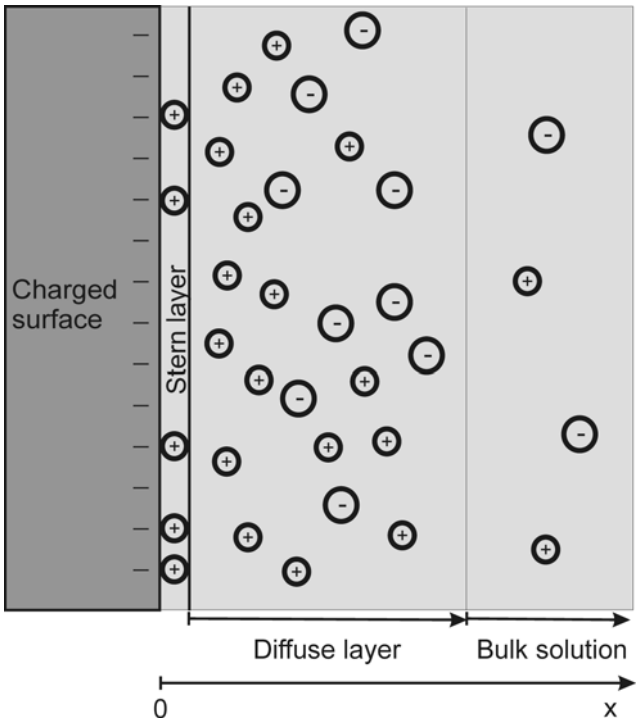

Figure 1-1. Schematic representation of the Stern model of the electric double layer, present in the proximity of a charged surface in solution.

Chapter 2. In the case of a monovalent salt, the pressure of the interacting plates is given by

$$P = 2c_b k_B T\left[\cosh(\frac{e\psi}{k_B T}) - 1\right] - \frac{\varepsilon\varepsilon_0}{2}\left(\frac{d\psi}{dx}\right)^2 \qquad (1.4)$$

where c_b is the bulk concentration of the electrolyte. For the case of two equally charged plates, we need to solve the Poisson-Boltzmann equation and substitute the potential ψ in equation (1.4) to obtain the pressure P. To solve equation (1.3), one needs to define boundary conditions according to the studied system. One possibility is to consider the surfaces as having constant charge. Another solution can be extracted by considering the potential at the surfaces as constant. The solutions can be viewed graphically in Figure 1-2. Herein, one observes that both solutions coincide at long separation distances. At smaller separations, if no binding of the counterions occurs, the surface charge remains constant, and

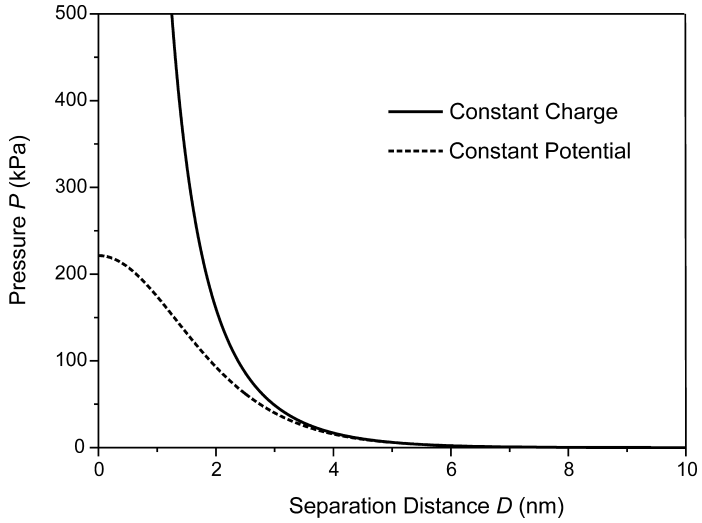

Figure 1-2. Pressure between two charged plates as a function of separation distance. The surface potential is ψ_d = 25 mV and the ionic strength of the solution is I = 0.1 M.

pressure and energy tend to infinite when the surfaces come closer. This behavior can be observed in the upper curve of Figure 1-2 (constant charge boundary condition). If specific ion binding can occur, the limiting case is considering the surface potential as constant. Thereby, the values of the pressure converge to a finite value upon close approaching of the surfaces, as shown in the lower curve of Figure 1-2. The pressure between two charged surfaces may be transformed in interaction energy per surface area W by a simple integration

$$W = \int_D^\infty PdL \tag{1.5}$$

For most of the experimental situations, the symmetry between two interacting surfaces is not that of two plates. To calculate the force between two spheres from the interaction energy per surface unit between two plates, it is of great utility to use the Derjaguin approximation, providing the distance between the interacting spheres is small compared to their radii. For two spheres, this approximation can be summarized in the expression

$$F(D) \approx 2\pi R_{eff} W(D) \tag{1.6}$$

where

$$\frac{1}{R_{eff}} = \frac{1}{R_1} + \frac{1}{R_2} \tag{1.7}$$

being R_1 and R_2 the radii of the interacting spheres.

c) Polymer-induced steric forces

Due to the higher number of contact points, polymers usually adsorb strongly, and often irreversibly on surfaces. In particular, a polyelectrolyte will adsorb strongly on an oppositely charged surface. The configuration of the polymer on the surface depends on a large number of parameters such as the forces that bring the polymer down to adsorption. Polymer-covered surfaces will interact through the outer part of the polymer in solution. The typical separation distance in which both opposing coils will overlap is in the order of two times the radius of gyration of the polymer. Normally, the effect of van der Waals is negligible at these distances, and polymer-polymer overlap and electrostatic forces (provided that the polymer is charged) will be predominant. In good solvents, the interaction between adsorbed polymers is repulsive. The coil of a polymer expands from the surface into the solution to gain configurational entropy. If the coils of the adsorbed polymers overlap, their conformations in solution are decreased, increasing the free energy of the system. Hence, a repulsive force between the surfaces is generated referred to as steric interaction. When the adsorbed polymers are charged, this interaction is sometimes called *electrosteric*. If the polymer is in a bad solvent, it may find more favorable to reach the vicinity of the opposing surface to increase its configurational entropy, and an attractive interaction between the surfaces can arise[13].

The saturation of a surface with linear polymers may drive to the formation of polymer brushes. Herein, a high density of linear polymers is attached to the surface at one end, while the coils extends into the solution, avoiding contact with the neighbors. The interaction between such surfaces is described by the theory developed by Alexander and de Gennes[7, 14]. The pressure between two plates bearing neutral monodisperse polymer brushes can be expressed as

$$P(D) \approx \frac{k_B T}{s^3}\left[\left(\frac{2L}{D}\right)^{9/4} - \left(\frac{D}{2L}\right)^{3/4}\right] \quad (1.8)$$

for $D < 2L$, where D is the separation distance, L is the contour length of the polymer, and s is the mean distance between attachment points. In the case of polyelectrolytes, a more complex behavior is observed that depends on both the grafting density s and the charge density of the polyelectrolyte. On the other hand, when the regime of adsorbed polymers is far from saturation, an attraction can occur even for good solvents. In this situation, a polymer can extend reaching a bare region of the opposing surface and making molecular contact on both sides. It results in an attractive interaction called "bridging". This last effect has dramatic consequences in systems of particles with small amounts of polyelectrolytes. Indeed, the polyelectrolyte may easily bind to two surfaces inducing an attractive interaction, and driving the system to rapid aggregation[15, 16].

1.3 Atomic force microscopy (AFM)

The scanning tunneling microscope (STM) invented in 1982[17] was the precursor of the development of a new class of techniques, summarized as scanning probe microscopy (SPM). All SPM techniques are based on measurements of the local interactions between a sample and a probe separated by a small distance. These techniques allowed to improve the measurements of many physical properties at a local scale, such as interaction forces, magnetic and electrostatic forces or chemical properties. Among the SPMs, AFM is more commonly used due to the large number of applications in which non-conductive samples are imaged in various media, including gases and liquids. Originally, the AFM was developed for imaging surface topography[18], although it is also possible to study interactions by measuring the force acting between the probe and the sample.

AFM consists of a tip at the end of a cantilever that is approached to the scanned object by means of a piezoelectric scanner. The deflection of the cantilever due to the tip-sample interactions is measured by a simple optical technique, in which a laser light is reflected from the back of the cantilever onto a

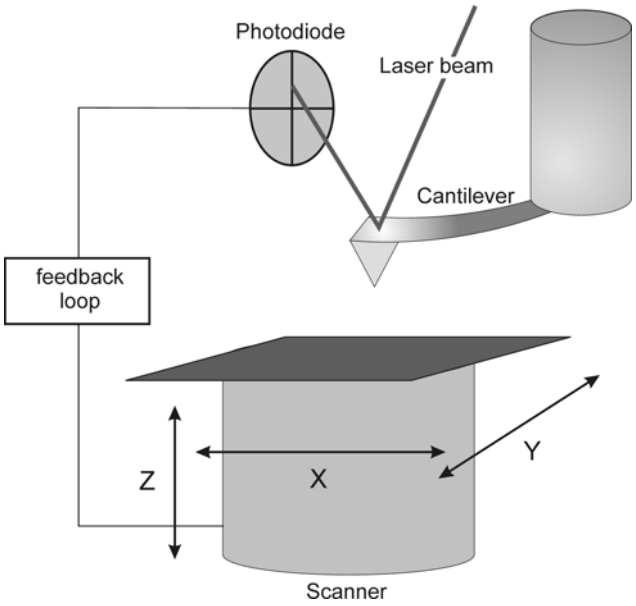

Figure 1-3. Schematic representation of an atomic force microscope set-up.

highly sensitive photodiode (see Figure 1-3). The signal of this photodiode is either registered or used to control the movement of the piezoelectric translation stage by a feedback mechanism.

a) Direct force measurements

The possibility of measuring directly interaction forces between surfaces has played an important role to develop a better understanding of colloidal interactions. The determination of such forces was firstly possible with the surface force apparatus (SFA)[19]. This technique has certain restrictions, such as the requirement of smooth, semitransparent, macroscopic surfaces as part of the experimental set-up, which limits enormously the amount of materials that could be examined. A significant improvement was achieved with the development of the colloidal probe technique[9, 10]. By attaching a micrometer-sized particle to the end of an AFM cantilever, the restrictions owing to the nature of the tip material were overcome, and it was possible to have a well-defined tip-sample geometry and higher force resolution. In these terms, the colloidal probe technique can be

used to measure the forces between surfaces of any kind of material, provided that they are microscopically flat enough. Additionally, this technique can laterally resolve the interaction forces, with the consequent increase in adaptability with respect to SFA.

In force measurements, the sample or the tip holder is moved vertically by a piezoelectric device, while the other components remain in place. The deflection of the cantilever is recorded during the vertical piezo movement, generally by the optical lever technique (see Figure 1-3). In this, a segmented photodiode act as a position sensor of the laser spot, registering the cantilever deflection by the reflected laser beam. The sensitivity of the optical lever can be characterized by the "inverse optical lever sensitivity" or *InvOLS*, where $x = InvOLS \cdot \Delta V$, and ΔV is the voltage measured by the photodiode[20, 21]. The most common method for quantifying the *InvOLS* requires that the lever be brought into contact with a rigid surface and then moved a known distance (a force curve). The slope of the resulting cantilever deflection vs. distance yields *InvOLS*. On the other hand, the voltage applied to the piezoelectric stage is transformed by means of an implemented *LVDT* in displacement. Thus, the raw data as cantilever deflection vs. piezo displacement must be transformed in force vs. separation distance. The conversion of the deflection to the force is done using the Hooke's law

$$F = k \cdot Y \tag{1.9}$$

where k is the spring constant of the cantilever, Y is the cantilever deflection and F is the resulted bending force.

Figure 1-4 shows a representative curve resulting from direct force measurements that displays some of the characteristic features of the interactions between two surfaces. In the region of large separation, where probe and sample still do not interact, the cantilever is not deflected by external forces. This interval is called *non-contact region* (Figure 1-4a). When raw data in form of cantilever deflection against piezo displacement are transformed in force versus separation, this region is fixed at force $F = 0$. When probe and sample are approached and start to interact, the cantilever is deflected (Figure 1-4b). Further, a short-range attractive interaction can overcome a threshold and trigger an instability of the

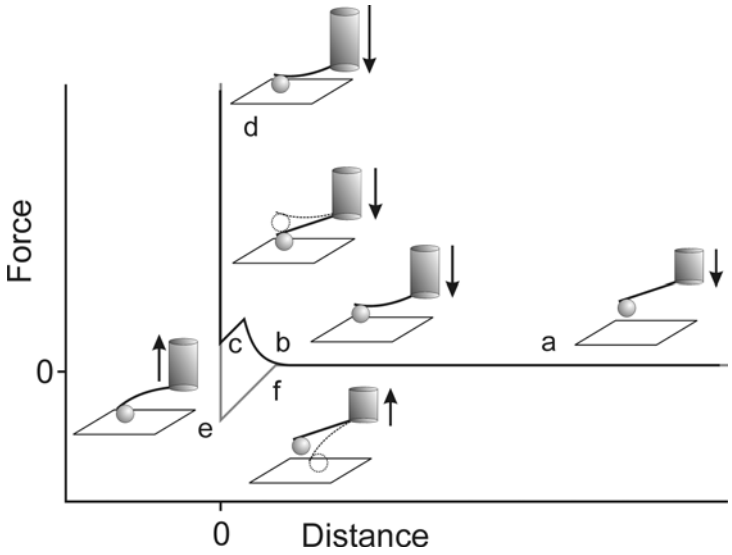

Figure 1-4. Exemplary force curve showing characteristic features of interactions between two surfaces. Approach curve in black: a) Non-contact region, b) repulsive interaction, c) probe jump-in due to short-range attraction, d) constant compliance region. Retraction curve in gray: e) adhesion event, f) jump-out and return to non-contact region.

probe, which results in a jump of the probe onto the sample or *jump-in* (Figure 1-4c). For incompressible surfaces, the probe and the sample remain in contact and the deflection of the cantilever follows the movement of the translation stage (Figure 1-4d). This part, which corresponds to a straight line in the deflection versus piezo displacement curve, is called the *constant compliance region*, and it is set as zero-separation distance when transforming to force vs. separation. In the absence of plastic deformation, the deflection observed during retraction of the cantilever follows the constant compliance region of the approach. During retraction of the probe, an adhesion hysteresis is often observed when the attractive force between the surfaces is higher than the restoring force of the cantilever. Thus, probe and substrate continue in contact (Figure 1-4e). Next, when the spring force overcomes this adhesion force, the probe pulls back (*jump-out*) from the surface to its equilibrium position (Figure 1-4f).

Quantitative analysis of the direct force measurements requires an accurate knowledge of the cantilever spring constant in order to convert a cantilever

deflection to a corresponding force value. Unfortunately, although the dimension and the density of the materials of a cantilever would suffice to establish its spring constant, it is difficult to obtain constant values during its production process, and there are often considerable variations. Hence, it is essential to calibrate cantilevers that are used in direct force measurements. One can find several methods in literature[22-25], although only two of them have been used in this thesis, namely the *Hutter-Bechhoefer* method, and the *Sader* method. The *Hutter-Bechhoefer* or *thermal noise* method is based on the equipartition theorem[22], which states that at thermal equilibrium, any harmonic term in energy with one degree of freedom possesses an energy equal to $\frac{1}{2}k_BT$, where k_B is the Boltzmann constant and T is the temperature (K). For an AFM cantilever, one can write

$$\frac{1}{2}k < Y^2 >= \frac{1}{2}k_BT \tag{1.10}$$

where k is the spring constant of the cantilever and $< Y^2 >$ is its time averaged square deflection in the vertical direction due to thermal motion. The thermal noise spectrum is obtained by transforming time series data of the cantilever deflection into the frequency domain using a fast Fourier transformation. Plotting the thermal noise curve as a power spectral density, where the thermally excited cantilever spectrum has the shape of a Lorentzian curve, the area under the curve corresponds to $< Y^2 >$. The optical lever sensitivity is required to convert the photodiode signal to the cantilever deflection Y. It is determined by an additional measurement from the constant compliance region on a hard surface using exactly the same laser alignment as was used for the acquisition of the power spectrum.

The *Sader* method allows for the determination of the cantilever spring constant for rectangular, single-beam cantilevers by measuring the easily accessible top-view dimensions and by evaluating the quality factor, Q, and a resonance frequency, v, from the thermal noise spectrum[23]. The spring constants can be obtained without knowledge of the optical lever sensitivity, and it eliminates the requirement of an *a priori* knowledge of the mass density and the elastic properties of a given cantilever and accounts for the effects of the surrounding medium[23]. The spring constant, k, is given by

$$k = 0.1906 l Q (w 2\pi\nu)^2 \rho_f \Gamma_i(\nu) \quad (1.11)$$

where w is the width (top view) of the cantilever, Q is the quality factor, ρ_f is the density of the fluid in which the cantilever is immersed and $\Gamma_i(\nu)$ is the imaginary part of a hydrodynamic function which depends on the Reynolds number of the cantilever in the medium[26].

b) Tapping mode AFM imaging

The imaging modes of AFM depend mainly on the type of contact between the tip and the sample, and the registering signal. Originally, AFM was developed for topographic imaging in the so-called contact mode[18]. Here, the AFM cantilever is brought in contact with the surface keeping a constant deflection by means of a feedback circuit. However, this mode was not suitable to be used in soft samples, such as polymer surfaces, due to the strong shear forces applied to the sample. In the case of tapping mode, the AFM cantilever oscillates at its resonance frequency with given constant amplitude. The tip is brought to intermittent contact with the surface, tapping it slightly, while the piezoelectric scanner moves the sample horizontally. The tip-sample interaction alters the cantilever oscillation. Thus, the scanner is moved vertically via a feedback signal to maintain the oscillation at constant amplitude (set-point amplitude) (see Figure 1-5). This signal and the one from the horizontal position of the scanner are used to generate the topographical image of the surface. In order to keep low dissipation energies, the set-point amplitude is adjusted typically at 90-95% of the free oscillation one. This mode allows to image samples bearing weakly bound elements, such as particles, polymers or other soft materials. As well as topographical imaging, it is possible to register changes in the phase angle of the resonance frequency of the cantilever to produce a second image, a technique that is called phase imaging[27]. The phase change of the oscillation depends on the dissipation energy of the sample, which can be related to its mechanical properties, namely adhesion, stiffness or viscoelasticity. The phase imaging mode is ideal to image surfaces bearing different materials. Although the properties of those images are mostly qualitative,

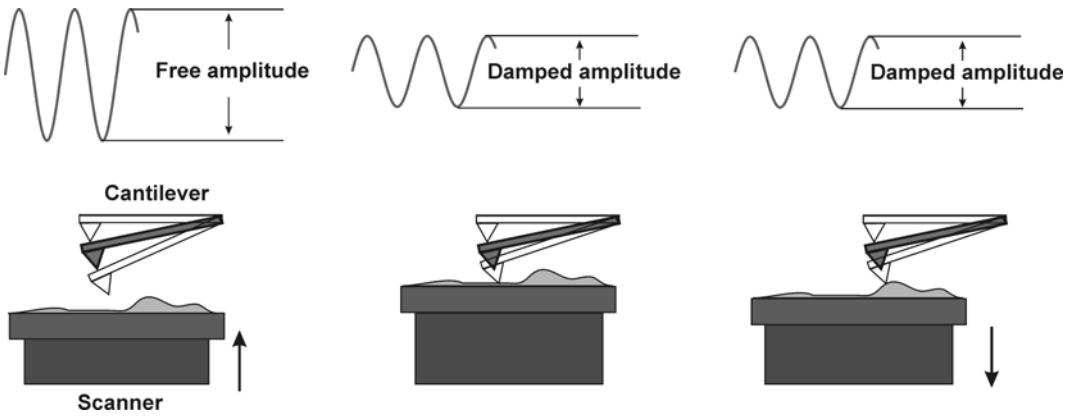

Figure 1-5. Schematic picture of tapping mode atomic force microscopy.

they provide a contrast between the materials present on the surface, or even between different phases of the same material. Hence, they are often used to complement topographic images[28].

1.4 Force measurements between polyelectrolyte layers

With the colloidal probe technique, one can monitor long-range interactions or adhesive properties that cannot be predicted a priori. It is appropriate to stress that this technique allows to resolve laterally interaction forces. As well, it is possible to investigate interactions between any kind of materials, including particulates, membranes, lipid layers or fibrous materials. In its origin, the colloidal probe technique was developed in order to measure interactions between similar mineral surfaces[9, 29, 30] and dissimilar ones[31]. As it has been commented above, the presence of polymers can change dramatically the interaction forces between surfaces. Due to the great versatility of the colloidal probe technique, it was soon used to investigate the effect of adding polymers to those systems[32, 33]. Interaction forces of surfaces in the presence of synthetic polymers[32], proteins[34], polyelectrolytes[35], copolymers[36], or even combinations of some of these[37] were studied, and investigations in several system conditions could be realized. For

some of these experiments, the polymers were previously adsorbed, forming layers on the substrate[38], multilayers[39], or polymer brushes[40].

The study of the interaction forces between surfaces by direct force measurements is extremely useful, for instance, to address the interactions between dispersed colloidal particles. These interactions determine the colloidal stability of those dispersions. Among those systems, one can include those bearing polymers as stability modifiers. Recently, it has been observed that for various systems, the aggregation behavior of colloidal particles in the presence of polyelectrolytes showed events that could not be explained by the classical DLVO theory. For instance, some previous results on colloidal aggregation in presence of polyelectrolytes have shown aggregation rates that are faster than the ones measured in the absence of polyelectrolytes[16, 41]. As a first hypothesis, it was stated that the lateral heterogeneity of the charge of polyelectrolyte-adsorbed particles could drive to local attraction of oppositely charged regions despite of net similar charge. It becomes necessary to be able to use a technique with which these interactions can be addressed, and that is capable to resolve them laterally, to test the influence of the local polymer distribution. In this framework, direct force measurements, and more precisely, the colloidal probe technique, is revealed as an ideal method to address these questions. Furthermore, it is necessary to tailor the interacting surfaces depending on the desired system. Additionally, it is specially suited to resolve the surface interactions laterally. The dependence of surface interactions on the surface charge heterogeneity has been approached to a large extend only from the theoretical point of view[42-44]. The main inconvenience comes from the difficulty of elaborating appropriate model systems with well-defined tunable surface charge. Some advances have been done in this direction recently[45], although more research is needed to obtain a better knowledge of these systems.

1.5 Outline of the thesis

The aim of this thesis is to study the dependence of the surface interactions on the lateral distribution of their surface charge. The adsorption behavior of different highly branched polyelectrolytes on mineral surfaces will be investigated. By the understanding of their adsorption behavior one can control and tune the lateral charge distribution on these surfaces. This allows to measure and compare the forces between different well-defined charged surfaces. The outline of this thesis is as follows:

In Chapter 2, a theoretical study of electrostatic interactions between charged surfaces will be formulated. Herein, a new solution scheme of the Poisson-Boltzmann equation is developed, which will be used to describe the electrostatic interactions of the direct force measurements in following chapters.

Chapter 3 will describe experimental interaction forces between homogeneously charged polyelectrolyte surfaces. Both the long-range interactions and the adhesion behavior between the surfaces will be discussed.

The adsorption behavior and the lateral distribution of adsorbed dendritic polyelectrolytes on mineral surfaces will be addressed in Chapter 4. We will study the possibility of tuning the charge of the surfaces by varying the different polyelectrolyte adsorption conditions.

To conclude, direct force measurements between heterogeneously charged polyelectrolyte surfaces will be presented in Chapter 5. The interacting surfaces will be designed following the conditions established by the adsorption experiments.

Chapter 2

Electrostatic interaction between charge regulating surfaces

2.1 Introduction

The electrostatic forces between ionizable surfaces are typically treated on the Poisson-Boltzmann (PB) level, which invokes a mean-field approximation for the electrolyte solution[4]. The solving of the PB equation requires a choice of boundary conditions, and usually, either the constant charge (CC) or the constant potential (CP) boundary condition. Inspection of available direct force measurements reveals that normally neither the CC nor the CP condition represents a good approximation[4, 10, 46-48]. The measured forces typically lie between these two cases, a situation which is referred to as charge regulation[4, 49-53]. In this situation, neither the diffuse layer charge nor the diffuse layer potential remain constant, but both quantities vary with the separation as a result of an interplay between the charge-potential relationships of the diffuse layer and of the surface. The charge-potential relationship of the surface reflects how the surface charge varies as a function of the diffuse layer potential and is dictated by the dissociation reactions occurring at the surface (i.e., surface complexation)[54, 55]. Charge regulation has been treated by several authors employing detailed models of the dissociation behavior of the surface[51-53, 56-59]. From these theoretical studies, it becomes clear that consideration of the charge regulation normally leads to results between the case of CC and the case of CP, and calculated force-distance curves do resemble the experimental results. Unfortunately, however, such calculations are cumbersome, highly model-dependent, and for this reason of limited practical use for routine data analysis. Based on these studies, one might

in fact suspect that without detailed models of the surface dissociation behavior, no calculations of the regulation behavior are possible. The resulting restriction would be severe, because for many systems of interest accurate surface charging models are not available (e.g., adsorbed polyelectrolytes).

Carnie and Chan[60] were the first to suggest how to circumvent this dilemma by considering a regulation parameter interpolating between the CC and the CP cases. This parameter was defined in terms of the diffuse layer capacitance C^D and a regulation capacitance C^I, both capacitances referring to the charge-potential relationships of the diffuse layer and of the surface, respectively. Both relationships have been linearized, and, consequently, the diffuse layer was treated within the Debye-Hückel approximation. The latter approximation is rather restrictive, however, because it linearizes the PB equation and is, therefore, applicable up to surface potentials of only 20-30 mV. For this reason, many realistic systems fall outside the range of this approximation.

More recently, it has been shown that the regulation parameter can be generalized to the PB level[51, 52]. This parameter p can be obtained from the capacitances of the diffuse and the surface layer and typically assumes the values $0 < p < 1$, with $p = 0$ for CP and $p = 1$ for CC. In the symmetric situation, an approximate scheme was further proposed to construct the force-distance curves from this regulation parameter and the CP and CC force profiles[51]. Nevertheless, the utility of the regulation parameter to calculate force-distance curves in the asymmetric PB case remained unclear.

This chapter shows how the regulation parameter p can be used to define a constant regulation (CR) boundary condition in the nonlinear PB regime. With this boundary condition, one can treat symmetric and asymmetric situations in the PB regime to excellent accuracy. The spirit of this approximation is that the diffuse layer is treated exactly within the PB equation, while the charge-potential relationship of the surface is linearized around the potential of the isolated surface. This approximation characterizes each surface with two parameters, namely, the diffuse layer potential $\psi^{D,\infty}$ and the regulation parameter p. The key advantage of this approximation is that these two parameters suffice to approximate the detailed

charge-potential relationship. This parametrization is completely generic and entirely independent of the molecular details of reactions occurring on each particular surface. Both parameters can be extracted from experimental force-distance curves or derived from models for dissociation equilibria for the isolated surface. Within this chapter, we shall demonstrate the high accuracy of the CR approximation by comparing the corresponding results with an exact treatment of the surface dissociation equilibria for realistic systems. The comparison with experimental data is discussed in the next chapters.

2.2 Interaction forces on the Poisson-Boltzmann level

We consider two charged, parallel plane surfaces immersed in a monovalent electrolyte solution separated by a distance L. The spatial coordinate normal to the surface will be denoted by x, and the position of the surface 1 (left) will be chosen at $x = 0$ and of the surface 2 (right) at $x = L$. The charges on the surface will create a diffuse layer in their vicinity. These diffuse layers overlap for small separations between the surfaces. The properties of these diffuse layers are determined by the dissociation equilibria at both surfaces.

a) Diffuse layer profile

The electrostatic potential $\psi(x)$ within the diffuse layer is described with the PB equation

$$\frac{d^2\psi}{dx^2} = \frac{\kappa^2}{\beta e}\sinh\left(\beta e\psi\right) \tag{2.1}$$

which is equation (1.3) for monovalent salt solutions. Thereby, e is the elementary charge, $\beta = 1/(k_B T)$ is the inverse thermal energy, and κ^{-1} is the Debye length defined by $\kappa^2 = 2\beta e^2 n/(\varepsilon\varepsilon_0)$, whereby n is the number concentration of the monovalent salt in the bulk and ε_0 is the dielectric permitivity of water. At the boundaries, the potential profile satisfies

$$\psi_1^D = \psi(0) \tag{2.2}$$

$$\psi_2{}^D = \psi(L) \tag{2.3}$$

where the $\psi_1{}^D$ and $\psi_2{}^D$ are the diffuse layer potential of the surfaces 1 and 2, respectively. Fixing these two parameters leads to the CP boundary conditions. Furthermore,

$$\sigma_1{}^D = -\varepsilon\varepsilon_0 \left.\frac{d\psi}{dx}\right|_{x=0} \tag{2.4}$$

$$\sigma_2{}^D = -\varepsilon\varepsilon_0 \left.\frac{d\psi}{dx}\right|_{x=L} \tag{2.5}$$

where the $\sigma_1{}^D$ and $\sigma_2{}^D$ are the diffuse layer charge densities of the surfaces 1 and 2, respectively. Fixing these two parameters leads to the CC boundary conditions.

In the general case, neither the CC nor the CP boundary conditions represent a good approximation, and one must use an explicit model of surface dissociation equilibria and derive a charge-potential relationship for the inner (compact) layer of each surface. This charge corresponds to the total charge on the surface and will be a function of the diffuse layer potential. Let us denote these relations for both surfaces as $\sigma_1{}^I(\psi_1{}^D)$ and $\sigma_2{}^I(\psi_2{}^D)$. Note that these relations only depend on the properties of the surface but not on the surface separation *L*. The above system of equations can be closed by realizing that the diffuse layer charge must be neutralized by the inner layer charge, namely,

$$\sigma_1{}^D = \sigma_1{}^I\left(\psi_1{}^D\right) \tag{2.6}$$

$$\sigma_2{}^D = \sigma_2{}^I\left(\psi_2{}^D\right) \tag{2.7}$$

These relations complete the system of equations, and eqs. (2.1)-(2.7) can be solved. Several authors have proposed solutions in terms of elliptic functions[51, 53, 56, 58, 59]. However, we find a direct numerical solution of the PB equation with a deferred correction technique and Newton iteration equally accurate, efficient, and much easier to implement in the asymmetric case[61].

At large separation distances, the diffuse layer charge is given by the Grahame equation

$$\sigma^D = \frac{2\varepsilon\varepsilon_0\kappa}{\beta e}\sinh\left(\frac{\beta e\psi^D}{2}\right) \quad \text{for} \quad L \to \infty \tag{2.8}$$

while the diffuse layer capacitance is given by its derivative

$$C^D = \frac{\partial \sigma^D}{\partial \psi^D} = \varepsilon\varepsilon_0\kappa \cosh\left(\frac{\beta e \psi^D}{2}\right) \tag{2.9}$$

The solution of eqs. (2.6) and (2.7) yields the surface potentials for each isolated surface, denoted as $\psi_1^{D,\infty}$ and $\psi_2^{D,\infty}$. Equivalently, one may also specify the diffuse layer charge of the isolated surface, $\sigma_1^{D,\infty}$ and $\sigma_2^{D,\infty}$. Both quantities are often loosely referred to as the *diffuse layer potential* and *diffuse layer surface charge*, although they refer to infinite separation. At finite separations, the potential and charge of the diffuse layer vary as a function of the distance.

Figure 2-1 illustrates the situation for a symmetric system. The diffuse layer charge σ^D increases with the surface potential, while the inner layer charge σ^I typically is a decreasing function. The crossing point of these two functions defines the surface potential. With decreasing distance between the plates, surface charge normally decreases, and the crossing point shifts to higher surface potentials.

b) Constant regulation boundary conditions

Let us now discuss the charging properties of the compact layer in more detail. For clarity, we shall drop the subscript referring to the surface 1 or 2. The compact layer capacitance can be defined as

$$C^I = -\frac{\partial \sigma^I}{\partial \psi^D} \quad \text{for} \quad L \to \infty \tag{2.10}$$

At large separations, we may expand the charge-potential relationships around the potential at infinite separation in a Taylor series

$$\sigma^I = \sigma^{I,\infty} - C^I\left(\psi^D - \psi^{D,\infty}\right) \tag{2.11}$$

and replace the charge-potential relationship of the inner layer by a straight line (see Figure 2-1, dashed line). In a first approximation, each surface can be characterized by the diffuse layer potential $\psi^{D,\infty}$ and the inner layer (regulation)

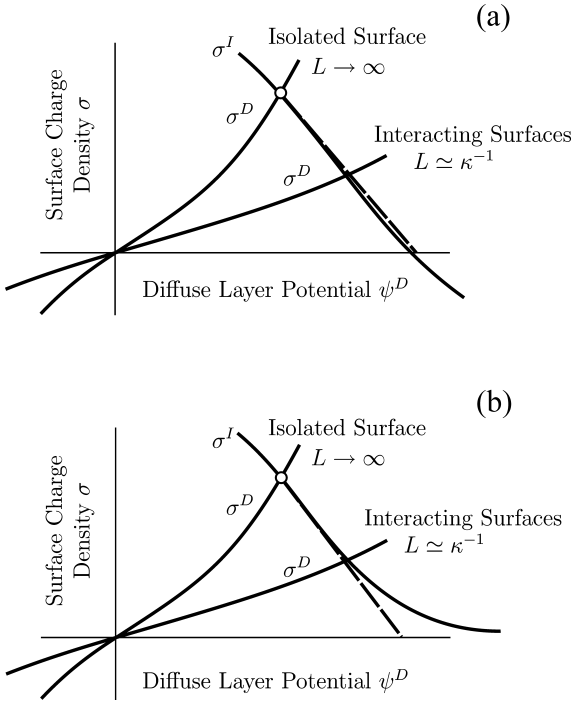

Figure 2-1. Schematic representation of the charge-potential relationships for two equal interacting surfaces. The inner layer charge density σ^I typically decreases with increasing double layer potential. It is independent of the surface separation L but depends on the surface chemistry. The diffuse layer charge density σ^D increases with increasing double layer potential. It depends on the separation L but is independent of the surface properties. For an isolated surface this relation is given by the Grahame equation (cf. equation (2.8)). The magnitude of σ^D decreases with decreasing separation L, and it vanishes at contact. The equilibrium point is given by $\sigma^I = \sigma^D$ at any separation and is marked for the isolated surface (O). The dashed line is the CR approximation for the inner layer charge density σ^I. The approximation works well even down to contact for part (a), but fails near contact for part (b).

capacitance C^I, both quantities being evaluated for the isolated surface. The inner layer capacitance describes the regulation characteristics of the surface, whereby a small capacitance corresponds to the CC case, while a large (positive) capacitance corresponds to the CP case. Because the regulation capacitance C^I used in the charge-potential relationship is a constant, we will be employing the term *constant regulation*. Instead of this capacitance, we prefer to introduce the regulation parameter[51, 52]

$$p = \frac{C^D}{C^I + C^D} \tag{2.12}$$

to characterize the regulation properties of each surface. Applying eq. (2.11) to each surface, we obtain a closed system of equations, and this approximation will be referred to as the CR boundary condition.

The substantial advantage of the above formulation is that the regulation characteristics of each surface are contained in merely two quantities, namely, the diffuse layer potential $\psi_1^{D,\infty}$ and the regulation parameter p, both being properties of an isolated surface. The quality of the approximation can be deduced from Figure 2-1. This approximation is asymptotically exact for large distances, even at large surface potentials. The latter aspect makes the present CR approximation much more versatile than the approach of Carnie and Chan[60], which is only applicable at low surface potentials.

The performance of the CR approximation near contact is not obvious, but its validity can be assessed by considering the charge-potential relationship for the inner layer. Naturally, when this relationship is close to a linear function, the approximation will be excellent (see Figure 2-1a). This situation applies particularly for surfaces with a well-defined PZC, such as most metal oxides. On the other hand, if the curvature of the charge-potential relationship is large, the approximation may fail at short distances (see Figure 2-1b). This situation is commonly encountered for surfaces that become neutral upon full desorption or full saturation of the charge-determining ion. In this case, as σ^I tends toward 0, the magnitude of the surface potential increases dramatically. An important example of such a situation is silica. We shall see, however, that even for such a surface, the CR approximation remains excellent except for small separations.

c) Basic Stern model

To investigate the quality of the proposed CR approximation, we shall use established models of surface dissociation equilibria for realistic systems and compare the exact results with the CR approximation.

The basic Stern model has been shown to be valid for a number of interfaces of metal oxides, and for that reason this model will be used in the following[54, 55]. This model considers a surface whose charge varies by means of the adsorption of

protons to different surface sites. The mass action law for each type of site j can be written as

$$K_j = \frac{\theta_j}{\left(1-\theta_j\right) a_H(0)} \tag{2.13}$$

where K_j is the microscopic association constant, θ_j is the degree of protonation, and the surface activity of protons is given by $a_H(0) = a_H \exp(-\beta\varepsilon\psi^0)$ where ψ^0 is the surface potential and a_H is their bulk activity with pH = -log a_H. The association constant is usually reported as pK_j = log K_j. The surface charge can be then evaluated as

$$\sigma^I = e\sum_j \Gamma_j \left(\theta_j + z_j\right) \tag{2.14}$$

where z_j is the charge of the site j in its deprotonated state and Γ_j is its total site density. The diffuse layer potential is related to the surface potential ψ^0 by the Stern capacitance, which is defined as

$$C^S = \frac{\sigma^I}{\psi^0 - \psi^D} \tag{2.15}$$

From eqs. (2.13)-(2.15) the charge-potential relationship for the inner layer $\sigma^I(\psi^D)$ can be constructed. This nonlinear relationship can be then used to solve the PB equation. For large separations, the solution reduces to the classical solution of the basic Stern model for isolated surfaces, which invokes the Grahame equation (cf. eq (2.8)). An equivalent approach was adopted earlier[52, 53].

d) Interaction forces

Once the potential profile is known, the force between two bodies can be evaluated from the pressure between the plates[4]. The pressure follows from equation (1.4). This expression is an invariant, meaning that it holds at any position x. This feature represents a useful check of the numerical accuracy of the solution. Once the pressure is known, the surface free energy can be evaluated by integration of equation (1.4). Based on the Derjaguin approximation, the force between two bodies becomes

$$F = 2\pi R_{eff} \int_L^\infty P(L')dL' \tag{2.16}$$

where R_{eff} is the mean curvature radius defined in equation (1.7). This integration is performed numerically. Equivalent procedures have been used by others[4, 56].

2.3 Exemplary oxide surfaces

To illustrate the utility of the CR approximation, we shall present exact numerical solutions of the interaction forces on the PB level between different oxide surfaces. The charging behavior of these surfaces will be treated within a classical surface complexation model[54, 55, 62, 63]. We shall present a few results for symmetric systems but mostly focus on asymmetric systems. As we shall see, in the vast majority of the situations, the CR approximation is extremely accurate even down to contact.

Three oxide surfaces will be used to illustrate the rich behavior of the electrostatic forces, which may be encountered in asymmetric situations. The surfaces considered are rutile (TiO_2), goethite (FeOOH), and silica (SiO_2). The charging properties of the surfaces can be described by the 1-pK basic Stern model[54, 55]. The charging behavior will be modeled as originating from one surface group, namely, as

$$\begin{aligned} \text{Ti-OH}_2^{+1/2} &\rightleftharpoons \text{Ti-OH}^{-1/2} + \text{H}^+ \\ \text{Fe-OH}_2^{+1/2} &\rightleftharpoons \text{Fe-OH}^{-1/2} + \text{H}^+ \\ \text{Si-OH}_2 &\rightleftharpoons \text{Si-OH}^- + \text{H}^+ \end{aligned} \tag{2.17}$$

where we introduce for rutile and goethite the charge of +1/2 in the protonated state and -1/2 in the deprotonated state, while for the silica surface the silanol group is neutral when protonated and has a charge of -1 when deprotonated. Table 2-1 summarizes the relevant parameters used to describe these systems. In all three cases, this parametrization provides a rather accurate description of the overall charge of these oxides as determined by potentiometric titrations[54, 55]. As an alternative, various authors have used so-called 2-pK models, largely with equivalent results[62, 63]. Because of its simplicity, we focus on the 1-pK picture

Table 2-1. Parameters of the 1-pK basic Stern model for oxide surfaces

		pK	z	Γ (nm^{-2})	C^S (F/m^2)
Rutile	TiO_2	5.8	-1/2	12.2	1.33
Goethite	FeOOH	9.5	-1/2	6.15	1.10
Silica	SiO_2	7.5	-1	8.00	2.90

here. The charging behavior of these three surfaces as a function of pH and for different ionic strengths is summarized in Figure 2-2. The columns refer to different oxides, while the rows refer to different surface properties. The top row shows the surface charge density, the middle row the diffuse layer potential, and the last row the regulation parameter. Note that all these properties are evaluated for an isolated surface.

Rutile and goethite are classical examples of amphoteric oxides, which are positively charged at low pH and negatively charged at high pH. At one particular pH value, the surface is uncharged, and one refers to the PZC. When the surface charge density is plotted as a function of pH for different ionic strengths, the PZC is immediately recognized as the common crossing point. The surface charge density depends more strongly on the pH for high ionic strength, while for low ionic strength its dependence is weaker.

The diffuse layer potentials decrease with increasing pH from positive to negative values and vanish at the PZC. The magnitude of the diffuse layer potential decreases with increasing ionic strength, as a result of more pronounced screening. At the same time, charging of the surface is facilitated by screening of the interactions between the sites. The combination of these two effects explains why the surface charge density and the diffuse layer potential show the opposite trends with the ionic strength.

For amphoteric oxides, the regulation parameter exhibits a minimum as a function of pH at the PZC. This minimum becomes more pronounced with decreasing ionic strength. Because the inner layer capacitance varies little near the

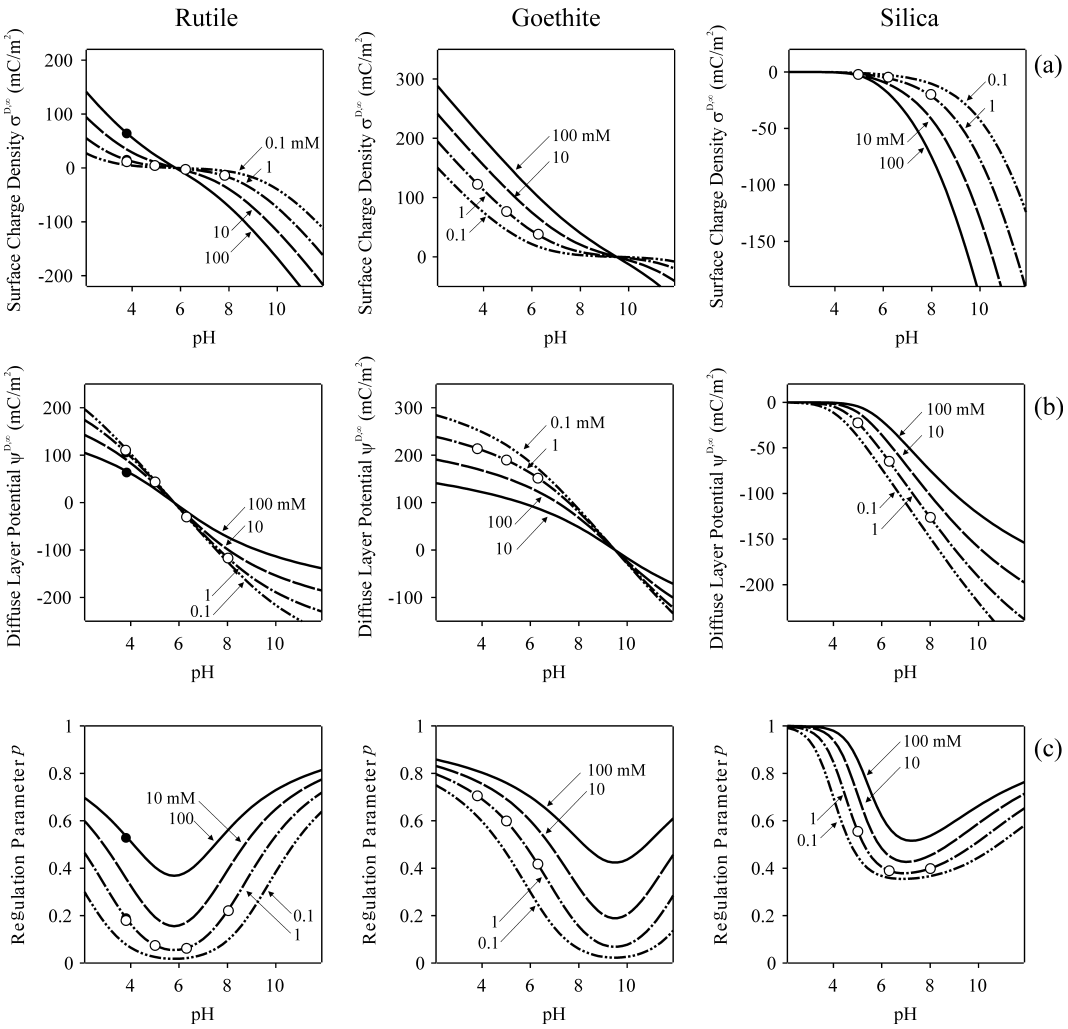

Figure 2-2. Charging behavior obtained from the basic Stern 1-pK model of three representative oxide surfaces, namely rutile, goethite and silica (from left to right). Various surface properties are represented for different ionic strengths as a function of pH. (a) Surface charge density $\sigma^{D,\infty}$, (b) diffuse layer potential $\psi^{D,\infty}$, and (c) regulation parameter p. The first two oxides show a PZC, while silica remains negative. The conditions used in the force calculations in symmetric (●) and asymmetric (○) cases are indicated.

PZC, this minimum reflects the dependence of the diffuse layer capacitance on the surface potential (cf. equation (2.9)). The latter is lowest for a weakly charged surface and increases strongly with increasing magnitude of the surface potential. Furthermore, the diffuse layer capacitance increases with increasing ionic strength. The regulation parameter follows, therefore, the same trends. Recall that $p = 1$ corresponds to the CC boundary condition, while $p = 0$ corresponds to CP.

We, thus, conclude that metal oxide surfaces near the PZC can be well approximated by CP boundary conditions, particularly at low ionic strengths. Further away from the PZC, however, their regulation behavior may be very different and eventually approaches CC conditions.

Silica behaves differently. The surface charge density vanishes at low pH and decreases with increasing pH. The behavior of the surface charge density and of the diffuse layer potential qualitatively resembles the discussed behavior of a metal oxide above the PZC. However, as a result of the low surface density of the charged groups at low pH, the surface charge density varies in this region only marginally. As a consequence, the diffuse layer capacitance also remains close to constant. The regulation parameter, thus, shows a minimum as a function of pH, but its values always remain relatively high. Therefore, silica will rather resemble CC conditions. At very low pH, the neutral silanol groups start to protonate, and silica acquires a weakly positive charge[54, 55]. However, this effect is negligible in the situations discussed here and, therefore, not considered.

The reason for the different behavior of the amphoteric oxide and silica surfaces at low charge densities originates from their different surface chemistries (see eq (2.17)). For the oxide surface, there is a large number of ionized groups, bearing either a positive (protonated group) or a negative charge (deprotonated group). The adsorption of protons to such a surface is easy, and its charge, thus, strongly depends on solution pH. For the silica surface, on the other hand, most sites are neutral (protonated group), and only very few are charged (deprotonated group). To charge up such a surface is more difficult, and its charge hardly depends on solution pH at low charge densities.

Within the CR approximation, each surface is characterized only by two basic parameters, namely, the diffuse layer potential $\psi^{D,\infty}$ and the regulation parameter p. Both parameters are properties of a *single* isolated surface and only depend on the solution composition (e.g., salt concentration, pH). Once these parameters are known, the properties of *two* interacting surfaces can be calculated. This idea simplifies the description of interacting surfaces enormously, be it in symmetric or

asymmetric situations. In the latter case, the two basic parameters must be specified for each individual surface and will be of course different.

While the evaluation of the complete charge-potential relationship for the surface is somewhat tedious in the present examples, it is nevertheless straightforward. Charge-potential relationships can be also obtained from more complicated models of the surface dissociation behavior. In many situations, however, models of the surface dissociation behavior are not available, and the charge-potential relationship cannot be evaluated. In such situations, the regulation behavior cannot be treated rigorously. However, the regulation behavior can still be discussed within the CR approximation for such a surface.

2.4 Forces in symmetric systems

Let us first demonstrate the usefulness of the CR approximation in symmetric systems. We shall consider two cases, one at low ionic strength, where we expect a behavior resembling CP, and the other one at higher ionic strength resembling CC.

To be specific, let us focus on the interaction between two identical rutile surfaces at pH 3.8 and an ionic strength of 1 mM. The results are shown in the left column of Figure 2-3. The corresponding surface charge densities, diffuse layer potentials, and regulation parameters for the isolated surface are summarized in Table 2-2 and indicated in Figure 2-2 with markers.

Consider first the variation of the surface charge density and of the diffuse layer potential upon approach (see left column of Figure 2-3a and b). One observes that the charge density decreases substantially, while the potential increases only marginally. At contact, the charge density vanishes, and the surface potential attains a value of 118 mV, which is close to the value of 111 mV for the isolated surface. The behavior is indeed not too different from the CP conditions, which is also indicated by the low value of the regulation parameter $p = 0.191$. When this parameter is used in the CR boundary condition, the results for the charge density and the potential are indistinguishable on the scale of the graph

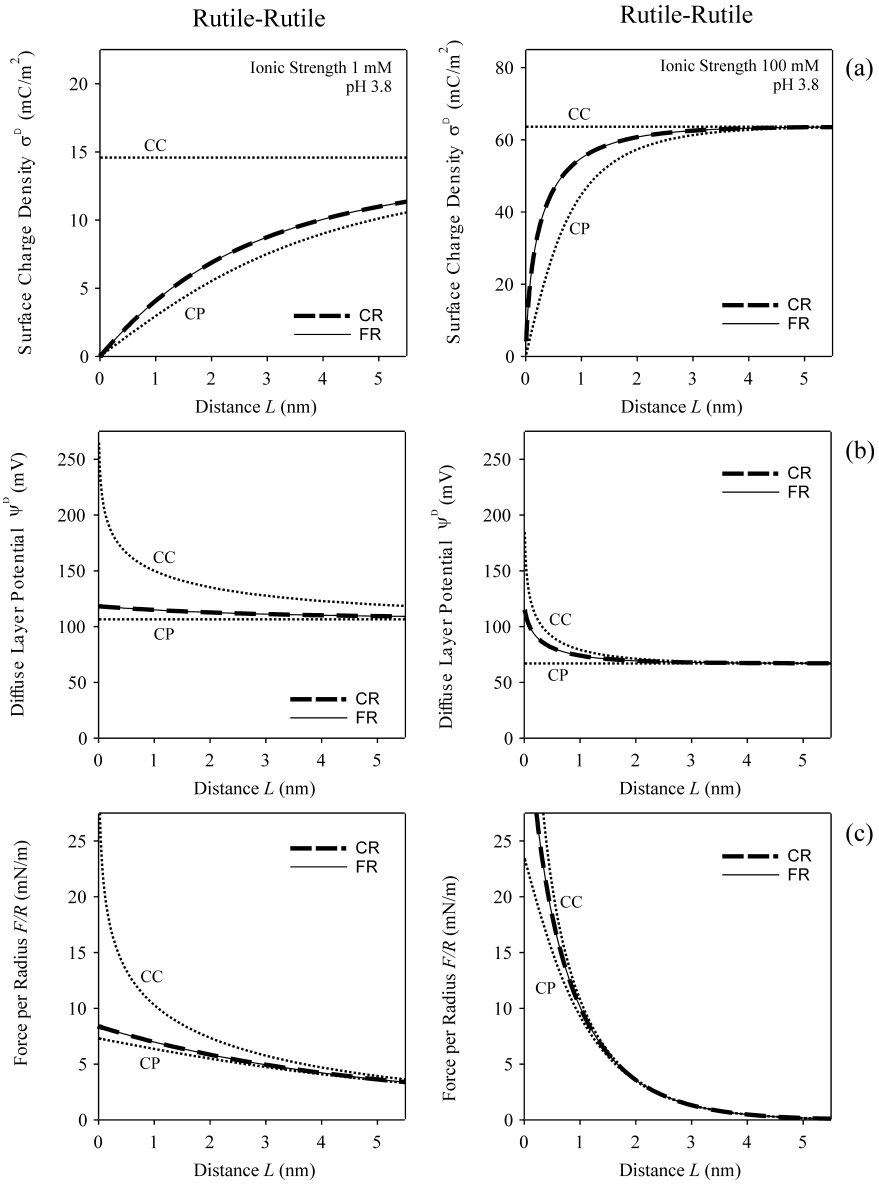

Figure 2-3. Interaction of two rutile surfaces as a function of separation at pH 3.8 and ionic strengths of 1 mM (left column) and 100 mM (right column). Results of the full regulation (FR) calculations are compared with those of the CR approximation. The limits of CC and CP are indicated. For this symmetric system we show (a) surface charge density, (b) diffuse layer potential, and (c) force per unit curvature radius.

from the results obtained by the full regulation calculation. The latter uses the above-described basic Stern model. The interaction forces are repulsive and governed by double layer overlap (see left column of Figure 2-3c). The CR approximation yields basically an identical result as the full regulation calculation.

Table 2-2. Diffuse layer potentials and regulation parameters for the systems considered[a]

	Figure	pH[a]	$\psi_1^{D,\infty}$ (mV)	p_1	$\psi_2^{D,\infty}$ (mV)	p_2
Rutile-rutile	2-3(left)	3.8	+106	0.191	+106	0.191
	2-3(right) [b]	3.8	+67.0	0.536	+67.0	0.536
Rutile-goethite	2-4a	3.8	+106	0.191	+214	0.706
	2-4b	5.0	+44.4	0.075	+190	0.598
	2-4c	6.3	-27.8	0.063	+152	0.418
Rutile-silica	2-5a	5.0	+44.4	0.075	-22.3	0.556
	2-5b	6.3	-27.8	0.063	-64.5	0.390
	2-5c	8.0	-116	0.220	-126	0.399

[a]Ionic strength is 1 mM, except in case *b* where it is 100 mM.

The resulting force is relatively close to the result for CP boundary conditions and far away from the CC case.

The right column of Figure 2-3 illustrates the analogous results at an ionic strength of 100 mM. The relevant parameters are summarized in Table 2-2. The regulation parameter p = 0.536 is situated closer to the CC condition. With decreasing distance, one observes that the charge density remains relatively constant at larger distances but decreases rapidly near contact. At the same time, the surface potential increases substantially. At contact, the surfaces are neutral and attain a potential of 115 mV, while for the isolated surface one has 67 mV. This pronounced change in the surface potential leads to a force that lies closer to the CC condition. The distance dependence is again accurately captured by the CR approximation.

To conclude our discussion on the symmetric system, let us compare the results with a superposition approximation for the regulating case suggested earlier[51]. These authors have proposed to approximate the force in the regulating case by a linear superposition of the CP and CC force obtained from the PB equation weighted with the regulation parameter p. This result is asymptotically exact on the PB level for large distances and coincides with the CR approximation

in this regime. On the other hand, the superposition approximation fails near contact, while the CR approximation can be exact in this regime, provided that the charging curve of the inner layer is a linear function of the potential. Thus, the present CR approximation is similar in spirit to the superposition approximation but more accurate in practice. The computational effort is the same in both cases.

2.5 Forces in asymmetric systems

The main advantage of the CR boundary condition consists of the simplicity it offers to treat asymmetric systems. While effects of charge regulation are much more important in asymmetric than in symmetric systems, the only way to describe these systems so far was to explicitly include all relevant chemical equilibria on both surfaces[53, 56, 64]. Needless to say, such calculations are cumbersome and highly model-dependent. Moreover, an equilibrium model for the surface is not available in many situations.

The CR condition packs the entire surface chemistry into two parameters, namely, the diffuse layer potential and the regulation parameter. For an asymmetric system, one naturally has to consider these two parameters for each surface, thus, dealing with four parameters $\psi_1^{D,\infty}$ and p^1 for surface 1 and $\psi_2^{D,\infty}$ and p_2 for surface 2. The CR condition represents a natural extension of the existing charge regulation treatment on the linearized Debye-Hückel level[60] to the nonlinear PB regime. For low surface potentials, both approaches coincide.

As the first asymmetric example, let us consider the forces between a rutile and a goethite surface at an ionic strength of 1 mM as a function of pH. Note that the PZC of rutile lies below the PZC of goethite. For this reason, the forces at large distances will be repulsive at low pH, attractive at intermediate pH, and again repulsive at high pH. Figure 2-4 summarizes some of the important cases in the transition from the repulsive to the attractive regime. Because this transition is somewhat complex, let us first discuss the dependence of the forces and then the quality of the CR approximation.

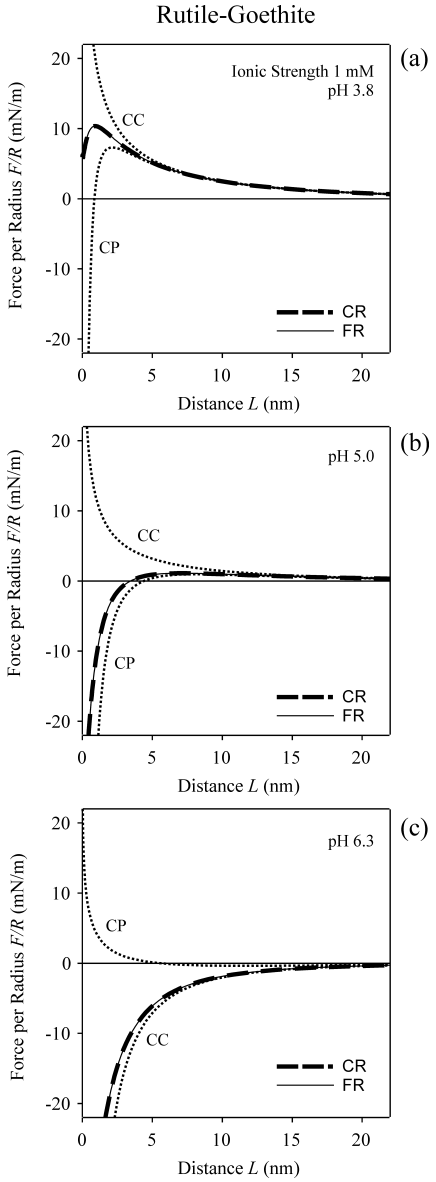

Figure 2-4. Interaction of a rutile and an iron oxide surface as a function of separation at an ionic strength of 1 mM. Results of the full regulation (FR) calculation are compared with those of the CR approximation. The limits of CC and CP are indicated. For this asymmetric system we show the force per unit curvature radius for pH values of (a) 3.8, (b) 5.0, and (c) 6.3

At very low pH, both surfaces are highly charged, strongly repulsive, and resemble the behavior in the symmetric system. With increasing pH, the force becomes progressively attractive near contact, and the force profile develops a characteristic maximum. Such a situation is encountered at pH 3.8 (see Figure 2-

4a). The force is repulsive at large distances but decreases at small distances. This behavior differs strongly from the fully repulsive CC case but resembles the CP case, where a maximum in the force is observed at larger separations. Upon approach, the highly charged goethite surface maintains its surface charge and surface potential, but the surface charge of rutile becomes negative, while the surface potential remains positive. This charge reversal is the origin of the weaker repulsion near contact.

With increasing pH, the force at small separations decreases continuously and eventually becomes attractive. For example, this situation occurs at pH 5.0 (see Figure 2-4b). Because both surfaces are still positively charged, the force remains repulsive at large separations. At smaller separations, the force becomes attractive as a result of a similar charge reversal mechanism as discussed above. At this point, however, the surface potential of the goethite surface decreases upon approach, while its surface charge increases.

With further increase of the pH, rutile goes through the PZC, and its charge becomes negative. This surface will be attracted to a positively charged iron oxide surface. This case is encountered at pH 6.3 (see Figure 2-4c). The attraction persists down to contact, and the behavior starts to resemble the CC case. Increasing the pH further, the forces become repulsive along a similar scenario. In any case, the CR approximates the results based on full regulation extremely well.
As a second example of an asymmetric system, consider the interaction forces between rutile and silica, again at an ionic strength of 1 mM. In contrast to the previous situation, silica always remains negative, which means that the forces at large distances will be attractive at low pH and repulsive at high pH. Figure 2-5 summarizes the results. Again, we first discuss the dependence of the forces and then discuss the quality of the CR approximation. At low pH, the silica surface is neutral, which leads to weak interaction forces and strong charge regulation effects. This situation is encountered at pH 5.0 (see Figure 2-5a). One observes a weak attractive force, which lies between the CP and the CC cases. The rutile surface behaves similarly to a CP surface, while the surface charge of the silica surface decreases and its potential increases and becomes positive. At higher pH,

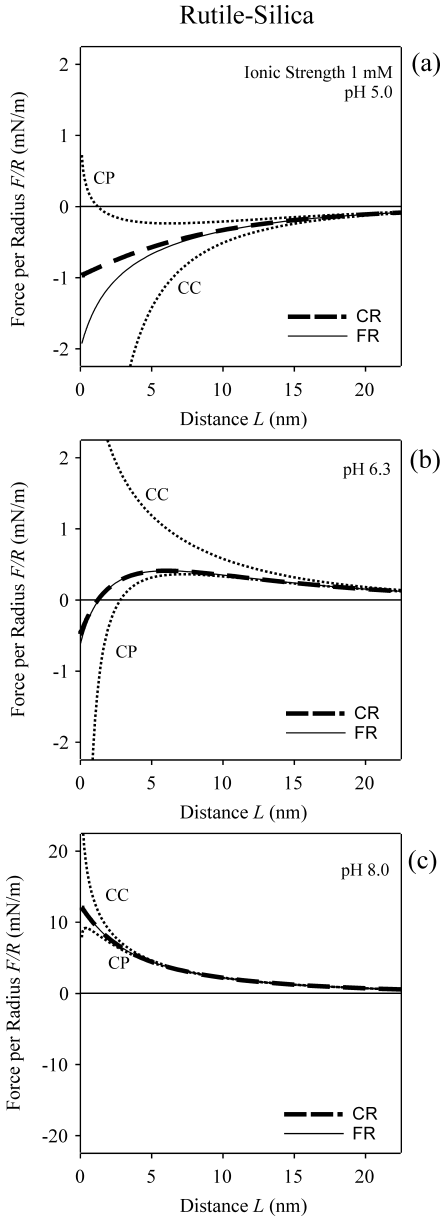

Figure 2-5. Interaction of a rutile and a silicon oxide surface as a function of separation at an ionic strength of 1 mM. Results of the full regulation (FR) calculation are compared with those of the CR approximation. The limits of CC and CP are indicated. For this asymmetric system we show the force per unit curvature radius for pH values of (a) 5.0, (b) 6.3, and (c) 8.0

the surface charge of rutile changes its sign and the force becomes repulsive at large distances. One finds this case at pH 6.3 (see Figure 2-5b). Because of regulation effects, however, the force becomes attractive close to contact. With decreasing separation, the surface charge of rutile increases, while the surface

potential decreases. The surface charge of silica increases at first but starts to decrease at shorter distances. This nonmonotonic behavior leads to the attractive force at smaller separations. At even higher pH values, negative charge builds up on both surfaces, and the system again resembles the symmetric case. This situation is found at pH 8 (see Figure 2-5c). The CR approximation works again very well, but with one important exception. As can be seen in Figure 2-5a, the results for full regulation are in substantial disagreement with the CR approximation near contact. This possibility was already invoked above (see Figure 2-1b). The intrinsic surface charge density of silica vanishes asymptotically with increasing diffuse layer potential, and the approximation of this function by a straight line is insufficient near contact. At larger distances, the CR approximation works well, as it should.

At higher pH, on the other hand, the CR approximation is accurate again despite the strongly nonlinear character of the charge-potential relationship for the surface. We, therefore, suspect, that situations where the CR approximation fails are infrequent, and the gain in simplicity largely outweighs this minor disadvantage.

2.6 Conclusion

The CR approximation provides an accurate description of the interaction forces of ionizable surfaces across an electrolyte solution on the PB level. The spirit of the approximation is to linearize the charge-potential relationship of the surface around the potential of the isolated surface but otherwise to solve the PB equation for the diffuse layer exactly. This approximation eliminates the need to treat the interacting surfaces simultaneously with the chemical adsorption equilibria of charged species to each surface. In fact, no mathematical model for the ionization of the surface is necessary, and the entire chemical response of the surface is expressed in terms of two parameters, namely, the diffuse layer potential $\psi^{D,\infty}$ and the regulation parameter p. Both parameters refer to an isolated surface only and,

thus, can also be obtained from classical surface equilibrium models or by probing the interfaces by surface-sensitive techniques (i.e., electrokinetic measurements). The classical boundary condition of CP corresponds to $p = 0$ and that of CC corresponds to $p = 1$. In the general case, the regulation parameter p typically assumes values in between. This parameter can be related to two capacitances, the diffuse layer capacitance C^D and the inner layer capacitance C^I (cf. eq (2.12)). When the inner layer charge remains constant, the inner layer capacitance is larger than the diffuse layer capacitance, and the surface behaves CC-like ($p = 1$). When the inner layer charge can be easily regulated by adsorption of charged species, the inner capacitance is small, and the surface behaves CP-like ($p = 0$). The diffuse layer capacitance increases with increasing magnitude of the surface potential and with increasing ionic strength. As a consequence, the regulation parameter will show a similar dependence.

The CR approximation represents a natural generalization of the linearized theory of Carnie and Chan[60]. The latter theory is based on the linear Debye-Hückel equation and is, thus, of rather limited validity in practice. By treating the PB equation exactly and linearizing the charge-potential relationship around the state of the isolated surface, we retain the simplicity of the Carnie and Chan approach[60] but are able to substantially extend its range of validity. Based on our experience so far, the approximation is excellent in most practical situations even at small separations, in symmetric as well as in asymmetric systems. Several successful examples have been presented here.

In some cases, however, the CR approximation might become poor at small separations. One important case concerns a nearly neutral surface, to which only traces of the charge-determining ions are adsorbed. In this situation, the charging curve of the inner layer approaches asymptotically 0 for high potentials, and the CR approximation might produce unsatisfactory results near contact. Nevertheless, we suspect that these situations are probably of minor importance in practice, and for this reason we expect that the CR approximation will provide a most useful framework to discuss electrostatic interactions between charged surfaces.

Chapter 3
Interactions between homogeneous polyelectrolyte surfaces

3.1 Introduction

Poly(ethylene imine) (PEI) is a cationic branched weak polyelectrolyte (see Figure 3-1), which strongly adsorbs on negatively charged surfaces, and thereby leads to their charge reversal. It is used in a wide variety of industrial applications, for example, as stabilizer of colloidal slurries, as flocculant in water purification, or as retention aid in papermaking [8, 65, 66]. Besides these classical applications, PEI has gained importance in the design of flat or spherical polyelectrolyte multilayers[39, 67-69]. Their permeability and surface functionality can be controlled by judicious choice of their building blocks, and such systems are therefore becoming interesting for drug delivery, cosmetics, or in-situ sensing[68, 70]. Multilayers are prepared by alternating adsorption of two of oppositely charged polyelectrolytes on a suitable substrate, whereby PEI is often used as the precursor layer[39, 69]. In between the adsorption steps, the substrate is washed in a polyelectrolyte-free solution, and thus such pre-adsorbed polyelectrolyte films are no longer in contact with a bulk solution of the polyelectrolyte in question. This situation is different to many of the applications mentioned above, where the surface is always in contact with a polyelectrolyte solution.

The adsorption of PEI to water-solid interfaces has been examined by adsorption experiments[66, 71], electrokinetic methods[41, 72], or optical reflectometry[73, 74]. Besides these classical techniques, direct force measurements with the surface force apparatus (SFA) or the atomic force microscope (AFM) have substantially

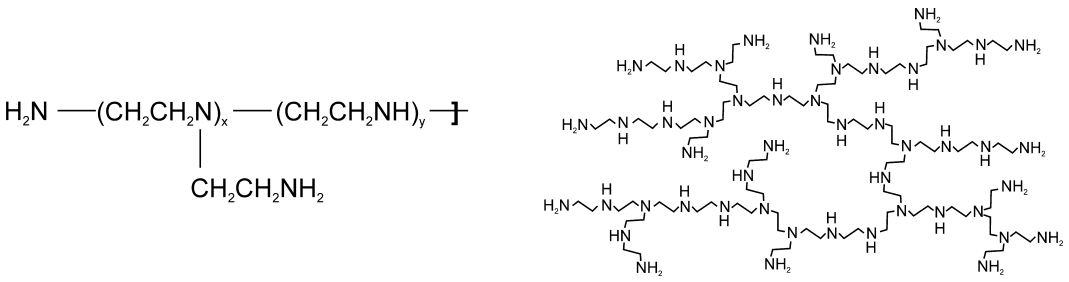

Figure 3-1. (Left) Semi-developed chemical formula of the monomer of highly branched poly(ethylenimine) (PEI), and representation of its random branched structure (right).

contributed to our understanding of the interactions between adsorbed polyelectrolyte films[5, 74-76]. Interaction forces between mica or glass surfaces in PEI solutions have been systematically examined with the SFA or its non-interferometric counterpart, which is commonly referred to as MASIF (i.e., measurement and analysis of surface interaction forces)[75, 76]. These studies conclude that adsorbed PEI leads to long-range electrostatic interactions, whose magnitude increases with increasing PEI concentration[75]. The pull-off forces decrease with increasing PEI concentration and thus follow an opposite trend to the long-range forces[76]. Pre-adsorbed films of PEI were investigated in lesser detail, primarily with respect to polyelectrolyte multilayer build-up[39, 77], or as base for the covalent coupling with further polymers[74].

In this chapter, we use the colloidal probe technique to measure the interaction forces between pre-adsorbed PEI layers on quartz. Due to the use of an AFM-cantilever with a low spring constant, the colloidal probe technique is also sensitive to the bridging of single polymers during the separation of probe and sample[32, 38, 78, 79]. Thus, this technique is ideally suited to study the long-range interactions as well as the adhesion forces between adsorbed polyelectrolyte layers.

The adsorption conditions of the PEI layers were chosen to mimic the PEI-precursor layer used for the preparation of polyelectrolyte multilayers[69, 80-82]. With respect to long-range interaction forces, we studied the charge regulation of the

weak polyelectrolyte PEI layers for the first time, and examined the effect of the molecular mass. The bridging adhesion between pre-coated PEI layers was measured for different ionic strengths, and examined on the level of single detachment events.

3.2 Experimental section

a) Pre-adsorbed layers and AFM imaging

Fractions of highly branched poly(ethylene imine) (PEI) with molecular masses of approximately 2, 30, 300, and 5000 kDa were used. The first one was purchased from Sigma-Aldrich, and all other PEI fractions were isolated in the BASF laboratories (Ludwigshafen, Germany). The aqueous solutions of 33% to 50% weight percent of the polymers were used without further purification. The degree of ionization of PEI is about 70-80% at pH 4 in aqueous solution[83]. All solutions were prepared with Milli-Q grade water (Millipore).

Polished quartz plates (Schott SA, Switzerland) were used as substrates for PEI adsorption in order to mimic the surface of the silica spheres used as colloidal probes. The substrates were initially treated with 65% nitric acid at 95°C, subsequently with in a 1:4 hot mixture of H_2O_2 (35%) and H_2SO_4, and finally rinsed extensively with Milli-Q water. Pre-adsorbed PEI layers were prepared by immersing the substrates in a PEI solution with a concentration of 200 mg/L at pH 9.5 and a KCl concentration of 0.1 M during 12 hours at room temperature (high salt conditions). For comparison, the PEI layers were prepared in a PEI solution of the same concentration at pH 9.8 without any added salt (low salt conditions). Afterwards, the surfaces were thoroughly rinsed with Milli-Q water.

The bare quartz substrates or the pre-adsorbed layers were imaged in dry state with a Nanoscope IIIa AFM (Veeco) in the tapping mode. Better resolution for AFM imaging was obtained when naturally oxidized silicon wafers (Silchem, Freiburg, Germany) were used as substrates. The wafers were cleaned with the RCA method, which consists of incubating the wafer in a 1:1:5 mixture of hydrogen peroxide (35%), ammonia (25%), and water at 75°C for 10 min[84].

b) Direct force measurements

The colloidal probe technique was used for the force measurements with a closed-loop AFM (MFP-3D, Asylum Research, Santa Barbara, CA). Colloidal probes were prepared with colloidal silica particles (Bangs Laboratories) with a diameter in the range of 6-7 μm. Their actual diameters were determined with optical microscopy to an accuracy of about 0.3 μm. The particles were attached to the end of a tip-less AFM-cantilever (CSC 12, μ-masch, Estonia) with UV-curable glue (NO 63, Norland Adhesives) utilizing a dedicated micromanipulator (Märzhäuser, Germany). The glue was cured by illuminating the probe with the mercury lamp in the optical microscope for about one minute. The spring constants of the AFM-cantilevers were determined by analyzing their thermal fluctuations in air[22, 85]. The results were compared with values obtained from the procedure proposed by Sader *et al*.[86], which uses the frequency response of the cantilever, its top-view geometrical dimensions, and the properties of the surrounding medium. Both methods are described in more detail in section 1.3a). The results deviated by less than 25% in all cases.

Prior to the adsorption experiments, the colloidal probes and the quartz substrates were cleaned in air-plasma at 35 W for 5 min (Harrick Scientific, NY). The substrates were fixed with the UV-curable glue to the bottom of petri dishes, which served as open AFM fluid cells. The pre-adsorbed PEI films on the substrates and the probes were prepared as described in the previous section. The petri dish was subsequently filled with a KCl solution of desired ionic strength, which was previously adjusted to pH 4 with dilute HCl. The pH was checked before and after each measurement with a microelectrode. The force curves were acquired at a cycling frequency of 0.3 Hz resulting in approach and retraction velocities of 0.2-0.6 μm/s. Force distance curves were measured at three different positions on the substrate, and 50 force curves were measured for each position. All measurements were carried out at room temperature of 23±2 °C.

The approximate symmetry of the system consisting of a colloidal silica particle and a quartz substrate in respect to the electrostatic interactions was

verified by yet unpublished force measurements in the sphere-sphere geometry. For this purpose, a colloidal silica sphere was glued to a solid substrate, while another silica sphere was used as colloidal probe. These measurements were compared with the ones obtained on a quartz surface and were found to be equal for the bare surfaces within experimental error. We conclude from these measurements that also the PEI-covered surfaces are approximately symmetric in respect to their electrostatic interactions.

c) Force data analysis

Force versus distance curves were calculated from of the cantilever deflection and the piezo crystal displacement. The force F was determined from the deflection and the spring constant with a sensitivity of about 20 pN. The separation distance D is obtained from the displacement of the piezo-crystal and by determining the zero separation from a linear fit of the constant compliance region. In the present case, this point can be determined with an accuracy of about 0.5 nm, since the pre-adsorbed polyelectrolyte layers are sufficiently thin and become incompressible under load. Further details on this technique can be found in literature[87, 88].

The interaction forces upon approach were obtained by averaging about 50 force curves measured at the same location, and normalized by the probe radius R. Derjaguin approximation suggests that the resulting normalized force F/R is proportional to the free energy of interaction per unit area[4]. The force versus distance profiles were fitted to the full numerical solution of the Poisson-Boltzmann equation for CC, CP and CR boundary conditions (see Chapter 2), for two symmetric plates for distances above $\kappa^{-1}/2$ for ionic strengths <10 mM and κ^{-1} for ≥ 10 mM. When the parameters entering the CR model are determined in this fashion, one can accurately predict the force at smaller distances down to a few nanometers.

The surface charge was assumed to be localized in a plane positioned at zero separation as obtained from the constant compliance region, whereby the extension of the polymer layer was not taken into account[89]. In general, van der Waals forces were not taken into account, except for comparison. In the latter

case, the plane of origin of the van der Waals force was displaced by a distance d, whereby $d > 0$ corresponds to a shift towards the solid substrate.

Molecular adhesion events were identified from the retraction force curves by an automated procedure based on an algorithm for the detection of local minima in the force profile[90]. In order to classify a minimum in the force as an adhesion event, the slope within the jump-off instability had to agree with the spring constant of the cantilever within 50%, and the magnitude of the force prior to the jump-off had to exceed the noise in the non-contact region by a factor of 5. The work of adhesion was evaluated from the area between approach and redraw parts, the force curves were smoothed with piece-wise parabolic fits and integrated with the trapezoidal rule.

3.3 Results and discussion

Direct force measurements between pre-adsorbed layers of branched poly(ethylene imine) (PEI) on silica substrates were carried out in KCl solutions at pH 4 with the colloidal probe technique. The influence of salt concentration and molecular mass of PEI on the interaction forces was investigated in detail. The PEI layers were adsorbed at pH 9.5-9.8 at a concentration of 200 mg/L and two different salt concentrations, in order to mimic conditions for the preparation of pre-cursor layers for multilayers[69, 80-82]. In the following, we shall focus on PEI layers adsorbed at high salt conditions. For the low salt adsorption conditions, similar results were obtained.

The surface topography of the pre-adsorbed PEI layers is shown in Figure 3-2. The layers are relatively uniform and homogeneous. The quartz substrates show few scratches and irregularities, and the flat parts of the surface are relatively rough with a root mean square (RMS) roughness of about 0.3 nm (Figure 3-2a). Even the PEI of high molecular mass (5000 kDa) cannot be reliably identified on such substrates, and upon its adsorption the roughness of the substrates remains basically unchanged (Figure 3-2b). For this reason, we have imaged the pre-adsorbed PEI layers on oxidized silicon wafers, which were much more smooth

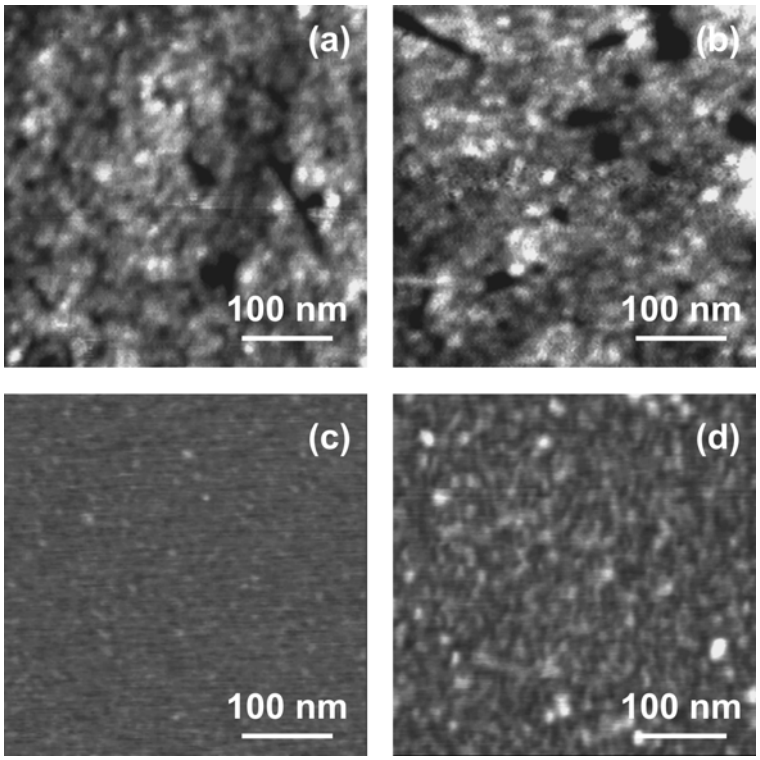

Figure 3-2. Surface topography for pre-coated poly(ethylene imine) (PEI) films by tapping mode AFM. (a) Bare quartz substrate and (b) 5 MDa PEI on quartz. Oxidized silicon wafers with pre-adsorbed PEI of (c) 2 kDa and (d) 5 MDa.

over large areas with RMS roughness of 0.16 nm. Adsorbed PEI of low molecular mass (2 kDa) forms very homogeneous layers with RMS roughness of 0.06 nm (Figure 3-2c). The fact that this roughness is smaller than the roughness of the bare silicon wafers suggests that the PEI adsorbs in the dints on the surface, and thereby flattens the substrate. For the adsorbed PEI of the high molecular mass (5000 kDa), the RMS roughness increases to 0.15 nm and becomes comparable to the roughness of the bare substrate (Figure 3-2d). The characteristic length scale of the lateral surface heterogeneities is on the order 20-50 nm. These heterogeneities probably correspond to individual adsorbed PEI molecules, which show almost a closed packed structure on the surface, but leaving small patches of uncovered substrate in between. The lateral extent of individual PEI molecules with a molecular mass of 1000 kDa adsorbed on mica was reported around 60 nm

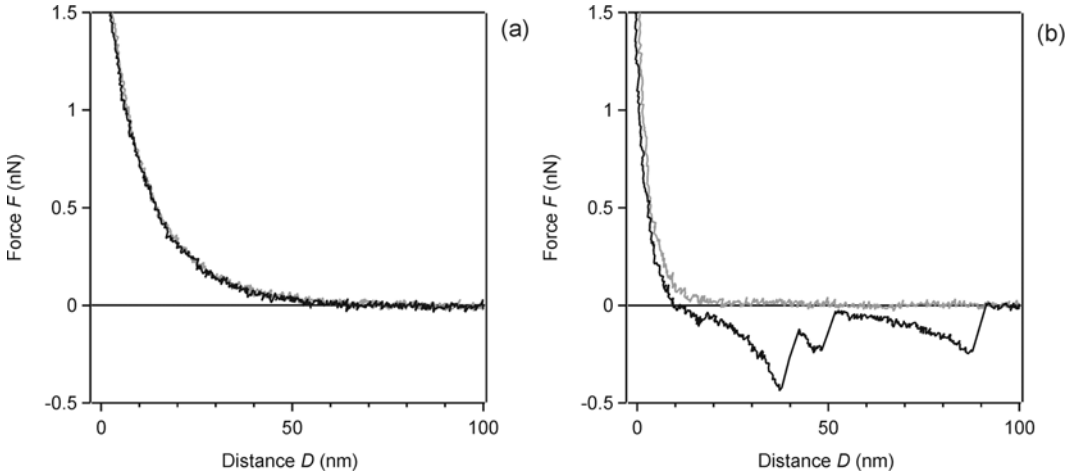

Figure 3-3. Representative force profiles between colloidal silica probe and quartz substrate with pre-adsorbed layers of 5000 kDa PEI prepared at high salt adsorption conditions. The approach (grey) and retraction (black) force curves were measured at pH 4 and different ionic strengths in KCl. (a) Reversible force curve at 1 mM, and (b) molecular adhesion events upon retraction at 100 mM.

with an average height of mere 1.5 nm[91]. The reported flat pancake-like structure of adsorbed PEI results primarily from the strong electrostatic attraction between the positively charged polyelectrolyte and the negatively charged substrate. A similar adsorption mechanism is likely to be operational in the present situation, and will result pre-adsorbed layers, which correspond to monolayers with a thickness of few nanometers only.

The relevant features of the interaction forces between such pre-adsorbed PEI layers are summarized in Figure 3-3. In order to ensure a symmetric system, the measurements were carried out with a silica probe against a quartz surface. For all conditions investigated, the forces between the surfaces are repulsive upon approach. At low ionic strengths, these forces are long-ranged and always repulsive, upon approach as well as upon retract (Figure 3-3a). At higher ionic strengths, the repulsive part is shorter ranged, and upon retraction one frequently observes molecular adhesion events (Figure 3-3b). The erratic adhesion events occur due to bridging of PEI molecules at contact and their subsequent pulling upon retraction. Due to the branched architecture of the PEI, however, they cannot

be easily decomposed into contributions from individual molecules. In the following, we shall first quantitatively analyze the repulsive forces, and later discuss the nature of the molecular adhesion events along with a statistical analysis.

We found no difference between forces measured for freshly prepared substrates and for substrates, which were stored in a solution of pH 4 for several hours. These findings confirm the good stability of pre-adsorbed PEI films in contact with electrolyte solutions, and they are in full accord with similar conclusions based on optical reflectivity[73].

a) Repulsive forces upon approach

The repulsive force profiles measured upon approach can be quantitatively interpreted in terms of interactions between charged surfaces across an electrolyte solution. The experimental force data, which were normalized to the probe radius, were interpreted in terms of the exact solution of the non-linear Poisson-Boltzmann (PB) equation for interacting, symmetric plates, including constant charge (CC), constant potential (CP), and constant regulation (CR) boundary conditions, which were already described in Chapter 2. All three solutions coincide at larger distances. In this region, they only depend on the diffuse layer potential ψ_d and the Debye length

$$\kappa^{-1} = \sqrt{\frac{\varepsilon\varepsilon_0 k_B T}{2 N_A e^2 I}} \tag{3.1}$$

where $\varepsilon\varepsilon_0$ the total permittivity of water, $k_B T$ the thermal energy, N_A the Avogadro's number, e the elementary charge, and I the ionic strength of the solution. At shorter distances, boundary conditions on the surface become important, since the surface charge may regulate upon approach due to adsorption of charged species (e.g., protons, salt ions). The simplest way to consider this effect is the constant regulation (CR) boundary condition, which is explained in detail in Chapter 2. This approximation stipulates a linear response of the surface charge to the diffuse layer potential, and characterizes the ability of the surface to

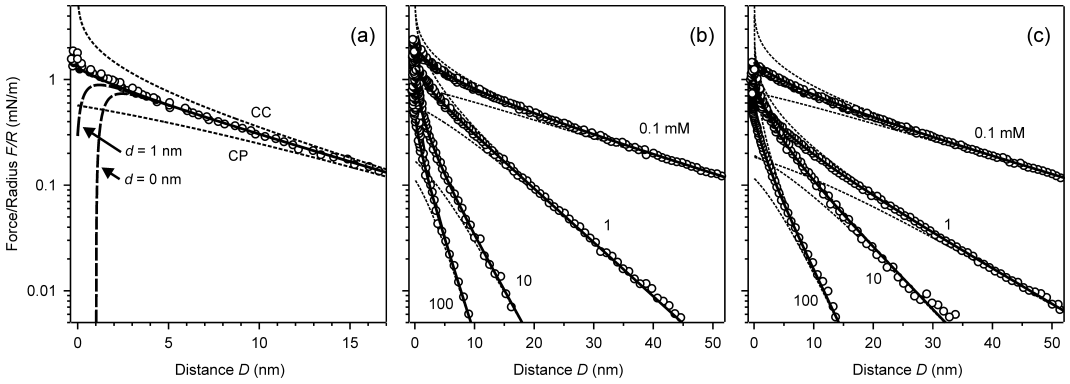

Figure 3-4. Force profiles measured upon approach between pre-adsorbed PEI layers on silica prepared at high salt conditions and measured at pH 4 and different ionic strengths. Lines are best fits with the PB model with constant charge (CC, dotted curve top), constant potential (CP, dotted curve bottom), and constant regulation (CR, solid line). (a) Detail of the force profile for 2 kDa PEI at 1 mM whereby the effect of the van der Waals force and relative shift of the planes of origin *d* are shown (dashed). Force profiles at different ionic strengths with PEI of molecular mass (b) 2 kDa and (c) 5000 kDa.

regulate its charge by introducing a regulation parameter p. For a surface that does not modify its charge (CC), we have $p = 1$, while for a surface that regulates its charge easily (CP), we have $p = 0$. For a realistic surface, the regulation parameter p usually lies in between these two limits.

Let us first discuss the interpretation of a typical force-distance curve in terms of the PB model without considering van der Waals forces. The latter will be shown to be negligible in the next paragraph. Figure 3-4a compares illustrative experimental data points measured at an ionic strength of 1 mM for 2 kDa PEI with model calculations. The employed PB model assumes that the point of contact between the surfaces coincides with the plane of origin of the electrostatic force. While neither CC nor CP conditions are capable of describing the experimental data correctly, the CR model fits the data very well almost down to contact. The fitted parameters extracted from the data are the Debye length κ^{-1} = 8.7 nm, the diffuse layer potential ψ_d = 32 mV, and the regulation parameter p = 0.69. These parameters are also summarized in Table 3-1. Based on the ionic strength of 1 mM, the expected Debye length is 9.6 nm, which is reasonably close

Table 3-1. Poisson-Boltzmann (PB) Model Parameters Obtained from Direct Force Measurements at pH 4

Molecular Mass (kDa)	Ionic Strength I (mM)	Debye Length κ^{-1} (nm)		Diffuse Layer Potential ψ_d (mV)		Regulation Parameter p	
		high[a]	low[b]	high[a]	low[b]	high[a]	low[b]
2	0.1	22.1[d]	24.6	58.2[d]	72.4	0.69[d]	0.63
	1	8.7[c,d]	9.0	31.6[c,d]	27.9	0.69[c,d]	0.67
	10	4.3[d]	3.5	15.2[d]	18.9	0.76[d]	-
	100	2.9[d]	-	7.4[d]	-	0.78[d]	-
30	0.1	-	34.1	-	83.0	-	0.76
	1	8.7	9.6	23.2	24.0	0.72	0.78
	10	5.1	5.9	13.2	12.6	0.77	0.85
	100	2.0	-	6.9	-	0.71	-
300	0.1	-	26.6	-	66.8	-	0.67
	1	10.9	8.6	30.3	24.7	0.84	0.69
	10	5.8	4.8	25.5	13.0	0.60	0.72
	100	1.5	-	9.1	-	0.42	-
5000	0.1	23.5[e]	25.8	58.7[e]	101.9	0.58[e]	0.42
	1	13.5[e]	9.0	24.7[e]	41.1	0.79[e]	0.65
	10	7.0[e]	4.2	17.9[e]	16.9	0.79[e]	0.86
	100	3.6[e]	-	10.7[e]	-	0.64[e]	-

[a]High salt (100 mM at pH 9.5) and [b]low salt (no salt added at pH 9.8) adsorption conditions for PEI. [c]Figure 3-4a, [d]Figure 3-4b, and [e]Figure 3-4c show the corresponding curves.

to the decay length extracted from the fit. These values were obtained from a fit at larger distances (see Experimental Section). Fits over the whole distance range lead to very similar parameters.

The existence of very short-ranged repulsion and the absence of jump-in instabilities indicate that short-ranged electro-steric repulsion overrides the attractive van der Waals forces. Similar trends were already reported for interactions between adsorbed PEI layers as measured by MASIF or the colloidal probe technique[39, 74, 76]. Figure 3-4a shows clearly that the experimental data are inconsistent with the assumption that the planes of origin for the van der Waals force and of the diffuse layer coincide ($d = 0$). We have used a Hamaker constant of 8.3×10^{-21} J as appropriate for quartz[4], and neglected the contribution of the polymer layer. Agreement with the experimental force profiles can be obtained by

displacing the plane of origin of the van der Waals force towards the solid substrate by at least 1 nm ($d > 0$, Figure 3-4a). This shift can be interpreted in terms of the finite thickness of the polymer layer, which gives only a negligible contribution to the van der Waals force. The Hamaker constant of the layer will be close to the one of water, since the water content of the layer is relatively high. For these reasons, neither van der Waals forces nor electro-steric forces were taken into account in the data analysis.

The results of the force measurements between pre-adsorbed layers prepared at high salt with PEI of low and high molecular mass are summarized in Figure 3-4b and c for different ionic strengths. The force versus distance curve can be well described by the solutions of the PB equation with CR boundary conditions, and deviations from this model are only observable for very small separation distances below approximately 2 nm. For the two extreme molecular masses there are no significant differences between these results. The fitted parameters are summarized in Table 3-1 and Figure 3-5, along with very similar results from the pre-adsorbed layers prepared at low salt. We did not find significant differences for the interaction forces between pre-adsorbed layers when the pure electrolyte solution (1 mM KCl, pH4) was replaced by solution of the same background electrolyte concentration and pH but contained additionally 50 mg/L PEI (30 kDa).

Figure 3-5a shows that the fitted Debye lengths are always in good agreement with the ones expected from the ionic strength of the solution at sufficiently low ionic strengths (equation (3.1)). Disagreement is observed at high ionic strength, whereby deviations are noticeable at 10 mM, and they are very pronounced at 100 mM. In the latter case, range of the interactions is small, but larger than expected on basis of the PB model. While its exponential dependence can be described with this model reasonably well, the observed averaged decay lengths of 2.9 ± 0.9 nm exceed significantly the expected Debye length of 0.9 nm. While no systematic trend with the molecular mass is observed, we suspect that this repulsive force originates from the short-ranged electro-steric repulsion between PEI layers. The relative independence of the electro-steric forces on the molecular mass suggests a

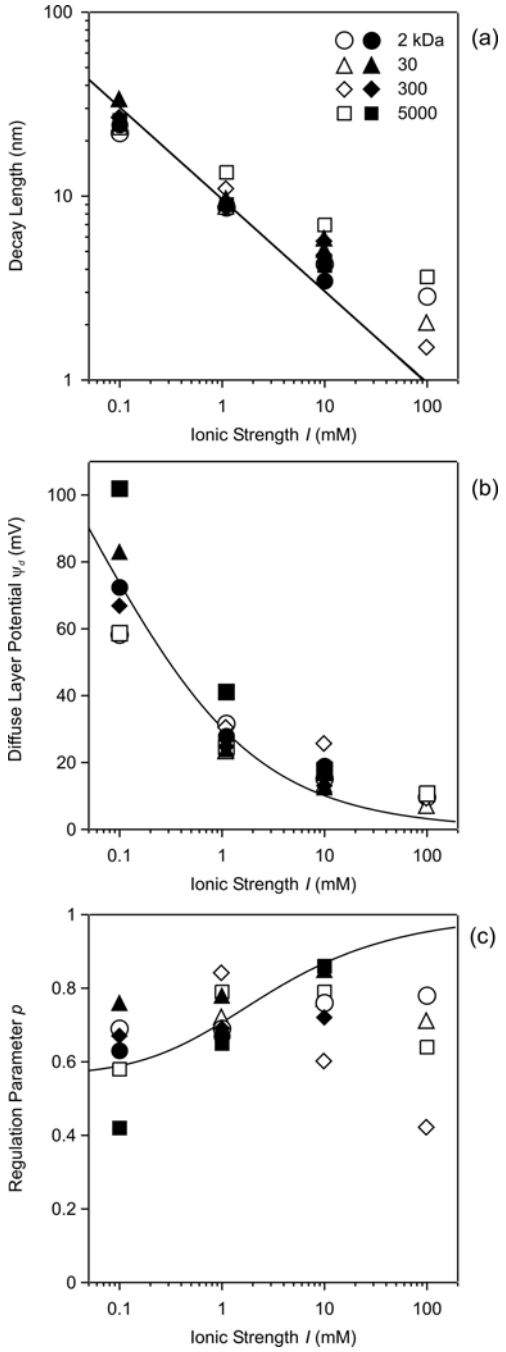

Figure 3-5. Parameters resulting from the PB model and the constant regulation (CR) approximation as a function of the ionic strength for PEI layers pre-adsorbed at low (full symbols) and high (open symbols) salt conditions. The solid line indicates predictions of the PB theory. (a) Debye length (cf. equation (3.1)), (b) diffuse layer potential from the Grahame equation with a charge density of 2.3 mC/m^2 (cf. equation (3.2)), and (c) regulation parameter with an inner capacitance of 36 mF/m^2 (cf. equation (2.12)).

flat configuration for the pre-adsorbed PEI molecules. This electro-steric force also prevents the jump-in of the surfaces at short distances, similar to steric repulsion between adsorbed polymer layers in good solvents[4].

Similar decay lengths to the ones reported here were derived from interaction forces between PEI layers in 50 mM NaCl near neutral pH[74]. These authors report decay lengths in the range of 2.1 ± 0.3 nm, which in their case also exceed the expected Debye length of 1.4 nm. These decay lengths are comparable to the thickness of individual adsorbed PEI molecules[91].

The diffuse layer potentials ψ_d are shown as a function of the ionic strength in Figure 3-5b. In spite of the fact that we cannot determine the sign of the potential, we are confident that the adsorbed PEI leads to a charge reversal and that the surfaces are positively charged. The clearest evidence for this charge reversal stems from electrokinetic data[41, 72]. The presently measured diffuse layer potential increases with decreasing ionic strength, and features a marginal dependence on the molecular mass and preparation conditions. The only exception are the pre-adsorbed layers prepared with the PEI of highest molecular mass of 5000 kDa, as they show somewhat higher surface potentials, particularly when prepared at low salt adsorption conditions. The diffuse layer potentials at 0.1 mM reported here agree reasonably well with values based on force measurements between similar PEI layers, which were around +60 mV when measured with the colloidal probe[74] and about +90 mV with MASIF[76]. However, these measurements cannot be directly compared with our findings, since the mentioned studies used higher pH and lower ionic strengths. Electrokinetic data of adsorbed PEI on silica at concentrations of 50 mg/L indicate a strong dependence of the surface potential as a function of pH[72]. At pH 4, the streaming potentials of oxidized silicon wafers in the presence of PEI are reported near +30 mV and +55 mV at ionic strengths of 10 mM and 1 mM, respectively. These values are in reasonable agreement with the presently measured values, and the small discrepancies could be related to the uncertainties in positioning the plane of shear.

The ionic strength dependence of the diffuse layer potentials can well be described with the inverse Grahame equation (cf. equation (2.8))

$$\psi_d = \frac{2k_BT}{e}\operatorname{arcsinh}\left(\frac{e\sigma}{2k_BT\varepsilon\varepsilon_0\kappa}\right) \tag{3.2}$$

where the diffuse layer potential is expressed as a function of the surface charge and the ionic strength, which enters through the Debye length κ^{-1} (cf. equation (3.1)). As shown in Figure 3-5b, the Grahame equation describes the ionic strength dependence with a surface change density σ = 2.3 mC/m^2 rather well. While the adsorbed PEI leads to charge reversal, it only corresponds to one positive charge per 70 nm^2. This value indicates that only a small fraction of the PEI charge contributes to the diffuse layer charge, and that the PEI is neutralized by both, the silica surface and the bound counterions. The fact that all data are consistent with the same value of the surface charge represents a strong indication that the adsorbed amount of PEI is independent of the molecular mass, and is in accord with the weak molecular mass dependence of the adsorbed amount of PEI on colloidal silica particles[66, 71].

The regulation parameter obtained from the fits is plotted in Figure 3-5c as a function of the ionic strength. The values lie mostly in the range of 0.6 – 0.8. At low ionic strength, the parameter increases with the ionic strength. This trend can be qualitatively understood since the diffuse layer capacitance increases with increasing ionic strength, while the capacitance of the inner layer remains approximately constant. One can attempt to quantify this trend with the relation proposed in Chapter 2 for the regulation parameter in equation (2.12), where C_i is the inner layer capacitance, and the diffuse layer capacitance is given by equation (2.9). As shown in Figure 3-5c, the trend in the experimental data can be approximately reproduced with an inner layer capacitance of $C_i \simeq 36\,\mathrm{mF/m^2}$. However, at higher ionic strengths, the regulation parameter shows a strong scatter and decreases with increasing the ionic strength. These features indicate that the PB model is inappropriate to describe the interactions at short distances, and provides further evidence that the nature of the interactions is modified due to the presence of electro-steric forces. In general, we observe very similar trends for

pre-adsorbed layers prepared at high salt and low salt adsorption conditions (see Table 3-1).

b) Molecular adhesion events upon retraction

We have already mentioned the molecular adhesion events observed upon retraction, particularly, at high ionic strengths (Figure 3-3b). Let us now discuss such events in more detail. Figure 3-6 shows additional force profiles, which illustrate the diverse nature of the molecular adhesion events observed. For high molecular mass PEI, multiple adhesion events with several minima are the rule (Figure 3-3c and Figure 3-6a). Occasionally, events with a single minimum are observed (Figure 3-6b, curve I), which strongly remind of single molecule pulling events as observed for linear neutral polymers and polyelectrolytes[38, 92-95]. It should be pointed out, however, that the present force-extension curves show typically much less curvature than in the case of linear polymers. These events probably originate from the stretching of individual polymer segments, several of which are being extended simultaneously within the branched structure. Simultaneous stretching of these interconnected segments results in rubber-like behavior, and leads to almost linear force-extension relationships (Figure 3-6a, second event). Such events occur frequently besides erratic events (Figure 3-6b, curve II). The latter are probably just a succession of several short rubber-like events, which remain unresolved given the noise of our experimental set-up. In some cases, desorption events are observed, which feature one or several force plateaus (Figure 3-6b, curve III). These plateaus resemble those found for linear polyelectrolytes[93], but they are much shorter in the present case, and hardly exceed a few nanometers. These desorption events occur most frequently for the low molecular mass PEI, which equally exhibits an unspecific adhesion minimum at small distances (< 10 nm, Figure 3-6b, curve III) directly after separation. While no molecular adhesion events are observed at the lowest ionic strength of 0.1 mM, they occur frequently at high ionic strengths. The adhesion events occur at larger distances, and with the exception of the 2 kDa sample, no unspecific adhesion minima at short distances are observed.

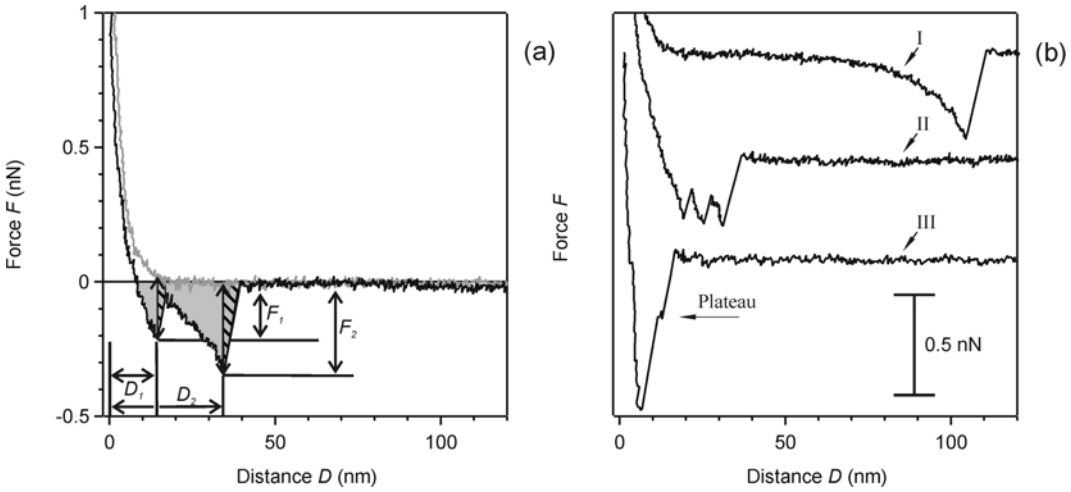

Figure 3-6. Representative force profiles between colloidal silica probe and quartz substrate with pre-adsorbed layers of PEI prepared at high salt adsorption conditions illustrating different molecular adhesion events. (a) Two rubber-like events with the corresponding forces and distances measured at 100 mM for 5000 kDa PEI. The area used for calculating the work of adhesion is indicated in grey and the contribution during jump-out is shaded. (b) Additional retraction force profiles, which were displaced vertically for clarity. Single molecule pulling event (I, 5000 kDa and 100 mM), sequence of erratic events (II, 5000 kDa and 10 mM), and short-range adhesion event (III, 2 kDa and 100 mM) showing a plateau due to desorption (arrow).

Analyzing these molecular adhesion events quantitatively is difficult due to their rich structure and random character. The most marked feature is the jump-off of the cantilever, which is accompanied with a local minimum in the force. Two of these events are indicated in Figure 3-6a, occurring at the rupture distances D_1 and D_2 with the corresponding maximal magnitude of the forces F_1 and F_2, referred to as pull-off forces. All molecular adhesion events are analyzed with respect to the rupture distance and the pull-off force. The results are summarized in Figure 3-7 and Table 3-2, where low molecular mass PEI (two left columns) is compared with high molecular mass PEI (two right columns).

Scatter plots of the pull-off forces as a function of the distance are given in Figure 3-7a. For low molecular mass PEI, one observes events at separation distances of few tenths of nanometers and maximum pull-off forces above one nN. For high molecular mass PEI, on the other hand, the events extend beyond 100 nm, but the forces are concentrated around 0.3 nN. The average distances and

Table 3-2. Typical Characteristics of Molecular Adhesion Events

Molecular Mass	2 kDa		5000 kDa	
Ionic Strength *I* (mM)	10	100	10	100
Mean events per curve	1.4	1.8	0.3	0.7
Probability of no event	0	0	0.82	0.56
Mean Force (nN)	0.58	0.9	0.19	0.25
Mean Distance (nm)	28	12	71	43
Mean Work ($\times 10^{-18}$ J)	7	12	0.8	1.7

pull-off forces reported in Table 3-2 also reflect these trends. At an ionic strength of 10 mM, we have an average distance of 28 nm and average pull-off forces of 0.58 nN for low molecular mass PEI, while for high molecular mass PEI these numbers are 71 nm and 0.19 nN. The rupture distances reported here are somewhat larger, but comparable to the lateral dimensions of adsorbed PEI molecules[91]. In general, the adhesion data are not as well reproducible as the long-range interaction forces, particularly, at intermediate ionic strengths. These difficulties can be partially attributed to sampling errors caused by the broad distributions encountered, and limited number of molecular adhesion events observed (typically 50-200). Furthermore, the adhesion on the single molecule level appears to be sensitive to the polyelectrolyte conformation in the adsorbed state, which might be time dependent and vary between the different preparations to some extent.

Nevertheless, the following trends can be established with confidence. Few or no molecular adhesion events are observed at low ionic strengths, while at high ionic strength these events are frequent. We explain this trend by the more effective screening of the repulsive interactions between the PEI molecules at higher ionic strengths due to the reduced Debye length (cf. equation (3.1)). These reduced interactions result in an increased probability of interpenetration of the PEI molecules upon approach and promote their consecutive adsorption at

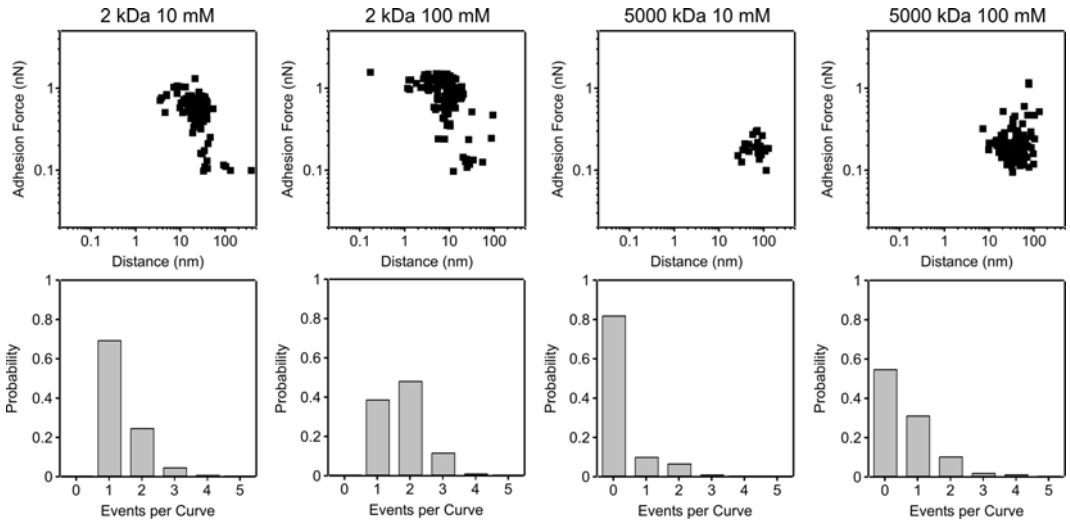

Figure 3-7. Molecular adhesion events between pre-adsorbed PEI layers on silica prepared at high salt adsorption conditions and investigated at pH 4 and different ionic strengths in KCl. (top) Scatter plot of the desorption force as a function of the corresponding distance. (bottom) Probability distribution of the number of events per curve. The columns correspond to the molecular masses of 2 kDa and 5000 kDa at ionic strengths of 10 mM and 100 mM.

uncovered patches on the other surface. At low ionic strength, there is little interpenetration of the layers and thus no adhesion events are observed.

The mean distances at which these events occur, increases with increasing ionic strength and with increasing molecular mass. The mean force of these events also increases with the ionic strength, but decreases with the molecular mass. Evidently, larger PEI molecules can be pulled further than smaller ones. On the other hand, the extension forces are lower since the large molecules are more flexible and less well anchored to the surface. These trends are rather well obeyed for all molecular masses and both adsorption conditions, with the exception of the 30 kDa fraction, where no adhesion is observed at ionic strengths ≤ 10 mM. Differences in the degree of branching or in the sample fractionation procedure could represent the reasons for this unusual behavior. Given the complicated structure of the retraction curves, the scatter plots as well as the number of events quantify the adhesion between PEI-coated surfaces only in approximate manner. For this reason, we have further estimated the work that is necessary to separate

the surfaces. This work of adhesion corresponds to the area under the force curve upon retraction, and it can be obtained by its numerical integration (see Figure 3-6a). The difficulty of this approach is that during the jump-off instabilities, the slope of force-distance curve reflects simply the force constant of the cantilever, but does not correspond to the actual retraction force profile. However, the contribution of these instabilities (hashed area, Figure 3-6a) to the adhesion work is relatively small, when compared to the other contributions (gray area, Figure 3-6a). This contribution is typically <20%, and only a small error will be introduced. The only exception was the PEI of 2kDa, where the contribution of the instability of the short-range adhesion cannot be neglected. Thus, the estimated work of adhesion must be viewed with caution for PEI of 2kDa.

The mean work of adhesion per each retraction was 1.7×10^{-18} J for PEI of 5000 kDa at an ionic strength of 100 mM (Table 3-2). At 10 mM, the work was 0.8×10^{-18} J, and this value decreases with the decreasing ionic strength. This decrease of the work of adhesion with decreasing ionic strength could be confirmed for all molecular masses. At 100 mM, we have observed a mean work of adhesion of $(6 \pm 2) \times 10^{-18}$ J for all samples and preparations, while at 0.1 mM this work was $<10^{-19}$ J. At intermediate ionic strengths, the data are less reproducible. The mean work of adhesion shows no clear trend with the molecular mass and is very similar for the two different adsorption conditions. The strong dependence on the ionic strength of the adhesion can be explained through the fact that the bridging between the surfaces necessitates the availability of free substrate patches on the other side. The accessibility of these patches is facilitated at high ionic strength through the reduced electrostatic repulsion between the polymer segments or eventually partial polymer desorption, leading to more free patches on the substrate where polymer from the other surface may adsorb.

In order to compare the work of adhesion with values available in the literature[39, 76], the work of adhesion obtained from the force curves has to be normalized to the unit area. In difference to the SFA, the necessary contact area cannot be measured directly with the colloidal probe, but a rough estimation can be made. Let us first consider the situation of two fully compressible, infinitely

soft PEI-layers with a thickness *l* in contact. The contact area is then defined by the overlap of the polymer layers and it represents an approximate upper limit of the area in which polymer segments can bridge directly to the other surface. The radius *r* of the outer rim of the circular overlap region in the sphere-plane geometry is obtained from a simple geometrical argument. In this approximation, the spherical colloidal probe of radius *R* and the planar substrate touch at the apex point of the sphere and of the rim is given by $r = \sqrt{4Rl}$. With a typical radius *R* of the colloidal probe of 3.4 μm and a layer thickness *l* of 4 ± 2 nm, we obtain contact radii of the order of 230 ± 60 nm.

This approximation of fully compressible layers introduces several assumptions. Two are the most important ones. Firstly, the approximation neglects the deformation of the silica and quartz surfaces. For bare silica surfaces, the radius of the circular contact area can be estimated by classical Hertz theory[4], and is on the order of 10 nm for a typical loading force of 10 nN and a bulk Young modulus of 72 GPa[96]. For this reason, this contribution can be neglected. Secondly, this approximation neglects the finite thickness of the PEI-layer upon compression, which was measured by SFA to be on the order of 2 nm[75]. For substantially thinner adsorbed layers, such as lipids, the elastic properties are given primarily by the underlying substrate[97, 98]. On the other hand, for an infinitely thick polymer layer with a bulk Young modulus of 10 MPa, the Hertz theory predicts a contact radius of 150 nm. This value for the Young modulus is in the upper range of values reported for gels and polymer layers[99]. The contact radius estimated in this fashion represents an upper limit, and for this reason the estimate given by the simple geometrical model should be appropriate. Nevertheless, it should be emphasized that the elastic properties of thin, soft polymer films on solid substrates are influenced by the substrate[100], and Hertz theory is inappropriate to describe the deformation of such a layer.

Taking the typical work of adhesion of 6×10^{-18} J, obtained from the bridging events at 100 mM KCl as discussed above, and a contact area of radius 230±60 nm, as estimated by the simple model above, we obtain a work of adhesion per unit area of 0.04 ± 0.01 mN/m. These values can be compared to the work of

adhesion W obtained from the unspecific adhesion force F_{adh} of 0.9 nN (cf. Table 3-2) observed for the low molecular mass PEI (2 kDa) at the same ionic strength. From the classical theory of Johnson, Kendall, and Roberts (JKR)[4] we estimate in this case from the relation $F_{adh} = (3/2)\pi R W$, a work of adhesion per unit area W of 0.06 mN/m.

Since these two estimated values for the work of adhesion per unit area agree reasonably well within the uncertainties of our approximation, we suspect that a similar adhesion mechanism is operating for all molecular masses, but the individual adhesion events cannot be resolved for the PEI of lowest molecular mass. This molecule consists of less than 100 monomers and it cannot be stretched very much. However, the steric repulsion it generates is similar to the higher molecular mass PEI, both in magnitude and in range. One may thus hypothesize that the magnitude of the electrostatic repulsion between the segments as well as the availability of free surface patches might be similar, even though the lateral length scales differ substantially.

The presently observed values for the work of adhesion per unit area of 0.04 ± 0.01 mN/m for PEI of all molecular masses should be compared with somewhat lower values around 0.01 mN/m based on earlier colloidal probe measurements[39]. On the other hand, the MASIF technique results in substantially larger values in the range of 10-30 mN/m[75, 76]. However, one must realize that we provided an upper estimate for the contact area and that the latter technique uses much larger radii of curvature, which result in much larger contact areas. Inhomogeneities in the film structure may result in the contact of PEI with patches of bare substrate and would contribute more strongly to the adhesion in the latter case. Moreover, these measurements were carried out at lower salt levels and higher pH, and therefore, they cannot be compared directly. Nevertheless, the discrepancies indicate that adhesive properties of PEI vary strongly, not only as a function of the solution composition, but also through the detailed preparation history of the sample. The history dependence is probably related to our difficulties to accurately reproduce the molecular adhesion events in the intermediate ionic strength range.

3.4 Conclusion

Interaction forces between pre-adsorbed layers of poly(ethylene imine) (PEI) of different molecular mass have been examined with the colloidal probe technique. During approach, the purely repulsive forces are mainly of electrostatic nature and originate from to the overlap of diffuse layers. The forces can be interpreted quantitatively down to distances of a few nanometers within the PB framework, provided charge regulation is being considered. Close to contact, the forces remain repulsive, probably due to electro-steric interactions between the PEI layers with a range of 2-3 nm. The forces upon approach are almost independent of molecular mass. During retraction, erratic attractive bridging forces are observed originating from molecular adhesion events, which are dominated by rubber-like adhesion. Single-molecule pulling events are less frequently noticed. This behavior is very different from linear polymers, which are normally dominated by pulling events of individual chains. The presently reported behavior is clearly related to the strongly branched architecture of the PEI. With increasing the ionic strength, one observes an increase in the frequency of the molecular adhesion events and the work of adhesion. Strong adhesion forces at short distances are frequent for low molecular mass PEI, while for high molecular mass, weaker adhesion forces at larger distances are the rule.

Chapter 4

Adsorption of dendrimers on mica surfaces

4.1 Introduction

The adsorption of colloidal particles, proteins, or other macromolecules at the liquid-solid interface is of substantial importance in many industrial, environmental, and biological processes, such as, wastewater treatment, chromatography, papermaking, or biocompatibility[1]. An improved understanding of this process has been achieved in recent years within the framework of the random sequential adsorption (RSA) model[101-108]. This model assumes the particles to adsorb irreversibly in a sequential manner to the surface at random positions, and treats the particles as hard objects, which are only allowed to adsorb at positions where no overlap with previously adsorbed particles occurs. The RSA model explains experimental adsorption data for colloidal particles[109-115], proteins[116, 117], or other macromolecules[118].

Several authors have studied the adsorption of rigid colloidal particles[109-112, 119]. While such systems are interesting for a number of applications, they are only of restricted applicability as model systems for proteins and other macromolecules, as the latter are flexible and may deform or undergo conformational transitions upon adsorption. In order to obtain a better understanding of the adsorption process in these situations, it is therefore essential to find alternative model systems. Dendrimers are most interesting in this respect. They are globular, highly branched polymers, which have attracted increasing interest in the last two decades[120]. Sequentially synthesized from a small core molecule, each complete reaction sequence results in a new generation, which has a well-defined molecular mass, diameter and number of terminal groups in close

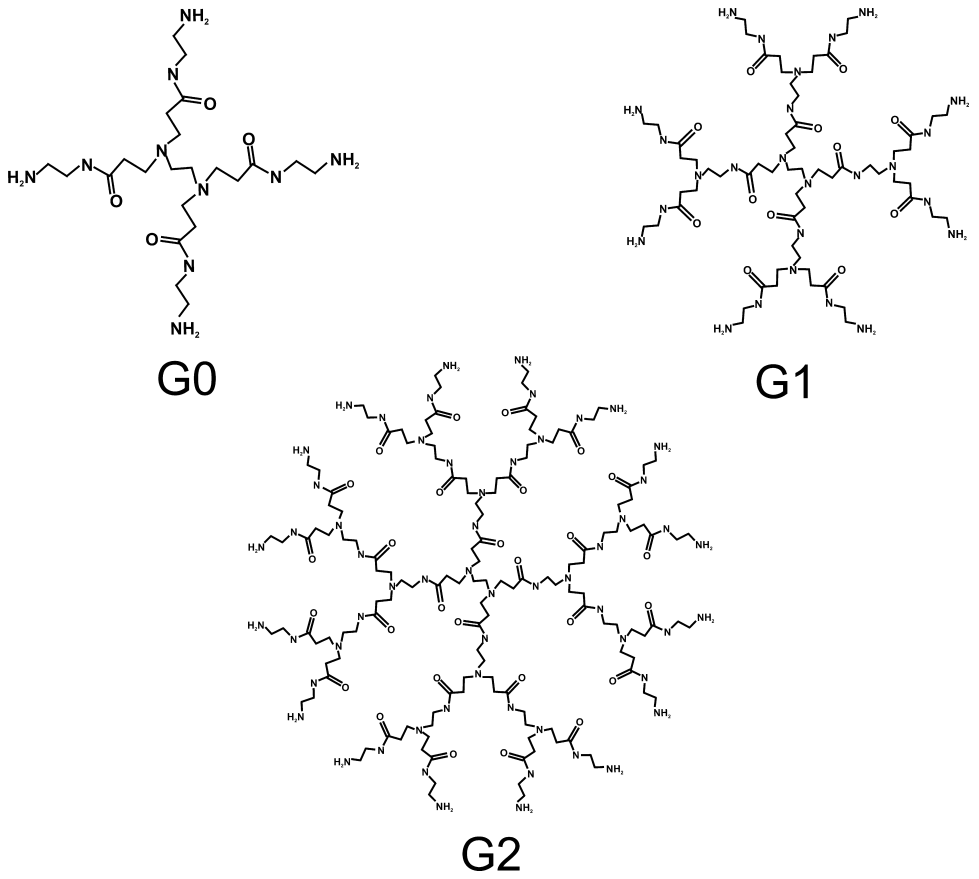

Figure 4-1. Chemical structure of poly(amido amine) (PAMAM) dendrimers of generation 0, 1 and 2.

proximity to the dendrimer surface. The increasing interest in these molecules is also due to their ability to mimic certain properties of proteins or micelles, or due to their applications in molecular recognition, self-assembly processes, or as catalysts[121, 122]. Among the first dendritic structures synthesized were poly(amido amine) (PAMAM) dendrimers[123] (see Figure 4-1). This extensively characterized class of water-soluble macromolecules can be considered as a suitable model system for proteins or branched polyelectrolytes, which are less well defined in many aspects. In particular, different molecular characteristics like size, charge and functionality can be controlled for PAMAM dendrimers in an independent fashion, allowing for a systematic study of their influence on the adsorption behavior.

The surface coverage of the adsorbed particles or macromolecules can be measured by various methods. However, the lateral distribution is only accessible by a limited number of techniques, especially when the size of the objects approaches the lower nanometer range. Atomic force microscopy (AFM) is in this context an extremely versatile method to directly image adsorbed nanoparticles, polymers, or proteins[124].

Adsorbed PAMAM dendrimers have been examined by AFM by several authors[125-130]. Their volume and molecular dimensions have been determined for a series of generations[127], also taking the effects of finite tip radius into account[129]. Furthermore, effects of the substrate and solution pH on the molecular dimensions have been discussed[128]. Recently, adsorbed PAMAM dendrimers were imaged in aqueous environment by AFM[130].

Controlled deposition of dendrimers has been realized by various methods[122, 131, 132], including spin-coating[128], aerosol deposition[133] and deposition from rapidly evaporating solvents[134]. The observed structures range from separated single molecules over domain patterns to monolayers. As recently demonstrated by *in-situ* AFM, different structures can be obtained by exploiting the effects of capillary forces, substrate chemistry, and dendrimer generation[130]. The adsorption process has been studied only for poly(propylene imine) dendrimers by optical reflectometry[118, 135, 136]. While this technique has the advantage to operate *in-situ,* it yields rather limited information concerning the details of the adsorbed dendrimer layer, in particular, in respect to lateral distribution of the molecules.

In this chapter, we use the AFM to study the adsorption process of PAMAM dendrimers from solution to molecularly flat mica. The substrate is for the whole pH-range investigated negatively charged[137, 138], whereas the PAMAM dendrimers carry the opposite charge[139]. The high resolution of AFM permits to obtain detailed information about the conformation of the adsorbed dendrimers and their lateral arrangement. These data allow for a quantitative test of the RSA model to the adsorption of PAMAM dendrimers. Experiments show that the adsorption density of the dendrimers can be precisely controlled and surfaces covered with dendrimers can be easily prepared in a well-defined way.

4.2 Experimental section

a) Sample preparation

PAMAM dendrimers of generations G8 and G10 were obtained as aqueous solutions from Dendritech (Midland, MI). All solutions were prepared with Millipore water, diluted to a concentration of 50 mg/L, and kept at 6°C until used. The concentrations of these stock solutions have been verified by total carbon and nitrogen analysis (Shimadzu TOC-V). Solutions for the deposition process were freshly prepared from the stock solutions and diluted to a range of 0.1-10 mg/L. The ionic strength and pH were adjusted with KCl, HCl, or KOH. Muscovite mica sheets (Ted Pella Inc., Redding, CA, USA) were freshly cleaved, and immediately immersed into the quiescent solutions of given dendrimer concentration, ionic strength, and pH. After a certain adsorption time, the samples were transferred into Millipore water for 1 min and finally dried in a stream of pure nitrogen. Experiments at variable pH were performed in a glove bag under a steady stream of nitrogen to avoid contamination by CO_2 from the air. In this case, the pH was monitored during the dendrimer deposition.

The employed drying procedure can induce formation of aggregates by capillary forces and therefore influence the relative positions of the deposited dendrimers. While for low pH values in general no formation of aggregates after drying occurred, this does not hold for pH>5. In the later case, the formation of aggregates with the simultaneous occurrence of sparsely or uncovered substrate areas have been observed. This point indicates that under different conditions the drying process can indeed result in a rearrangement within the adsorbed dendrimer layer. In any case, however, it should be noted that the amount of deposited dendrimers remains constant independently of the relative positions; therefore, the obtained surface coverages θ should remain unaffected by eventual drying artifacts.

b) AFM measurements

The imaging was performed in tapping mode with a Multimode Nanoscope III (Digital Instruments, Santa Barbara, CA, USA) using an "E" scanner. Standard tapping cantilevers (OMCL-AC160TS-W2, Olympus) were normally used. For each sample, 500-1500 dendrimers were imaged during five or more scans at different positions. Size determination of the dendrimers was carried out separately with super-sharp tips (SSS-NCH-10, Nanoworld AG, Neuchâtel, Switzerland) with a nominal tip radius of less than 5 nm, as verified with a Nioprobe standard (Aurora Devices, Edmonton, Canada).

Adsorbed dendrimers were automatically detected with the image analysis package implemented in IGOR PRO (Wavemetrics, OR, USA) and relying on an algorithm by Barret *et al*[140]. Additional procedures have been developed for manual counting of particles within aggregates or for the removal of artifacts. Particles that obviously belonged to aggregates were not used for the estimation of the dendrimer volume, but considered for the determination of the surface coverage. The mean numbers of adsorbed molecules per scan area were used for the calculation of the surface coverage. Dendrimer positions, as obtained from the center of gravity, were used for the determination of the pair correlation functions. The latter were calculated by sorting the distances between pairs of particles into equidistant shells of equal thickness, subject to periodic boundary conditions.

Due to the finite tip radius, the lateral dimensions obtained by AFM from single dendrimers are subject to a convolution with the tip shape. We have evaluated a tip-size corrected distribution of the dendrimer radii with two simple geometrical models, namely a sphere cap and an oblate ellipsoid. Both models take the deformation of the dendrimer upon adsorption into account, which has been previously observed experimentally by AFM[126-128, 141] and predicted theoretically[142]. The deviation between the models is not substantial, and for clarity, only the results for the ellipsoid model will be reported. The resulting volume distributions have been calculated from the determined geometrical dimensions (i.e., corrected radius, height) for each dendrimer and were then converted to the molecular mass distributions using a density of 1.23 g/mL[128, 143]

(see Appendix). The data derived in this way confirm that the dendrimer structures visible in Figure 4-2 are indeed single molecules.

4.3 Electrostatic interactions and the effective hard sphere model

In the RSA model, the particles are considered to adsorb randomly in a sequential fashion to the surface[101, 102, 105-108]. If there is no overlap between a newly approaching particle and the particles already adsorbed at the surface, then the new particle is assumed to adsorb at that point. Once a particle is adsorbed, it is allowed neither to desorb nor to move laterally on the surface. The resulting fractional surface coverage θ is defined as the ratio of surface area covered to the total surface area, and reads

$$\theta = n\pi < a^2 > \tag{4.1}$$

where n is the surface number density of adsorbed particles and $< a^2 >$ the second moment of the distribution of the radii of the adsorbed particles. Within the RSA model, the surface coverage attains a maximum value, which is referred to as the jamming limit θ_{jam}. For two-dimensional systems, this value cannot be derived analytically, but is accurately known from Monte-Carlo simulations[101]. In the case of monodisperse hard disks, the jamming limit is $\theta_{jam} \cong 0.547$.

The RSA model has been recently extended to charged particles[104, 108]. Their lateral electrostatic repulsion can be approximately described in the framework of an effective hard disk model[104]. The actual radius of the particles, a, is then replaced by a larger effective radius, a_{eff}, which is obtained by defining an energy threshold on the order of the thermal energy, k_BT. This threshold is considered as a maximum potential energy for the electrostatic interactions between the particles. Accordingly, assuming maximum RSA jamming limit, the surface coverage becomes

$$\theta_{max} = \theta_{jam}(a / a_{eff})^2 \tag{4.2}$$

At sufficiently large center-to-center separations r, a pair of identical colloidal particles interacts through the screened Coulomb potential[144, 145]

$$u(r) = \frac{Z^2 e^2}{4\pi\varepsilon\varepsilon_0}\left(\frac{\exp(\kappa a)}{1+\kappa a}\right)^2 \frac{\exp(-\kappa r)}{r} \tag{4.3}$$

where Z is the effective particle charge in units of the elementary charge e, $\varepsilon\varepsilon_0$ the dielectric permittivity of water, and κ the inverse Debye length. For high surface charge densities, the effective charge saturates to a constant value[146]. For sufficiently high salt concentrations (i.e. $\kappa a \geq 5$) this saturation charge is well approximated by[112]

$$Z = \frac{a}{L_B}(4\kappa a + 6) \tag{4.4}$$

where $L_B = e^2 / (4\pi\varepsilon\varepsilon_0 k_B T)$ is the Bjerrum length. In water at ambient temperature, one has $L_B \cong 0.72$ nm.

The effective radius a_{eff} can then be defined by the comparison of the potential $u(r)$ with the thermal energy $k_B T$ introducing the factor λ, namely as

$$\lambda\, u(2a_{eff}) = k_B T \tag{4.5}$$

This equation can be solved analytically in an approximate fashion with the result

$$a_{eff} = (2\kappa)^{-1} \ln(A / \ln A) \tag{4.6}$$

with

$$A = \lambda Z^2 \kappa L_B \frac{\exp(2\kappa a)}{(1+\kappa a)^2} \tag{4.7}$$

Setting $\lambda = 2.8$ one obtains results deviating not more than 4% from the original approach of Adamczyk *et al.*[105], which uses the low-density expansion of the radial pair correlation function on the surface to define the effective radius[112, 144]. Further details on RSA of charged particles are given in recent reviews[105-108].

4.4 Results and discussion

a) Adsorption kinetics of PAMAM dendrimers

Figure 4-2 presents some typical AFM images of G10 PAMAM dendrimers adsorbed to mica at an ionic strength of 10^{-3} mol/L and at pH = 3. The different images were taken for different adsorption times. For short adsorption times, the number of adsorbed dendrimers is low, and rapidly increases as a function of time. For sufficiently long adsorption times, the number of adsorbed dendrimers remains constant. From such images, the surface coverage has been calculated from equation (4.1) using the molecular dimensions given in Table 4-1. The molecular dimensions were determined with super-sharp tips and by considering tip-convolution. The polydispersity index (PDI) of 1.26 of the G10 PAMAM distribution agrees well with the previously reported value of 1.2[128]. Further details concerning the size determination are given in the appendix. For the investigated pH, the mica surface is negatively charged[137, 138] while dendrimers are carrying a large positive charge, due to complete protonation[139]. Therefore, the dendrimers adsorb very strongly to the surface.

The observed evolution of the surface coverage with time is presented in Figure 4-3 for various bulk concentrations ranging from 0.1 to 10 mg/L. One observes that the higher the dendrimer concentration, the more rapidly the plateau is reached. The plateau value itself is independent of the bulk concentration. The existence of such a universal plateau is a clear indication that a well-defined saturation value of the surface coverage for given ionic strength and pH exists. Due to the employed preparation method, a diffusion-limited process determines the early stages of the dendrimer adsorption. In this case, the time evolution of the surface coverage follows the relation[147]

$$\theta(t) = c\, a^2 \sqrt{4\pi D t} \tag{4.8}$$

where t is the time, D is the diffusion constant, and c is the number concentration of the dendrimers in the bulk. The diffusion constant has been calculated using the Stokes-Einstein equation for the G10 PAMAM radii in solution given in Table 4-1, and one obtains $D = 3.63\times10^{-11}$ m^2/s. The theoretical curves are represented in

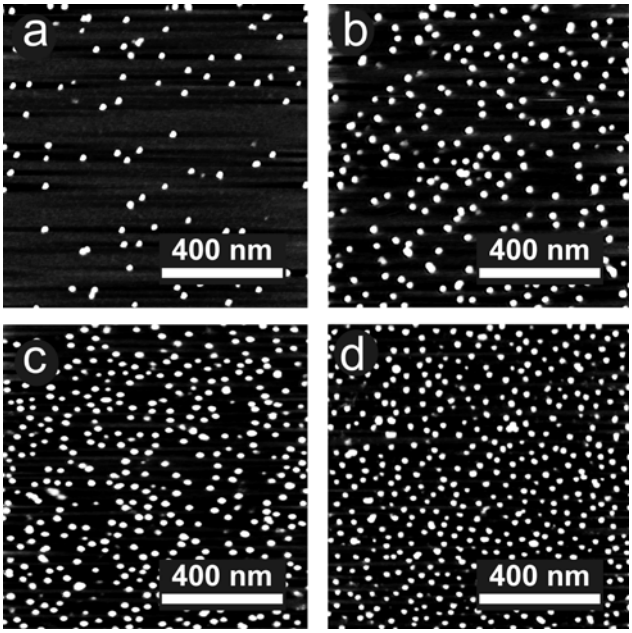

Figure 4-2. AFM Images of G10 PAMAM dendrimers on mica for different adsorption times. The samples were prepared at pH 3 at a dendrimer concentration of 2 mg/L, and no salt was added. Scan size is 1 x 1 µm. Adsorption times: (a) 30 s; (b) 8 min; (c) 15 min; (d) 90 min.

Figure 4-3 as dotted lines for the different bulk concentrations. For short adsorption times, the experimental data follow clearly the expected $\sqrt{t}$-dependence. Nevertheless, some deviations from the theoretical predictions are observed. Beside some scatter in the data, for short times one observes an offset of about 50%.

The reason for this discrepancy remains unclear. The concentration of the dendrimers has been verified by C/N analysis. It is further unlikely that the observed deviation can be attributed to an inaccurate value for the diffusion constant. Neutron spin echo spectroscopy measurements of PAMAM dendrimers in methanol[148] demonstrated an excellent agreement between the measured diffusion coefficients and the Stokes-Einstein equation, despite the fact that an eventual swelling of the dendrimers in an aqueous solution of pH 3 should lower the diffusion constant[149]. As stated previously, the existence of a universal plateau can be established for longer adsorption times. Its presence indicates a saturation of the adsorption process. However, an increased scatter of the data points is also observed. This scatter might be also due to the continuous growth of the diffusion

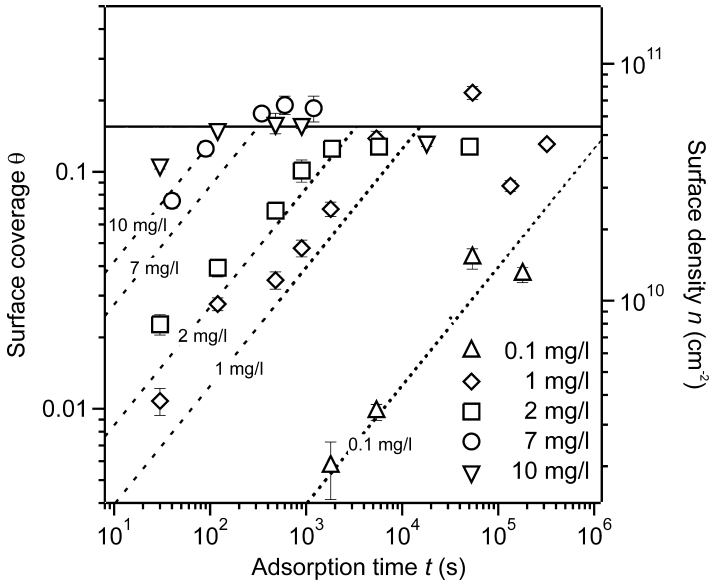

Figure 4-3. The fractional coverage θ and the surface density n of G10 PAMAM as a function of time t at pH 3 and ionic strength 10^{-3} M for different dendrimer concentrations. The dotted lines represent the diffusion-limited adsorption for the different bulk concentrations of G10 PAMAM. The drawn plateau is the average over all maximum coverages.

layer with increasing deposition times, which causes a higher susceptibility to distortions by convection currents generated by small thermal gradients or circulation of air. While the transition between the initial stages of adsorption and the plateau region has been of substantial theoretical interest[106, 113], poor time resolution of the method employed here does not allow any substantiation of this point. It should be noted, that the here employed deposition method is substantially different from the one where a small volume of PAMAM solution is allowed to dry slowly on the sample. In this case, the formation of dense, hexagonal packed areas of PAMAM dendrimers can be observed[127]. This behavior can be seen in analogy to latex particles, where the slow evaporation of the aqueous solvent leads to hexagonal packing[150], while diffusion limited adsorption, with subsequent washing and drying, follows the RSA model[110-112].

Table 4-1. Dendrimer size data as determined by AFM

Generation	Number of surface groups	Mean molecular dimensions (nm)			Mass weighted molecular mass M_W (kDa)		Polydisp. index [d]
		In solution[a]	Adsorbed (AFM)		Theory[c]	AFM	AFM
		Radius	Radius[b]	Height			
G8	1024	4.85	6.35	1.47	233	210	1.47
G10	4096	6.75	9.15	4.28	935	1234	1.26

[a]Light scattering data provided by Dendritech Inc. [b]Dendrimer modeled as oblate ellipsoid. [c]Determined from molecular structure. [d]Polydispersity index PDI = M_w / M_n , where $M_w = \sum N_i M_i^2 / \sum N_i M_i$, and $M_n = \sum N_i M_i / \sum N_i$.

b) Dependence of maximum coverage on ionic strength

Figure 4-4 represents AFM images obtained for adsorption at pH 4.0 but at different ionic strengths of the background electrolyte. The dendrimer concentrations were between 3-7 mg/L, and deposition times in the range of 2-3 hours. The ionic strength was varied from 0.1 mM to 50 mM. According to the kinetic measurements discussed above, these adsorption times and concentrations are sufficient to ensure the surface saturation. This point was also verified by choosing longer adsorption times. The AFM images demonstrate two effects. First, with increasing ionic strength the surface coverage increases. Second, the surface layers are structured and there is a preferred average distance between the dendrimers. The first effect concerns the decrease of the maximum surface coverage with decreasing ionic strength. Figure 4-5 illustrates the dependence of the maximum surface coverage θ_{max} at saturation as a function of the screening parameter κa. The dimensionless screening parameter is proportional to the square root of the ionic strength. The maximum surface coverage increases monotonically with increasing screening parameter κa. Even for the highest ionic strengths examined (50 mM), the values for θ_{max} are well below the jamming limit of $\theta_{jam} \cong 0.547$.

Besides the G10 PAMAM dendrimers, the adsorption of G8 dendrimers of smaller radius has been studied in a similar fashion. It is observed that the

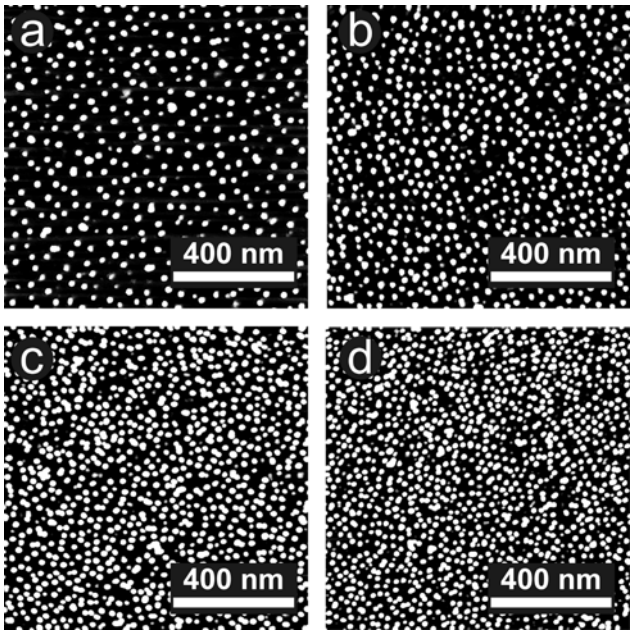

Figure 4-4. AFM images of saturated layers of G10 PAMAM dendrimers adsorbed from different ionic strengths. Samples were prepared at pH 4 and a dendrimer concentration in the range 3-7 mg/L. Scan size is 1 x 1 μm. Ionic strengths: (a) 0.1 mM; (b) 1 mM; (c) 10 mM; (d) 50 mM.

maximum coverages for both dendrimer generations follow a very similar trend. The effective hard sphere model has been used assuming a saturation charge of the dendrimers as given by equation (4.4) and using the appropriate radii for dendrimers in the adsorbed state. Figure 4-5 shows the results by the solid lines, and captures well the overall trend in the data. However, the experimental values are considerably larger than predicted by this simple model and the disparity is more pronounced at low ionic strengths. One observes that in this case the effective hard sphere RSA model overestimates experimentally observed values for the effective radii and thus underestimates the surface coverage. This model further represents an upper estimate for the repulsive interactions and therefore gives a lower bound for the surface coverage. The second effect concerning the structure of the adsorbed layer can be quantified by calculating the radial pair distribution $g(r)$ from the AFM images. The results are shown in Figure 4-6 for different ionic strengths. The observed maximum corresponds to the most

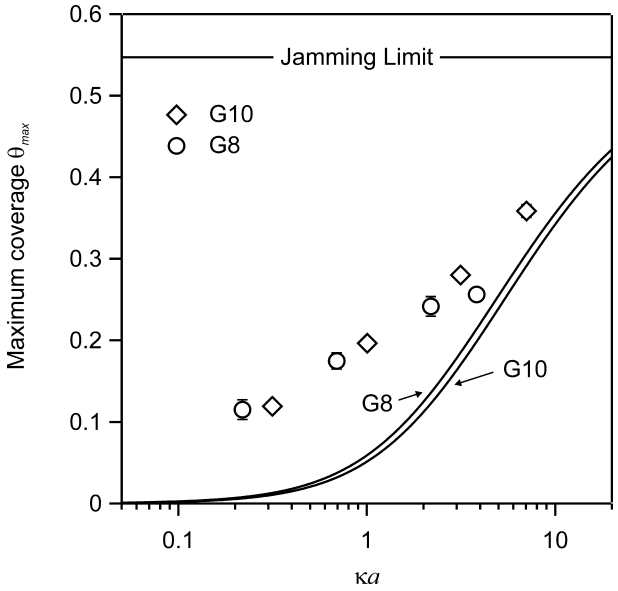

Figure 4-5. The maximum fractional coverage θ_{max} of G10 and G8 PAMAM as a function of the screening parameter κa (a is the molecular radius on the surface and κ is the inverse Debye screening length). The solid lines are calculations based on the effective hard sphere model with charge saturation. Electrostatic inter-particle repulsion decreases θ_{max} in comparison with the RSA hard sphere jamming limit, $\theta_{jam} = 0.547$.

probable distance to the next neighbor dendrimer and reveals the existence of a predominant length scale in the adsorbed structure. The peak positions are summarized in Table 4-2. The peaks shift to lower distances as the ionic strength of the solution is increased. This trend is exactly expected based on the effective hard sphere model, since at low ionic strength the effective radius a_{eff} of the particles is larger due to stronger electrostatic repulsion between the particles. Although a straightforward relation between a_{eff} and the maxima positions in $g(r)$ is not directly accessible without Monte Carlo simulations, the same trends are observed for both quantities in respect to the ionic strength. Furthermore, this observation provides an indication that artifacts due to the drying process are not governing the inter-particle distances.

Deviations from the RSA model, as seen for the PAMAM dendrimers, have been also observed for colloidal particles in recent studies[112], although to less pronounced degree. In the standard RSA model, the surface is considered only as

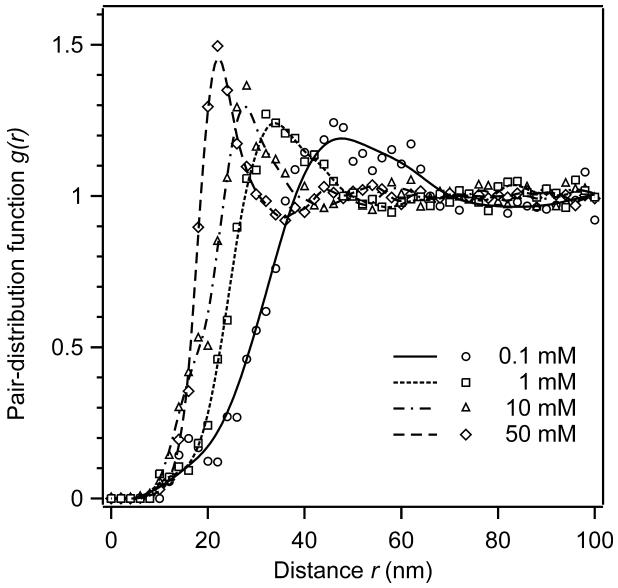

Figure 4-6. Radial pair distribution function $g(r)$ of G10 PAMAM dendrimers on mica surface adsorbed at different ionic strengths and pH 4. The data represent an average over at least 3000 molecules for each ionic strength condition. The lines are interpolation of the experimental data by smoothing spline. The positions of the maxima are given in Table 4-2.

an ideal collector for the adsorbing particles (i.e., the adsorption occurs with a sticking coefficient of one and adsorbed particles remain irreversibly in their initial position). In order to explain some of the observed deviations, it appears that the presence of a charged wall must be taken into account explicitly[151]. In Chapter 5, the adsorption of PAMAM dendrimers on naturally oxidized silicon wafers is studied at pH 4 as well. The values of maximum surface coverage as a function of the ionic strength of the adsorption solution are well below the ones obtained on mica. Indeed, the results on silica show a better agreement with the effective hard sphere model. It is well known that the charge of silica at pH 4 is very low, almost neutral[152]. Thus, the influence of the substrate, or more precisely, the surface charge, must be taken into consideration to explain the observed deviations of dendrimer adsorption on mica with respect to the theory. In the case of dendrimers, additional factors can influence the adsorption. Dendrimers deform upon adsorption, and the electrostatic repulsion will be overestimated when a spherical shape is being assumed. An extension of the effective hard sphere model

Table 4-2. Surface coverage and characteristic distances in dependence of ionic strength of G10 PAMAM

Ionic Strength (mM)	Characteristic Distance (nm)				Surface Coverage θ	
	Pair Correlation Function [a]		RSA Model [b]		Experimental	RSA Model
0.1	23.8	(2.6*a*)	67.7	(7.4*a*)	0.119	0.010
1	16.9	(1.8*a)*	30.6	(3.3*a*)	0.196	0.049
10	13.6	(1.5*a*)	16.5	(1.8*a*)	0.280	0.168
50	11.0	(1.2*a*)	12.6	(1.4*a*)	0.358	0.289

Characteristic distances given in the parenthesis are in units of molecule radius *a* for comparison.
[a] Half of the separation distance of the pair correlation function maximum.
[b] Effective radius a_{eff} as given by equation (4.6).

for charged hard ellipsoids was proposed recently[108, 153]. Although the dendrimers have a spherical shape in solution and undergo a conformational change only upon adsorption, an analysis of the present situation along those lines could resolve the mentioned discrepancies. Furthermore, a certain degree of surface mobility has been stated for dendrimers[133]. This effect could explain the observed increased surface coverages compared to the RSA model in a simple manner. Nevertheless, the pair correlation functions $g(r)$ indicate that the repulsive electrostatic interaction between the dendrimers imposes a minimum distance between neighboring dendrimers.

c) Dependence of maximum coverage on pH

Since the charge of PAMAM dendrimers decreases with increasing pH, the maximum surface coverage has been examined as a function of the pH. Figure 4-7 shows the surface coverage data for the generation G10 at a constant ionic strength of 10^{-3} M. The maximum surface coverage increases significantly with increasing pH. At low pH, the surface coverage stays approximately constant. Between pH 6 and 7, one observes a substantial increase with a new plateau at higher pH. The plateau at high pH should be interpreted with caution. At high

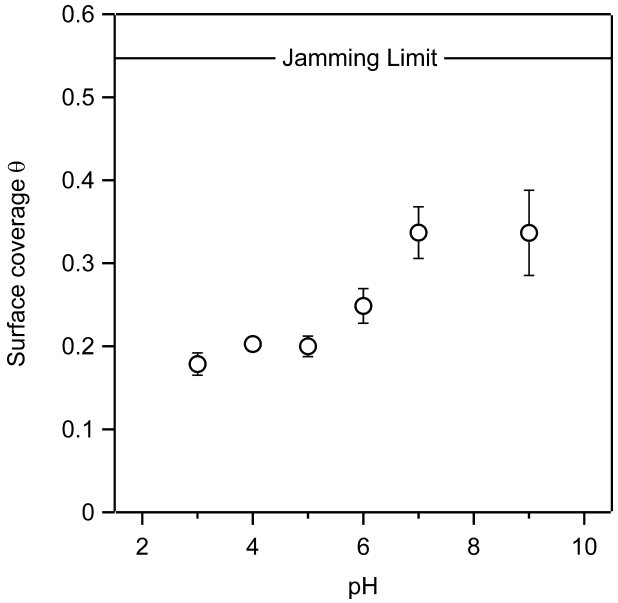

Figure 4-7. The maximum fractional coverage θ_{max} of G10 PAMAM dendrimers as function of pH at an ionic strength of 10^{-3} M.

coverages, it was difficult to resolve all adsorbed dendrimers, since a strong tendency towards aggregation has been observed. The formation of aggregates can be attributed partly to artifacts induced by the drying procedure, since the weakly charged dendrimers adhere less strongly to the substrate and are more susceptible to attractive capillary forces. Qualitatively, the increase of the surface coverage as a function of pH can be easily understood. At low pH, the PAMAM dendrimers are fully charged. Thus, the lateral electrostatic repulsion is strong (corresponding to a large effective radius) and the maximum coverage is low. At high pH, on the other hand, the dendrimers are weakly charged. The electrostatic repulsion is weak, and thus the maximum coverage is higher.

Quantitatively, however, the present observations are not as easily understood. The effective charge can be approximated by its saturation limit only when the bare charge is sufficiently high. For small charges, the bare charge and effective charge coincide. The crossover between these two regimes is relatively sharp, and occurs where both charges are comparable[154, 155]. As the pH is increased, the bare charge of the dendrimers decreases in a fashion that is well understood[139].

However, their bare charge remains high in comparison to the effective charge, and the effective charge remains close to the saturation value for most pH values. The effective charge decreases substantially only for pH > 8. When this situation is treated within a simple model, one obtains a sudden increase of the surface coverage in the pH range 8-9, which is not in agreement with the experiment.

4.5 Conclusion

The adsorption of PAMAM dendrimers of generations G8 and G10 to a mica surface has been studied by atomic force microscopy (AFM) as a function of ionic strength and pH. The initial steps of the adsorption of the dendrimers were consistent with a diffusion-limited process, while the surface coverage saturates at later stages. The maximum surface coverage and the corresponding pair correlation functions have been determined for different ionic strengths. The observed trends of the surface coverage can be described within the effective hard sphere model for random sequential adsorption (RSA). Particularly at low ionic strength, the experimentally observed coverage is larger than predicted by the RSA model. Similar but smaller discrepancies have been observed for colloidal particles. We suspect that this larger discrepancy partly originates from the fact that the dendrimers undergo a deformation upon adsorption to the surface, and that the simple hard sphere RSA model overestimates their electrostatic interaction. Measurements of the maximum surface coverage as a function of pH also suggest that the model needs refinement. Nevertheless, the main trends of PAMAM dendrimer adsorption were shown to be compatible with the RSA model.

This chapter shows that surfaces with a well-defined density of dendrimers with different surface coverages ranging from 0.05 up to 0.4 can be prepared by selecting an appropriate dendrimer generation, ionic strength of the background electrolyte and pH value. These surfaces, although of random nature, exhibit characteristic length scales in the nm-range for the distances between neighboring adsorbed dendrimer molecules. In this fashion, nano-patterned surfaces can be

obtained, exhibiting smaller length scales than obtainable by similar approaches employing colloidal particles[156, 157].

4.6 Appendix

Two simple models that represent two extreme configurations of dendrimer deformation upon adsorption have been compared: (a) a sphere cap and (b) an ellipsoidal shape. For these models the measured lateral dimensions are corrected using the independently determined tip size (Figure 4-8). For the ellipsoidal model, a symmetrical deformation perpendicular to the surface and approximate position of the contact point between the tip and the dendrimer at half of the measured height are assumed. The relationship between a and a' reduces then to $2(a'-a)^2 = 4Rh - h^2$, whereby the symbols are defined in Figure 4-8. By geometrical considerations, one arrives to a similar relationship for the sphere-cap model: $a'^2 - a^2 = 2Rh + 2h^2$. In Figure 4-9 a selection of typical AFM images with corresponding cross-sections are shown. In average, the PAMAM G10 dendrimers adsorbed from pH 4 have an uncorrected radius of approximately 13 nm as measured with a supersharp tip (R = 4.5 ± 1.1 nm). For the spherical cap model, this average diameter is reduced by 25 %, while for the ellipsoidal model one finds a reduction of 29 % (11 % and 27 % for G8 respectively, c.f. Table 4-3). The obtained distributions for the radii (cf. Figure 4-10) correspond well with ones obtained by transmission electron microscopy for the same PAMAM generations[158]. The determined diameters are similar to the ones of G9 PAMAM as measured in aqueous conditions by AFM[130], taking into account the different generations. For G10, the determined volumes and molecular masses match the expected ones based on the molecular structure, although the ellipsoidal model yields better agreement. The determined index of polydispersity by AFM is higher than determined by small angle x-ray and neutron scattering[148, 159]. Further analysis reveals that the polydispersity as measured by AFM is enhanced by an increased coefficient of variation for the heights of 0.29 in comparison to the ones for the radii of 0.19 (cf. Figure 4-10). This effect could be attributed to imperfect

transitions between the generations, which will not only lead to a wider molecular mass distribution, but also to defects in the structural network of the dendrimers. The existence of such defects could lead to a more pronounced deformation of the respective dendrimers perpendicular to the surface upon adsorption, and thus explain the larger polydispersity of the heights.

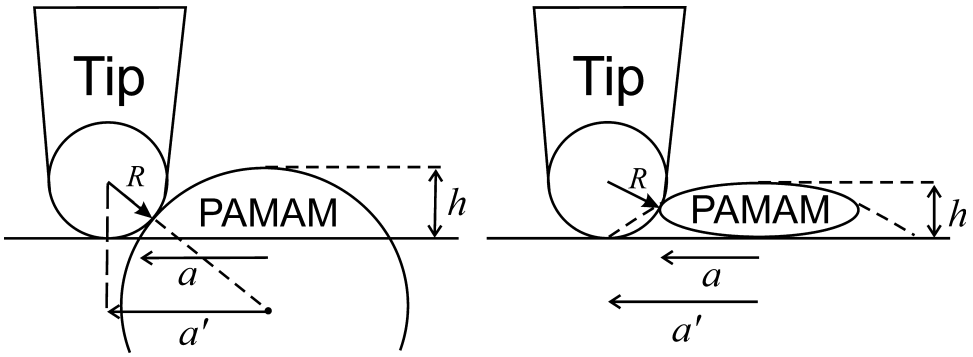

Figure 4-8. Scheme illustrating the convolution of the lateral dendrimer dimension with the tip radius in the sphere cap and oblate ellipsoid model (a' and h are the radius and the height of the dendrimers as measured by AFM, R is the tip radius).

Table 4-3. Comparison of sphere cap and oblate ellipsoid model

Generation	Molecule Radius (nm)		Mass Weighted Molecular Mass Mw (kDa)		Polydispersity Index	
	Sphere Cap	Oblate ellipsoid	Sphere Cap	Oblate ellipsoid	Sphere Cap	Oblate ellipsoid
G8	7.68	6.35	115	210	1.41	1.47
G10	9.54	9.15	524	1234	1.22	1.26

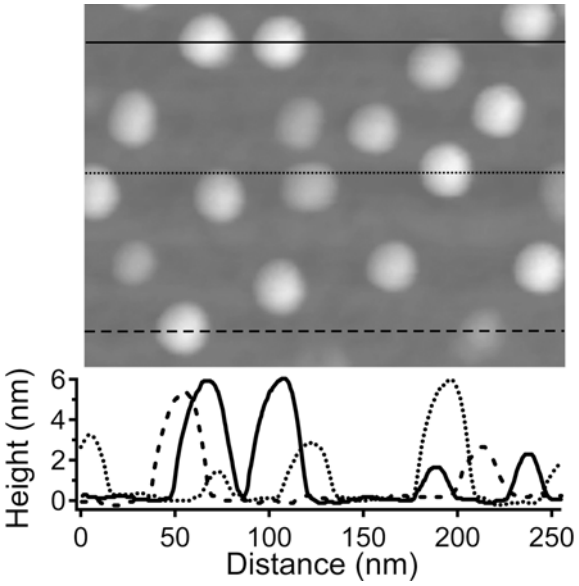

Figure 4-9. Selection of an AFM image with corresponding cross sections for some G10 PAMAM dendrimers.

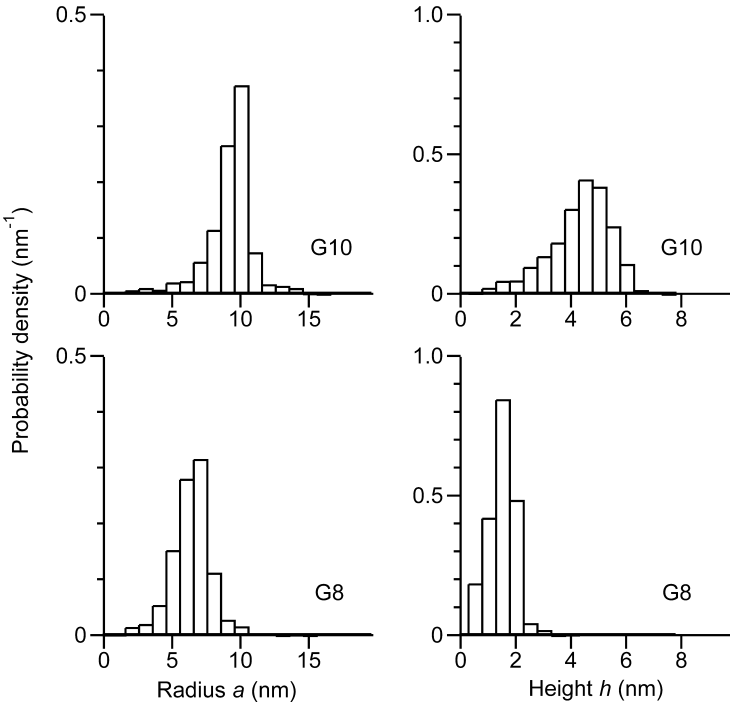

Figure 4-10. Distribution of the radii obtained by the ellipsoid model and the measured heights for G10 and G8 PAMAM adsorbed on mica from an ionic strength of 10^{-4} M and pH 4 as determined by AFM.

Chapter 5
Interactions between dendrimer coated surfaces

5.1 Introduction

The presence of oppositely charged polyelectrolytes influences strongly the aggregation behavior of colloidal systems[1, 16, 41, 160]. This is due to the possibility of charge neutralization or charge reversal of the colloidal particles caused by the adsorption of the polyelectrolytes. However, some phenomena observed in those systems cannot be explained by DLVO theory. For instance, some previous results on colloidal aggregation in presence of polyelectrolytes have shown aggregation rates that are faster than the ones measured in the absence of polyelectrolytes[16, 41]. These results may be explained by the lateral heterogeneity of the surface in systems of deposited highly branched polyelectrolytes with a high density of charge. In these situations, the surface consists of a distribution of highly charged patches, leaving bare areas of opposite charge on the surface. In situations where these bare areas are large enough, oppositely charged local areas of interacting particles may attract to each other, driving to aggregation beyond the charge neutralization point. When the lateral repulsion between the adsorbed polyelectrolytes is predominant over the local attraction of oppositely charged areas, further colloidal aggregation is impeded.

As has been shown in Chapter 3, direct force measurements have become an extremely useful tool to address the interactions between polyelectrolyte-covered surfaces as it has been shown in and in previous studies[37, 75, 89]. Nevertheless, there is a lack of studies concerning the influence of charge heterogeneity in the interactions between polyelectrolyte-covered surfaces. Some advances have been

achieved in the theoretical prediction of such interactions, but most of the studied systems are still too simplistic to be compared to the real ones[42-44, 161].

In this chapter, direct force measurements between silica surfaces with deposited poly(amido amine) (PAMAM) dendrimers are presented. The adsorption behavior of these dendrimers on silica substrates is also investigated, in order to have detailed information about both the adsorbed mass and the lateral distribution of the charge on the surface at hand. Tapping mode atomic force microscopy (AFM) images are analyzed, and information about the surface coverage and the lateral configuration of the adsorbed dendrimers on planar and spherical surfaces is acquired. The colloidal probe technique is used to measure the forces between different dendrimer surfaces and in various solution conditions (see Figure 5-1). Parameters such as the diffuse layer potential and the diffuse layer charge density are obtained from fitting the interaction curves to solutions of the Poisson-Boltzmann equation. Further, a qualitative analysis of the interaction occurring at short-range separation distances is presented.

5.2 Experimental section

a) Sample preparation

Poly(amidoamine) PAMAM dendrimers of generations G6, G8 and G10 were obtained as aqueous solutions from Dendritech (Midland, MI). All solutions were prepared with Millipore water, diluted to a concentration of 50 mg/L, and kept at 6 °C until used. The concentrations of these stock solutions have been verified by total carbon and nitrogen analysis (Shimadzu TOC-V). Solutions for the PAMAM deposition process were freshly prepared from the stock solutions and diluted to a range of 5-10 mg/L. The ionic strength and pH of the dendrimer solutions were adjusted with KCl and HCl. Silicon wafers (Silchem, Freiburg, Germany) with a natural oxide layer were used as planar substrates for PAMAM adsorption. The wafers were cleaned following the RCA method[84], which consists of incubating

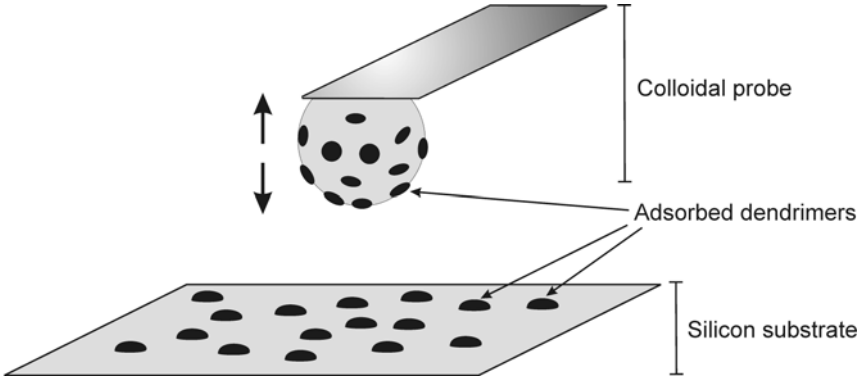

Figure 5-1. Schematic representation of the experimental set-up of the direct force measurements between dendrimer-covered surfaces (not to scale).

the wafer in a 1:1:5 mixture of hydrogen peroxide (35%), ammonia (25%), and water at 75 °C for 10 min, and finally rinsed extensively with Milli-Q water.

Colloidal probes were prepared using colloidal silica particles of 6-7 μm (Bangs Laboratories). To assemble a probe, a bead was attached to the end of a tip-less AFM cantilever (CSC 12, MikroMasch, Estonia) with UV-curable glue (NO 63, Norland Adhesives) using a dedicated micromanipulator (Märzhäuser, Germany). The glue was cured by illuminating the probe with a mercury lamp in an optical microscope for about one minute.

Before dendrimer adsorption, the silicon substrates and the colloidal probes were cleaned in air-plasma at 35 W for 5 min (Harrick Scientific, NY). After the cleaning process, they were immediately immersed into a quiescent solution of given dendrimer concentration, ionic strength, and pH for about 12 h. It has been previously verified that this adsorption time is sufficiently long to ensure saturation of the surface at PAMAM concentrations between 5 and 10 mg/l as has been demonstrated in Chapter 4. After the adsorption process, the samples were transferred into Millipore water for 1 min to remove loosely bound dendrimers, and finally dried in a stream of pure nitrogen. It should be noted that the adsorbed density of dendrimers is constant over the wafer. Therefore, the obtained surface coverages should remain unaffected by eventual drying artifacts.

b) Tapping mode AFM measurements

The imaging of adsorbed PAMAM dendrimers was performed in tapping mode with a Multimode Nanoscope III AFM (Digital Instruments, Santa Barbara, CA) using a "J" scanner. Standard tapping cantilevers (OMCL-AC160TS-W2, Olympus) were used. In the case of planar samples, 500-1500 dendrimers were imaged during five scans at different positions. Size determination of the dendrimers was carried out separately with high-resolution tips (DP14/HI'RES/Al BS, MikroMasch, Estonia). Because of the finite tip radius, the lateral dimensions obtained by AFM from single dendrimers are subject to a convolution with the tip shape. These effects are eliminated with a deconvolution software[162] (Deconvo 1.1, Silicon-MDT Ltd.). Adsorbed dendrimers were automatically detected with the image analysis package implemented in IGOR PRO (Wavemetrics, OR), which relies on an algorithm by Barret *et al*[140]. Additional procedures have been developed for manual counting of particles within aggregates. Particles that obviously belonged to aggregates were not used for the estimation of the dendrimer size but considered for the determination of the surface coverage. The mean numbers of adsorbed molecules per scan area were used for the calculation of the surface coverage.

For the case of spherical surfaces, silica particles were glued to silicon substrates, and they were submerged in solutions of PAMAM dendrimers with predetermined ionic strength, pH and dendrimer concentration, analogously to planar surfaces. Due to substantial roughness of the spheres, adsorbed dendrimers on the particles could be only identified in phase mode. The dendrimer adsorption density was calculated manually. We compared coverages of particles and flat substrates, and the difference between both substrates was found to be always below 15 %.

c) Direct force measurements

The force measurements were carried out with a closed-loop AFM (MFP-3D, Asylum Research, Santa Barbara, CA). Colloidal particles used as probes, which were glued to tipless cantilevers as described above, had diameters in the range of

6-7 μm. Their actual diameters were determined by optical microscopy to an accuracy of about 0.3 μm. The spring constants of the AFM cantilevers were determined by analyzing their thermal noise in air[22, 85]. The results were compared with values obtained from the procedure proposed by Sader *et al*.[86], which uses the frequency response of the cantilever, its top view geometrical dimensions, and the properties of the surrounding medium. The results of both methods deviated by less than 25% in all cases. After mounting the polyelectrolyte covered colloidal probe and the silicon substrate in the MFP apparatus, the gap between the cantilever holder and the substrate was filled with KCl solution of desired salt concentration adjusted to pH 4 with dilute HCl. The ionic strength of this solution is referred to as I_{sol}, and it must be differentiated in this chapter from the one of the adsorption solution of dendrimers, referred to as I_{ads}. The drop remained appended to the holder and the substrate by means of capillary forces, keeping the probe and the measuring region of the substrate submerged in the liquid during the experiment. The force curves were acquired at a cycling frequency of 0.3 Hz resulting in approach and retraction velocities of 0.2–0.6 μm/s. All measurements were carried out at room temperature of 23±2 °C.

The approximate symmetry of the bare surfaces was verified as follows. A silica sphere was glued to a silicon substrate, and force measurements were realized between this sphere and a colloidal probe under the same conditions used for measurements of the polyelectrolyte coated surfaces. In the same experiment, the probed sphere was displaced by moving the scanner plate of the AFM apparatus. In this way, further measurements were obtained gauging this time the silicon substrate with the colloidal probe. The obtained results for both symmetries agreed fairly well, and in any case the error was not higher than the inherent experimental inaccuracy.

d) Force data analysis

Direct force measurements were realized at three different positions on the substrate, and 50 force curves were measured per position. These 50 curves were averaged to obtain finally three curves per experiment. Force versus separation

distance curves were obtained by multiplying the deflection of the cantilever by the spring constant of the cantilever. The separation distance was determined by setting the constant compliance region, obtained from a linear fit, as the zero separation between the probe and the plane. The data were normalized by the probe radius R to compare the experimental data with the interaction free energy per unit area, as stipulated by the Derjaguin approximation[163]. The final force curves were fitted to a numerical solution of the Poisson-Boltzmann equation for the case of two symmetric plates, from distances above two times the Debye length $2\kappa^{-1}$ of the experiment solution. At this distance, no effects from charge regulation or charge heterogeneity of the surfaces are expected. It was considered as a boundary condition that both surfaces had constant charge, although both theoretical predictions for constant surface charge and potential coincide at this point.

5.3 Results and discussion

a) Adsorption of PAMAM dendrimers on silica

The adsorption of PAMAM dendrimers onto silicon surfaces with a natural oxide layer was studied using tapping mode AFM. The adsorption experiment was realized for various ionic strengths of the deposition solution. Two generations of dendrimers, namely G8 and G10, were examined to investigate the effect of dendrimer size. In Figure 5-2a and b, two images of adsorbed G10 PAMAM dendrimers on silicon substrate are displayed. They show the lateral distribution of dendrimers deposited in a solution at pH 4, with an ionic strength of 0.1 mM for Figure 5-2a, and 5 mM for Figure 5-2b. G10 PAMAM dendrimers were adsorbed onto a silica particle, and the resulting tapping mode AFM images are shown in Figure 5-2c and d. Both pictures correspond to the same scan. Figure 5-2c is the three-dimensional image of the particle measured in height mode. Here, the dendrimers cannot be clearly resolved, since their heights are of the same order as the particle roughness. For this reason, the surface was measured as well in phase mode and it is shown in Figure 5-2d. The brighter features correspond to

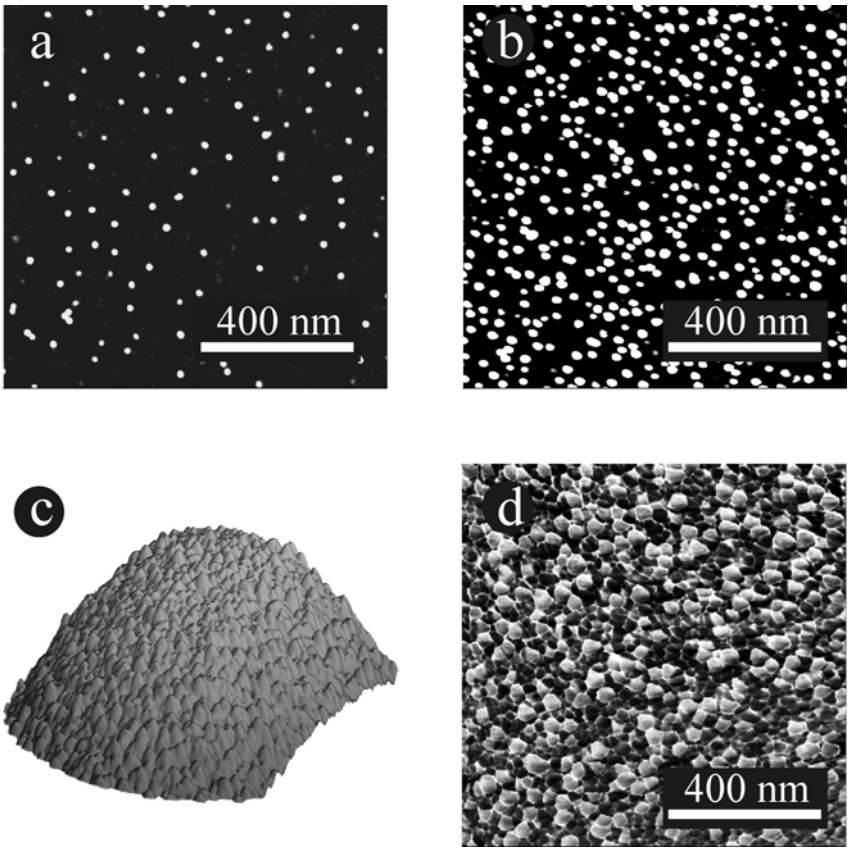

Figure 5-2. Tapping mode AFM images of adsorbed G10 PAMAM dendrimers scanned in air. (a) show height image of dendrimers adsorbed on a silicon substrate from a solution at pH 4 and an ionic strength of 0.1 mM. (b) displays height image of dendrimers adsorbed on a silicon substrate in a solution at pH 4 and an ionic strength of 5 mM. (c) is a stereographic image of dendrimers adsorbed onto a silica particle of 6.8 μm of diameter; dendrimers were adsorbed in a solution at pH 4 and an ionic strength of 5 mM. (d) is the same image as (c) but obtained in phase mode. Brighter regions correspond to adsorbed dendrimers.

the adsorbed PAMAM, and the darker regions are bare areas of silicon substrate. All images show the adsorbed dendrimers as charge patches randomly distributed laterally. As can be seen, the dendrimers adsorb individually, and very few aggregates can be observed, especially in the picture where the dendrimers were adsorbed at lower ionic strength. The density of molecules adsorbed in lower ionic strength solution is much inferior than for the case of adsorption at higher ionic strength. The reason must be found in the interactions between adsorbing dendrimers with the ones already deposited at the surface. At pH 4, a PAMAM

dendrimer is highly charged, and a diffuse layer of ions is formed around the molecule in solution. The thickness of this layer is given by the Debye length κ^{-1} of the solution[4], and it can be reduced when increasing the ionic strength of the aqueous medium. When a dendrimer approaches to the depositing surface, its diffuse layer may overlap with the one of a previously adsorbed molecule, and it is prevented from adsorption. This effect leaves an excluded region around an adsorbed dendrimer, which is characterized by defining an effective radius of the dendrimer (see eq. (4.5) and (4.6)), whose extension depends on the dendrimer size, its charge, and the ionic strength of the medium.

Figure 5-3 shows the coverage of G8 and G10 PAMAM dendrimers, which is given by

$$\theta = \pi a^2 n \tag{4.9}$$

In this expression, n is the surface density of dendrimers, and a is the mean radius of the adsorbed dendrimer. The sizes of adsorbed G8 and G10 PAMAM dendrimers were obtained from a dedicated experiment where images were taken using special fine tips. The measured radius of G10 PAMAM was 8.3 nm, and the height 4.0 nm. For the case of G8 PAMAM, the measured radius was 5.0 nm, and the height 2.0 nm. These values are of the same order as the ones obtained on mica (see Table 4-3). The differences in value must be taken with caution, since the sizes were obtained following dissimilar methods. The fractional coverage represents the surface ratio covered by the deposited dendrimers, and it has been plotted in Figure 5-3 as a function of the screening parameter κa, where κ stands for the inverse Debye length

$$\kappa = \sqrt{\frac{2N_A e^2 I_{ads}}{\varepsilon\varepsilon_0 k_B T}} \tag{4.10}$$

where $\varepsilon\varepsilon_0$ is the permittivity of water, $k_B T$ is the thermal energy, N_A the Avogadro's number, e the elementary charge, and I_{ads} is the ionic strength of the adsorption solution. The screening parameter κa relates the dendrimer size with the thickness of its diffuse layer, and it increases its value when the ionic strength of the solution is augmented. The graph shows that an increase of the ionic

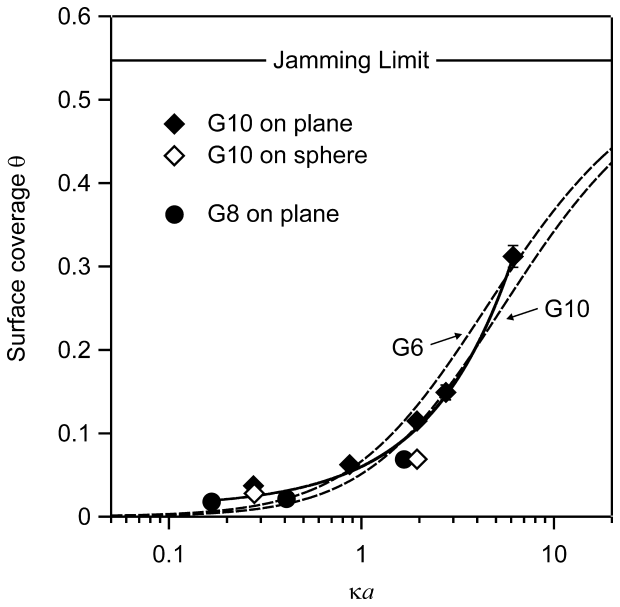

Figure 5-3. Fractional coverage θ of PAMAM dendrimers on bare silicon substrates as a function of the screening parameter κa, where κ is the inverse Debye length and a is the mean average radius of the deposited dendrimer. The markers represent the experimental data as obtained from the tapping mode AFM images. The dash lines are the theoretical prediction of the adsorption behavior according to the effective hard-sphere approximation for the two limiting dendrimer sizes, namely G6 and G10. The solid line is a smoothed interpolation of the experimental data.

strength causes an enhancement of the fractional coverage. This phenomenon is well understood since the interaction has shorter range when ionic strength is increased. Thus, the effective radius of the dendrimer becomes smaller, and a wider extension of bare surface becomes available for further deposition. It can be seen that a change in the size of the dendrimer of about 40 %, as corresponds to the sizes of G10 and G8 PAMAM, does not change the behavior of the coverage significantly. In any case, the coverage was well below the jamming limit $\theta_{jam} = 0.547$ that has been predicted for random sequential adsorption (RSA) processes[101]. All the values of the coverage on planar surfaces and on spheres were interpolated using a smoothing spline algorithm. The experimental data in Figure 5-3 are plotted together with the effective hard sphere model[105, 108], which is an extension of the random sequential adsorption (RSA) model[101, 102, 106]. A summarized explanation of this theory as used here is given in Chapter 4 for the adsorption of PAMAM dendrimers on mica and in the work of Semmler *et al*[112]

for deposition of latex particles onto silica. Our experimental data of the coverage fit quite well with this model. Besides, studies of particle adsorption of various composition and sizes show similar agreement with the effective hard sphere model[105, 111, 112, 164].

The behavior of dendrimer adsorption on silica is qualitatively analogous to the one already described in Chapter 4 for mica surfaces. For both substrates, silica and mica, the density of adsorbed dendrimers is enhanced when increasing the ionic strength of the adsorption solution. However, if we compare the absolute values of the fractional coverage of both cases, it is observed that the adsorbed amount of dendrimers is higher for mica. This phenomenon is especially enhanced at low ionic strength adsorption conditions, where the adsorbed dendrimer density using mica as collector surface can be almost three times higher than in the case of silica. The values of the coverage for both materials seem to converge for high ionic strength adsorption conditions. The reason for this difference is alleged to be the dissimilar charge of the substrate at the experiment pH. Indeed, at pH 4, silica is weakly charged[165], whereas mica has a fairly high negative charge under these conditions[138]. When a dendrimer approach a silica substrate, it may only interact electrostatically with a previously adsorbed dendrimer if both diffuse layers overlap, and its interaction with the surface can be neglected. For the case of approaching a mica surface, the dendrimer may interact not only with a previously adsorbed one, but also with the oppositely charged surface. In the latter case, the interaction is attractive, and the possibilities for the dendrimer to reach the surface and be adsorbed are enhanced with respect to the case of approaching a neutral surface. In terms of the effective hard sphere model discussed in Chapter 4, the negative charge of the mica reduces the effective radius of the positively charged dendrimer. Thus, the excluded region for further deposition around an adsorbed dendrimer is diminished.

The lateral distribution of the adsorbed PAMAM dendrimers can be also obtained from the tapping mode AFM images. We examine their radial pair-distribution on the surface as a function of the separation distance, as it is

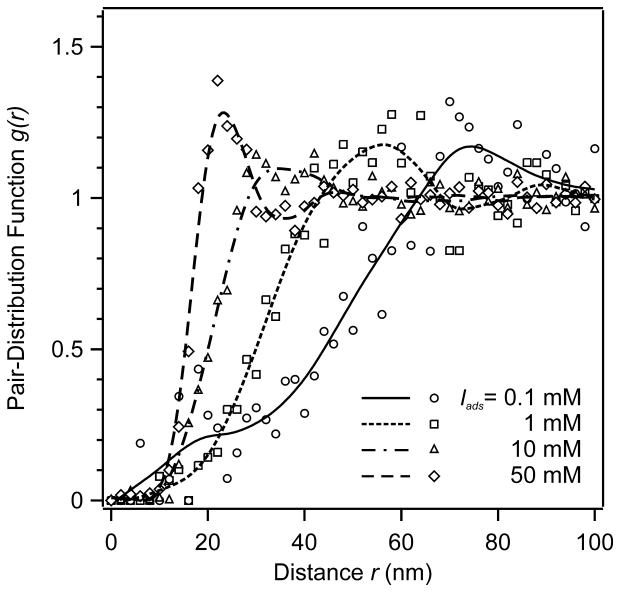

Figure 5-4. Pair-distribution function *g(r)* of the adsorbed PAMAM dendrimers on silica substrates. The symbols display the experimental data obtained from tapping mode AFM images. Lines show interpolation of the data by smoothing spline. Results from the PAMAM adsorption in solution at four different ionic strength I_{ads} and pH 4 are shown.

displayed in Figure 5-4. The first maximum of this function shows the most probable distance of an adsorbed dendrimer to its closest neighbor for every adsorption condition. The presence of this peak demonstrates a patterning of the surface with an underlying length scale, despite of the random nature of the adsorption process. It is observed that the peak shifts to closer distances when the ionic strength of the adsorption solution is increased. This trend is anticipated by the effective hard sphere model, where the effective radius of the particle diminishes for higher solution ionic strengths, allowing particles to adsorb at shorter distances between each other. The reported distances can be compared as well with the ones obtained on mica (see Table 4-2). One can see that the most probable closest-neighbor distances on silica are larger than in the case of mica, as it is expected from the comparison of the surface coverage on both substrates.

b) Long-range interactions between PAMAM-covered surfaces

Direct force measurements of the interactions between silica surfaces with adsorbed PAMAM dendrimers were realized. In Figure 5-5, the curves show the force between two surfaces with adsorbed PAMAM as a function of the separation distance. Both the cantilever approach and retraction curves are displayed. Some of the characteristic features obtained in the force curves are shown here. When approaching the probe to the planar surface at about 60 nm, the long-range interaction is repulsive. At short separation distances, a jump-in of the probe onto the substrate is observed. Then, the probe reaches the constant compliance region. When retracting the cantilever, an unspecific adhesion event is noticed. The probe remains adhered to the substrate while the cantilever is retracted until the adhesion force is equivalent to the pulling force of the cantilever. At this moment, the probe jumps off at a distance where repulsion can be still observed.

Various dendrimer generations, namely G6, G8 and G10, adsorbed from solutions with ionic strength ranging from 0.1 mM to 50 mM were investigated. The use of different generations and adsorption ionic strengths allow to tune the heterogeneous charge distribution of the surfaces. However, only representative force curves for G10 are shown for the sake of simplicity. The long range interactions between G10 PAMAM adsorbed surfaces may be analyzed from Figure 5-6. Every graph of this figure shows the force curves between silica surfaces with PAMAM adsorbed in solutions of ionic strength I_{ads} of 0.1, 1, 10 and 50 mM. The force is normalized by the radius of the colloidal probe. The curves were fitted to a numerical solution of the Poisson–Boltzmann equation, considering as boundary condition that the surfaces are constantly charged. It was possible to extract the diffuse layer potential ψ_d of the surface and the Debye length κ^{-1} of the solution as parameters of the fitting. From the four configurations, one can observe that repulsion between the surfaces decays exponentially at all ionic strengths. It can be stated that the decay length of the repulsion decreases with increasing the ionic strength of the solution. This tendency agrees with the behavior of a pure electrostatic repulsion. In order to test

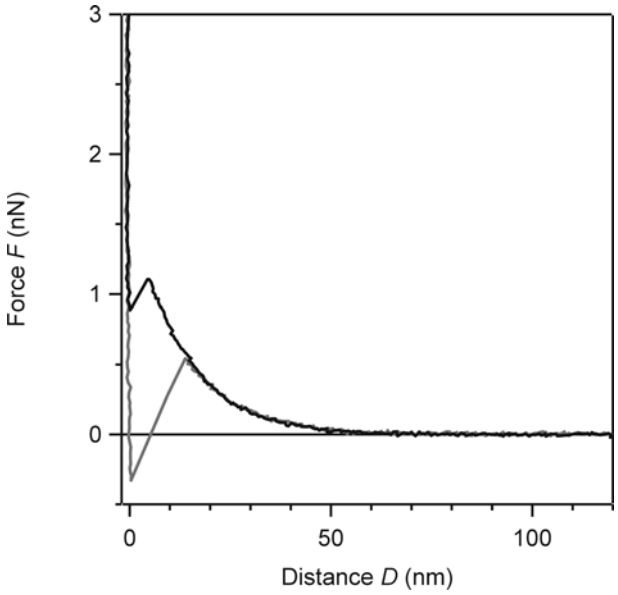

Figure 5-5. Force between two G10 PAMAM adsorbed surfaces as a function of the separation distance. The black trace represents the approach curve, and the gray one shows the retraction of the cantilever. The dendrimers were adsorbed in a solution at pH 4 and ionic strength of 0.5 mM. The force measurement was realized at pH 4 and an ionic strength of 0.6 mM.

the origin of the interaction, the decay lengths of all the obtained force curves are plotted against the ionic strength of the experiment solution in Figure 5-7. Further, they are compared with the theoretically expected Debye length. The agreement is very good for the whole range of ionic strengths. We conclude that the origin of the long-range interaction is purely electrostatic. This result differs from findings of previous studies, where the interaction between heterogeneously charged surfaces was investigated theoretically. In the work of Miklavic *et al*.[42], it is stated that the decay length of the interaction between two heterogeneously charged surfaces arranged as a square lattice is dependent on two values, namely the Debye length of the solution and the distance between the charged sites at the lattice. In a later work[43], it was found that the same dependence of the decay length may be applied to interactions between heterogeneously charged surfaces with random distribution. If we compare these results with our experimental data, we realize that our heterogeneously charged surfaces behave like substrates with

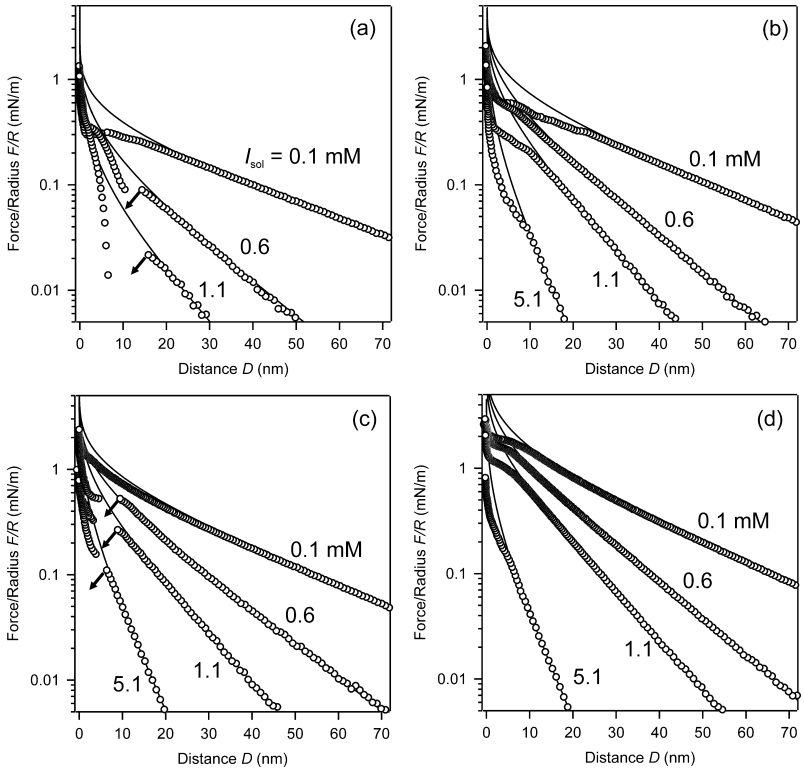

Figure 5-6. Interaction force normalized by the probe radius *F/R* displayed versus separation distance *D* between silica surfaces with G10 PAMAM dendrimer adsorbed at different ionic strengths I_{ads}. a) corresponds to dendrimers adsorbed at 0.1 mM, b) 1 mM, c) 10 mM, and d) 50 mM. Experiments were realized at pH 4 and at the ionic strengths indicated beside the curves. The markers are the experimental data as obtained from the colloidal probe technique. The arrows indicate where the probe jumps to the planar surface. The solid line is the best fit of the Poisson-Boltzmann equation at constant charge boundary conditions.

smeared-out charges when we investigate the long-range interactions. Figure 5-7b displays the diffuse layer potentials, as obtained from the fitting of the force curves at Figure 5-6, versus the ionic strength of the solution I_{sol}. Previous measurements of electrokinetic properties of latex particles with adsorbed PAMAM show that the overall surface charge is positive due to the adsorbed dendrimers, even at the lowest adsorption ionic strength[166]. Each symbol of the figure represents a different charge configuration of the interacting surfaces. As a general trend, the diffuse layer potential decreases when increasing the ionic strength of the solution. This trend is consistent with the inverse Grahame equation (cf. eq. (3.2)), which states that the diffuse layer potential ψ_d is a

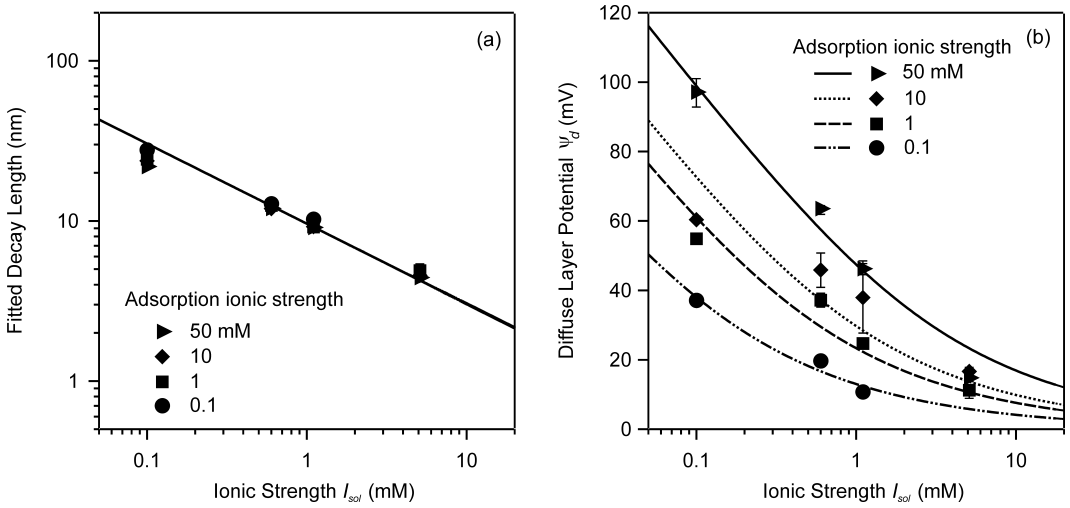

Figure 5-7. a) Decay length of the force curves measured with the colloidal probe technique experiments as a function of the ionic strength of the solution I_{sol}. This decay length is obtained from the fitting to the solution of the Poisson-Boltzmann equation. The markers correspond to experimental data for the different ionic strengths from which the dendrimers were adsorbed. The solid line represents the theoretical Debye length of the solution. b) Diffuse layer potential ψ_d, which was obtained from the fitting of the force curves, versus the ionic strength of the solution. Error bars show the maximum and minimum values for three different probed positions. The markers have the same meaning as in a). The lines show the best fit of the experimental data to the inverse Grahame equation.

function of the surface charge density σ and the ionic strength of the solution through the Debye length κ^{-1}. It is observed that the diffuse layer potentials measured at the same ionic strength vary according to the surface coverage of the dendrimers, and it can be seen that they are higher in a general trend for higher PAMAM fractional coverage. This result is consistent with the theoretical predictions stated in the work of Sader *et al.*[167], which affirmed that the effective potential of a heterogeneously charged surface is dependent on the surface charge distribution and the associated length scale. The force curves and fitting parameters obtained from the interactions for other generations and adsorption conditions show analogous trends to the ones discussed so far for G10 PAMAM surfaces.

The experimental potentials represented at Figure 5-7 have been fitted to the inverse Grahame equation (equation (3.2)) in order to obtain an effective surface

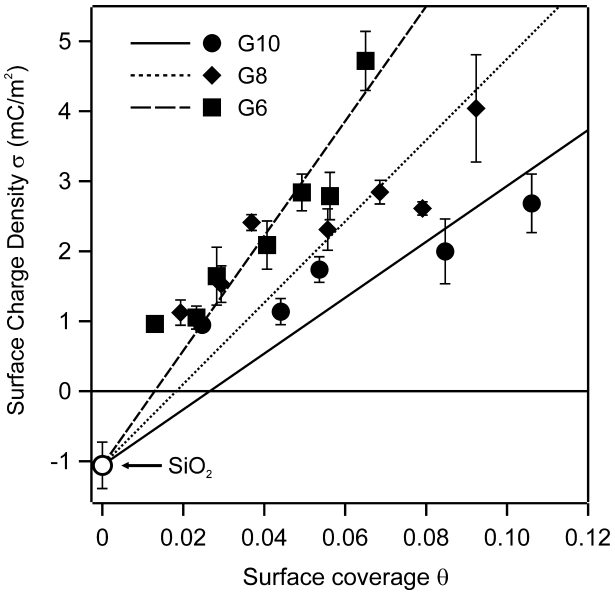

Figure 5-8. Surface charge density σ, obtained from the fitting of the diffuse layer potentials to the Grahame equation, is represented versus the fractional coverage θ of the silica substrates by the deposited dendrimers. Full markers are the experimental data for the studied PAMAM dendrimer generations, with error bars showing the standard deviation of the fits. The empty marker is the parameter obtained for bare silica surfaces. Lines are best linear fits of the experimental data.

charge of every configuration of PAMAM dendrimers on the surface. The results for various dendrimer generations and configurations on the surface at low coverage studied in this work are summarized in Figure 5-8, where the fitted surface charge is plotted as function of the fractional coverage of the surface by the PAMAM dendrimers. This coverage is extracted from the interpolation of the experimental data of PAMAM adsorption on silica in Figure 5-3. At the same graph, we mark the values of the surface charge of bare silica from direct force measurements between a silica particle and a bare silicon substrate at the same pH and ionic strength. These values are negative, as it has been confirmed for silica in electrokinetic measurements and potentiometric titrations[47, 152, 165]. The surface charge of silica as obtained from the force curves are of the same order as the ones from potentiometric titrations at pH 4 [166]. On the other hand, the values found by fitting the surface charge density of substrates with adsorbed dendrimers are substantially lower than the ones that we obtain by calculating its ionized site

density. The reason is that the fit of the interactions has been realized at long separation distances. In this regime, the diffuse layer potential of a surface with high density of ionized sites saturates in aqueous solution to a value called effective potential. The effective charge of the surface obtained from that potential is not dependent any more on the density of ionized sites, but on the ionic strength of the solution and the dimension of the element that bears the charge sites, in this case the probe and the silica substrate[145, 168]. The trends of the charge density of adsorbed PAMAM dendrimer surfaces for generation 6, 8 and 10 are displayed in Figure 5-8. It is observed that the charge increases when augmenting the substrate coverage by PAMAM for all generations. It can be stated as well from Figure 5-8 that this increase is enhanced for lower generations. This phenomenon is significant considering that the bare surface charge density of a PAMAM dendrimer is higher for higher generations, and that the coverage does not depend on the size of the adsorbing dendrimers. In fact, the density of adsorbed dendrimers increases when we adsorb lower generations at same solution conditions. On the other hand, as has been stated above, the effective charge of a dendrimer depends primarily on its size, keeping the same ionic strength at the solution. This shows, in terms of the overall charge, that the effect of deposition of a higher number of dendrimers per surface unit overcomes the decrease in effective charge of individual molecules.

The experimental data of the surface charge against the fractional coverage have been fitted to a linear relation

$$\sigma = \sigma_{PAMAM}\theta + \sigma_{SiO_2}\left(1-\theta\right) \tag{4.11}$$

that decomposes the charge into its sources, namely the surface charge density of the adsorbed dendrimers σ_{PAMAM} and the bare silica charge σ_{SiO_2}. From this, it is possible to extract the value of the effective charge Z_{AFM} for an individual adsorbed PAMAM dendrimer

$$Z_{AFM} = \frac{\pi a^2 \sigma_{PAMAM}}{e} \tag{4.12}$$

being a the adsorbed dendrimer radius, and e the elementary charge. Results are shown in Table 5-1, together with other parameters describing the charge of

Table 5-1. Charge characteristics of PAMAM dendrimers (see text for details)

Generation	Z	Z_{eff}	Z_{mob}	Z_{AFM}
6	514	34	47	18
8	2065	54	103	29
10	8272	82	207	53

PAMAM dendrimers in solution. From this table, Z shows the total number of protonated amine groups at pH 4[139]. Z_{eff} is the effective charge of a sphere in solution for sufficiently high surface charge densities, calculated from an analytical expression[146]

$$Z_{eff} = \frac{a}{L_B}\left(4\kappa a + 6\right) \tag{4.13}$$

at an ionic strength of 1 mM, where L_B is the Bjerrum length ($L_B \approx 0.72$ nm in water). Z_{mob} are the values of the effective charge of a G10 PAMAM dendrimer at 1 mM calculated from electrophoretic mobility measurements of latex particles with adsorbed dendrimers, as obtained by Lin *et al.*[166]. The main conclusion from comparing those values is that indeed, in all cases, the effective charge of the dendrimer is much lower that the number of ionized sites in those conditions of acidity and ionic strength. Additionally, it is observed that these values increase with the size of the molecule, which is expected due to the higher amount of ionized sites, and to the definition of effective charge in equation (4.13). However, there is a certain discrepancy between the methods for the determination of the effective charge. The value Z_{eff} as calculated from equation (4.13) corresponds to the effective charge of the dendrimer *in solution*. To estimate Z_{mob}, the amount of adsorbed dendrimers per latex particle at the isoelectric point is obtained to compute the particle charge that was neutralized by the PAMAM adsorption. Lastly, Z_{AFM} is the effective charge of the *adsorbed* PAMAM dendrimer. To compare this value with the previous ones, it has to be stressed that the adsorbed dendrimer is not spherical, since this is a restriction to use equation (4.13). As well, part of its charge in solution is compensated by the

underlying oppositely charged substrate. Anyhow, the number of ionized sites of an adsorbed PAMAM dendrimer in the experiment conditions is sufficiently high to be considered as saturated.

c) Short-range interactions between adsorbed PAMAM surfaces

We have seen so far that the heterogeneity of the surfaces has an important influence in the long-range interactions between PAMAM deposited substrates. This importance is manifested in the dependence on the surface charge configuration of the diffuse layer potentials, which are obtained from the fitting of the force curves at far separation. Besides, it is clear that a high influence must be observed when analyzing the forces at close separation distances, where local interactions between the heterogeneous surfaces may take place. Important features are shown in Figure 5-9. In those graphs, force curves show interactions between silica surfaces with adsorbed PAMAM dendrimers below 50 nm of separation distance. Both curves were measured at pH 4 and an ionic strength of 0.6 mM, and the dendrimer surfaces were prepared in a solution at pH 4 and an ionic strength of 0.5 mM. However, the curves have been measured in different positions of the substrate. The forces are predominantly repulsive for the whole range, although probe jump-ins are observed at short separation distances. The two different graphs were chosen to show limiting cases for the short-range interactions. In the left graph (Figure 5-9a), an electrostatic repulsion may be observed down to 17 nm approximately. The origin of the interaction is assured by analyzing the decay length, which coincides fairly well with the Debye length of the solution. At that distance, a jump-in of the probe is observed, and a new regime of repulsion is perceived. The profile of this repulsion corresponds to the one that may be observed between polymer brushes at short separation distances[40]. Hence, the force curve shows that there exists steric repulsion between adsorbed dendrimers upon approaching. The range of this interaction is of about 12 nm, which is in the range of the height dimension of two adsorbed dendrimers in solution[130]. This steric repulsion continues down to a distance of about 4 nm. At this distance, a second jump-in of the probe is observed. This is

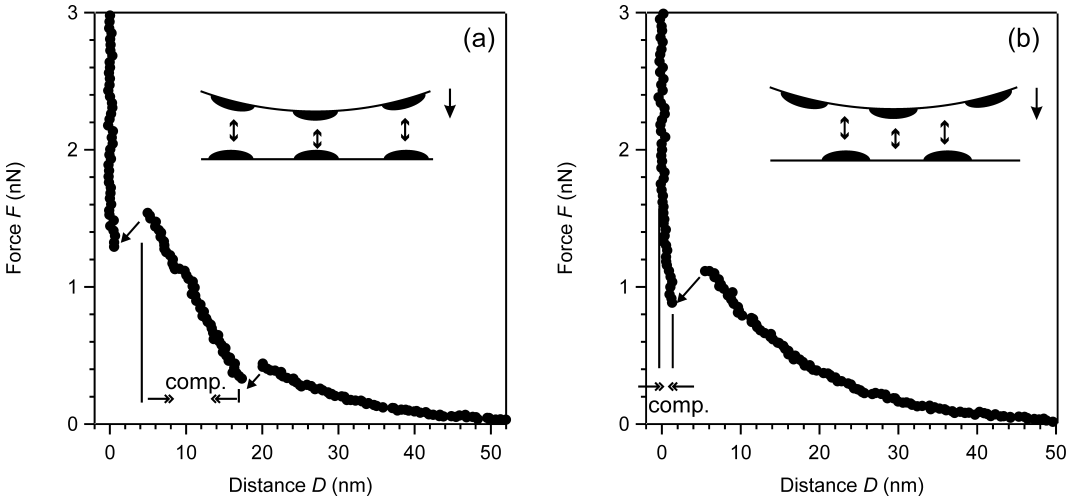

Figure 5-9. Approach force curves as a function of the separation distance between silica surfaces with adsorbed PAMAM dendrimers. Both curves were obtained in a solution at an ionic strength of 0.6 mM and pH 4. Dendrimers were adsorbed from a solution at ionic strength of 0.5 mM and pH 4. (a) and (b) are measured at different positions of the substrate. Diagonal arrows show positions where the probe bears a jump-in. "Comp" shows distance ranges where compression of dendrimer layers is taking place. The inset pictures show the approaching configuration of the opposing surfaces.

probably due to the reorientation of the dendrimer layers at conditions of high compression against each other. Below a distance of 2 nm, further layer compression cannot be resolved with respect to the constant compliance region. This profile corresponds to an approaching configuration of the surfaces in which steric interactions between opposite adsorbed dendrimers are predominant along the surfaces at short separations, as can be observed schematically at the inset of Figure 5-9a. It is significant that these steric interactions are observed, even though only about 4 % of the surface is covered by PAMAM dendrimers when they are adsorbed in a solution of an ionic strength of 0.5 mM. The other limiting case can be seen in Figure 5-9b. In this situation, the repulsive interaction upon approach is of electrostatic origin down to 7 nm approximately. At this point, the probe bears a jump-in down to 2 nm, showing an attractive interaction. At this point, a short regime of steric interactions of less than 2 nm is observed, which shortly give way to the constant compliance region. This short-range steric force

is likely due to the compression of dendrimers against bare silica areas. The profile indicates a predominant configuration of dendrimers locally opposing bare silica regions upon approaching. The origin of the attraction regime is the charge heterogeneity of the surfaces. At large separation distances, the interaction between two heterogeneously charged surfaces is similar to the one between two surfaces with equal smeared out surface charge density. In fact, for the case of surfaces with a square lattice of elementary charges, the electric field is the same as for a surface of spread-out charge down to a distance equal to the lattice constant[4]. The jump-in at our curve takes place at a distance of about 8 nm. The characteristic distance of closest neighbors of our dendrimer configuration is measured experimentally by the pair-distribution function of the imaged PAMAM dendrimers on the silica surface. This distance is approximately 60 nm for the case of dendrimers adsorbed from a solution of ionic strength of 0.5 mM, as it is extracted from the first maximum of its pair-correlation function in Figure 5-4. However, it has to be considered the special characteristics of our charged surface, which is far from being like an ideal regular lattice of charge sites. The finite size of the PAMAM dendrimers does not allow to consider them as point charges, but more like charge patches, as can be observed at the tapping mode AFM images. Moreover, the charge does not stand in one plane. Indeed, adsorbed dendrimers have a height in solution in the order of 5-10 nm[130], so most of the positive charges playing a role in the surface interaction are placed at least about 5 nm inside the solution with respect to the negative charge sites of the silica substrate. Therefore, the local interaction between opposite PAMAM dendrimers is enhanced with respect to the one between dendrimers and bare silica regions at short separation distance. The short-range attraction is not a van der Waals force, since they are often sufficiently pronounced at distances in the order of 2 nm. Furthermore, direct force measurements were realized between a bare silica probe and a silicon substrate, and no evidence of van der Waals interactions was found, in agreement with results obtained previously[29, 46].

The two limiting cases discussed above show how the short-range interaction may depend on the orientation of the opposing dendrimers on the probe and on the

silica substrate. This may have as well consequences in the long-range interactions, considering that the silica substrate plane coincides with the constant compliance region, and that the plane of positive charge may be at 5 nm away from the silica substrate. Indeed, for certain experiments, the values of the diffuse layer potential obtained from the fitting of the force curves have deviations of more than 50 % for three different probed positions.

5.4 Conclusion

In this chapter, the adsorption properties of poly(amidoamine) (PAMAM) dendrimers on silica surfaces, as well as direct force measurements between adsorbed PAMAM silica substrates, were presented. Using tapping mode atomic force microscopy (AFM), the adsorption of PAMAM dendrimers generation 8 and 10 was studied by imaging the topography of the dendrimers deposited on planar surfaces and on colloidal spheres. Its adsorption behavior examined for various ionic strength conditions was found to agree well with the random sequential adsorption (RSA) model. Further, direct force measurements were realized between silica surfaces with PAMAM dendrimers deposited as established in the adsorption experiments. In this way, the adsorbed mass and the lateral distribution of the dendrimers on the silica plate and the colloidal sphere were known a priori. The colloidal probe technique measurements showed that long-range interactions were purely electrostatic. The diffuse layer potentials were obtained from fitting the force curves, and they were found to decrease with the ionic strength of the medium. Additionally, the experimental potentials increased for a fixed ionic strength when augmenting the coverage of the probed PAMAM surfaces. The surface charge density was obtained for all the dendrimer adsorption conditions and it was found to increase with the fractional surface coverage. It was observed that the charge density augmented for lower generations at the same coverage. We achieved in obtaining values of the effective charge of individual adsorbed PAMAM dendrimers from the direct force measurements. This charge was found to be much lower than the density of ionized sites, and it increased when the size

of the dendrimer was augmented. These trends of the effective charge agree with the ones predicted in theory, and with the ones obtained from electrophoretic mobility measurements. A qualitative analysis of the short-range interactions was provided. It has been stated that the orientation of the approaching surfaces with respect to each other may well explain the scattering of the fitted diffuse layer potentials at various probed positions. A way to test the influence of the positioning of the surfaces when interacting would be to realize force volume imaging of the PAMAM adsorbed to surfaces. This would allow a mapping of the forces with higher resolution.

Chapter 6
Conclusions and outlook

In this thesis, interactions between surfaces with adsorbed highly branched polyelectrolytes were studied with the colloidal probe technique. By studying the adsorption behavior of highly branched polyelectrolytes, the lateral distribution of the surface charge could be tune by the appropiate adsorption conditions. By choosing different polyelectrolytes, namely highly branched poly(ethylene imine) (PEI) and poly(amido amine) (PAMAM) dendrimers, it was possible to investigate the forces between homogeneously charged layers, as well as surfaces composed of charge patches where both the patch size and the distance between them could be tuned. The output of the force measurements allowed not only to know its dependence on the surface charge heterogeneity, but also some properties of the individual adsorbed polymers. A detailed explanation of the main findings is as follows.

In Chapter 2, a novel approach to solve the Poisson-Boltzmann equation was developed. The model, called *constant regulation approximation*, approximates the full charge regulation of the surface by linearizing the relationship between the surface charge and the diffuse layer potential around the potential value of the isolated surface. This approach improves the accuracy of the frequently used constant charge and constant potential solutions in the application to real systems. The constant regulation approximation eliminates the need of treating the interacting surfaces as well as the chemical adsorption equilibria of charged species to each surface. Indeed, the entire chemical response is summarized in terms of only two parameters for an isolated surface, i.e. the diffuse layer potential and the regulation parameter. The approximation is excellent in most practical situations, and it has been used in this thesis to describe the charging behavior of interacting adsorbed polyelectrolyte surfaces.

The interaction forces between two homogeneously charged polyelectrolyte layers were studied in Chapter 3. In order to obtain such layers, highly branched poly(ethylene imine) was adsorbed to silica surfaces. Tapping mode AFM imaging showed that this polyelectrolyte forms relatively uniform and homogeneous layers. Direct force measurements between PEI layers were realized, and they showed that the repulsive forces upon approaching were of electrostatic nature. At decreasing separation distance below the Debye length, the effect of charge regulation becomes increasingly important. The charge regulation between polyelectrolyte-coated surfaces was described for the first time in the framework of the constant regulation approximation. It was found as well that the diffuse layer potentials obtained from the fitting of the force curves were independent of the molecular mass of PEI. Adhesion events on the molecular level were observed when the polyelectrolyte surfaces were retracted, indicating strong bridging adhesion. Those events were mainly rubber-like, behaving very differently to single molecule pulling events that are commonly observed for the case of linear polymers. This finding is compatible with the highly branched architecture of the PEI.

In Chapter 4, the adsorption of poly(amido amine) dendrimers to mica surfaces was studied as a function of ionic strength and pH. It was demonstrated that the early stages of adsorption were a diffusion-limited process, and that the surface coverage saturated at a value that was independent of the bulk concentration of dendrimers. The trends of the maximum coverage as a function of the ionic strength could be described qualitatively by the effective hard sphere model for random sequential adsorption. In all the studied conditions, the values of the coverage were found to be well below the jamming limit of random sequential adsorption processes, i.e. 55% of the surface. In this way, nanopatterned surfaces with a well-defined density of dendrimers with different surface coverages could be prepared by selecting the dendrimer generation, ionic strength of the background electrolyte, and pH value. These surfaces showed characteristic length scales as demonstrated by their radial-distribution function, despite of the random nature of the adsorption process.

The adsorption of PAMAM dendrimers onto silica surfaces was investigated in Chapter 5. The dependence on the ionic strength of the adsorption process was examined, analogously to the previous chapter. The coverage values obtained for adsorption on planar substrates and on spherical surfaces agreed very well with the effective hard sphere model. However, it was found that the values of the maximum coverage were significantly lower than the ones obtained on mica surfaces. Thus, a dependence of the random sequential adsorption process of PAMAM dendrimers on the collecting substrate was demonstrated. Following the developed adsorption methods of PAMAM dendrimers on silica, it was possible to tailor the lateral charge distribution of surfaces.

For the first time, the interaction forces between well-defined heterogeneously charged surfaces were measured. Various charge configurations were elaborated by varying the dendrimer generation and the ionic strength of the aqueous adsorption conditions. The interaction forces at distances larger than twice the Debye length were found to be purely electrostatic. These findings indicate that the surfaces could be considered as homogeneous, smeared-out charge distributions with a surface charge that increases with increasing the fractional coverage of the dendrimers. At equal surface coverage, it was observed that the surface charge increased when decreasing the dendrimer generation. Values of the effective charge of individual adsorbed dendrimers were obtained for the first time by means of direct force measurements. The qualitative analysis of the short-range forces between adsorbed PAMAM surfaces showed the importance of the mutual positioning in the interactions that take place locally.

The results of this work are expected to have impact in many areas of science and technology. Indeed, heterogeneous charge distributions are present in many natural systems, such as cellular membranes, and in technologic devices, like electronic microchips. For the first time, direct force measurements with tunable model systems in the nanometer scale were realized. The elaboration of nanopatterns by means of the controlled adsorption of poly(amido amine) dendrimers may be applied in nanolithography or in functionalization of surfaces.

However, more effort has to be done, for instance, in the elaboration of model systems of regular lattices of charge, where a full theoretical description is more easily achievable. The possibility of realizing direct force measurements between heterogeneously charged surfaces with regular distribution remains challenging. It is desirable as well to improve the study of local interactions in a quantitative way. The development of experiments with a finer positioning of the surfaces against each other might be achieved by realizing force volume measurements by means of atomic force microscopy, which show laterally resolved interaction forces.

Acknowledgements

First, I would like to thank Prof. Michal Borkovec for all his support, advice, and fruitful scientific discussion during these four years.

I am very grateful to Prof. Marcus Textor (ETHZ) and Prof. Claude Piguet (University of Geneva) for accepting to be part of the jury of this thesis. Their comments, corrections, and further discussion are especially valuable.

Special thanks to Dr. Georg Papastavrou for supervising this work, for his assistance in the daily tasks, and for helping me overcome the difficult times much more easily.

I would like to thank Prof. Christiane Helm (University of Greifswald) and Dr. Sven Behrens (BASF) for their useful advice and review of parts of this work. To Dr. Thomas Gutberlet (Paul Scherrer Institute) for providing us with X-Ray measurements. To Dr. Ger Koper (Delft University of Technology), for putting some light on our results in dendrimer adsorption. To Dr. Serge Stoll, for his corrections and advice in the French text. I recognize specially the contribution from Dr. Duško Čakara, Dr. Luke Kirwan and Dr. Cécile Gehin-Delval in various aspects of this thesis.

Thanks to all the present and past members of the LCSC group for their help, time, and all those pleasant scientific and non-scientific debates.

I recognize as well the help, kindness and patience of the secretaries, technicians and other PATs who made things much less complicated.

Finally, I would like to dedicate this thesis to *mamá* and *papá* for all their hard work, for having confidence in me, for their support, and for all their love. To my sisters, for their infinite affection. To Sonia, for her support, patience, trust, love and so much more.

This thesis is dedicated to the memory of my first Mathematics and Physics teacher, my grandfather Antonio, for awaking in me the passion for science and life.

References

1. Elimelech, M.; Gregory, J.; Jia, X.; Williams, R., *Particle deposition and aggregation: Measurement, modeling and simulation*. Butterworth-Heinemann Ltd.: Oxford, 1995.

2. Derjaguin, B.; Landau, L. D. *Acta Phys. Chim.* **1941,** 14, (6), 633-662.

3. Verwey, E. J. W.; Overbeek, J. T. G., *Theory of stability of lyophobic colloids*. Elsevier: Amsterdam, 1948.

4. Israelachvili, J. N., *Intermolecular and surface forces*. 2nd ed.; Academic Press: London, 1991; p 296.

5. Claesson, P. M.; Dedinaite, A.; Rojas, O. J. *Adv. Colloid Interface Sci.* **2003,** 104, 53–74.

6. de Gennes, P. G. *Macromolecules* **1981,** 14, (6), 1637-1644.

7. de Gennes, P. G. *Adv. Colloid Interface Sci.* **1987,** 27, (3-4), 189-209.

8. Borkovec, M.; Behrens, S. H., Stabilization of aqueous colloidal dispersions: Electrostatic and steric forces. In *Encyclopedia of colloid and surface science*, Hubbard, A., Ed. Dekker Publishers: 2002; pp 4795 - 4806.

9. Butt, H. J. *Biophys. J.* **1991,** 60, (6), 1438-1444.

10. Ducker, W. A.; Senden, T. J.; Pashley, R. M. *Nature* **1991,** 353, (6341), 239-241.

11. Dzyaloshinskii, I. E.; Lifshitz, E. M.; Pitaevskii, L. P. *Advances in Physics* **1961,** 10, 165-209.

12. Sabisky, E. S.; Anderson, C. H. *Phys. Rev. A* **1973,** 7, 790-806.

13. Evans, D. F.; Wennerström, H., *The colloidal domain*. 1st ed.; VCH Publishers: 1994.

14. de Gennes, P. G. *C. R. l'Academie. Sci., Ser. II Univers* **1985,** 301, (20), 1399-1403.

15. Adachi, Y.; Aoki, K. *Colloids Surf. A* **2003,** 230, (1-3), 37-44.

16. Gregory, J. *J. Colloid Interface Sci.* **1973,** 42, (2), 448-456.

17. Binnig, G.; Rohrer, H.; Gerber, C.; Weibel, E. *Phys. Rev. Lett.* **1982,** 49, 57-61.

18. Binnig, G.; Quate, C. F.; Gerber, C. *Phys. Rev. Lett.* **1986,** 56, (9), 930-933.

19. Israelachvili, J. N.; Adams, G. E. *Nature (London)* **1976,** 262, 774-7.

20. Meyer, G.; Amer, N. M. *Appl. Phys. Lett.* **1988,** 53, (12), 1045.

21. Alexander, S.; Hellemans, L.; Marti, O.; Schneir, J.; Elings, V.; Hansma, P. K.; Longmire, M.; Gurley, J. *J. Appl. Phys.* **1989,** 65, (1), 164.

22. Hutter, J. L.; Bechhoefer, J. *Rev. Sci. Instrum.* **1993,** 64, (7), 1868-1873.

23. Sader, J. E.; Chon, J. W. M.; Mulvaney, P. *Rev. Sci. Instrum.* **1999,** 70, (10), 3967-3969.

24. Cleveland, J. P.; Manne, S.; Bocek, D.; Hansma, P. K. *Rev. Sci. Instrum.* **1993,** 64, (2), 403-405.

25. Gibson, C. T.; Watson, G. S.; Myhra, S. *Nanotechnology* **1996,** 7, (3), 259-262.

26. Sader, J. E. *J. Appl. Phys.* **1998,** 84, (1), 64-76.

27. Garcıa, R.; Tamayo, J.; Calleja, M.; Garcıa, F. *Applied Physics A* **1998,** 66, S309–S312.

28. Tamayo, J.; Garcıa, R. *Langmuir* **1996,** 12, 4430-4435.

29. Ducker, W. A.; Senden, T. J.; Pashley, R. M. *Langmuir* **1992,** 8, 1831-1836.

30. Larson, I.; Drummond, C. J.; Chan, D. Y. C.; Crieser, F. *J. Am. Chem. Soc.* **1993,** 115, 11885-11890.

31. Larson, I.; Drummond, C. J.; Chan, D. Y. C.; Grieser, F. *J. Phys. Chem.* **1995,** 99, 2114-2118.

32. Biggs, S. *Langmuir* **1995,** 11, 156-162.

33. Rutland, M. W.; Senden, T. J. *Langmuir* **1993,** 9, (2), 412-418.

34. Pera, I.; Stark, R.; Kappl, M.; Butt, H.-J.; Benfenatiy, F. *Biophys. J.* **2004,** 87, 2446-2455.

35. Biggs, S.; Proud, A. D. *Langmuir* **1997,** 13, 7202-7210.

36. Pasche, S.; Textor, M.; Meagher, L.; Spencer, N. D.; Griesser, H. J. *Langmuir* **2005,** 21, (14), 6508-6520.

37. Meagher, L.; Maurdev, G.; Gee, M. L. *Langmuir* **2002,** 18, (7), 2649-2657.

38. Braithwaite, G. J. C.; Howe, A.; Luckham, P. F. *Langmuir* **1996,** 12, (17), 4224-4237.

39. Bosio, V.; Dubreuil, F.; Bogdanovic, G.; Fery, A. *Colloids Surf., A* **2004,** 243, 147-155.

40. Kelley, T. W.; Schorr, P. A.; Johnson, K. D.; Tirrell, M.; Frisbie, C. D. *Macromolecules* **1998,** 31, 4297-4300.

41. Bouyer, F.; Robben, A.; Yu, W. L.; Borkovec, M. *Langmuir* **2001,** 17, 5225-5231.

42. Miklavic, S. J.; Chan, D. Y. C.; White, L. R.; Healy, T. W. *J. Phys. Chem. B* **1994,** 98, 9022-9032.

43. Stankovich, J.; Carnie, S. L. *J. Colloid Interface Sci.* **1999,** 216, 329–347.

44. Sader, J. E.; Lenhoff, A. M. *J. Colloid Interface Sci.* **1998,** 201, 233–243.

45. Chen, J. Y.; Klemic, J. F.; Elimelech, M. *Nanoletters* **2002,** 2, (4), 393-396.

46. Vigil, G.; Xu, Z. H.; Steinberg, S.; Israelachvili, J. *J. Colloid Interface Sci.* **1994,** 165, (2), 367-385.

47. Hartley, P. G.; Larson, I.; Scales, P. J. *Langmuir* **1997,** 13, 2207-2214.

48. Toikka, G.; Hayes, R. A. *J. Colloid Interface Sci.* **1997,** 191, (1), 102-109.

49. Stahlberg, J.; Jonsson, B. *Anal. Chem.* **1996,** 68, (9), 1536-1544.

50. Zheng, J.; Behrens, S. H.; Borkovec, M.; Powers, S. E. *Environ. Sci. Technol.* **2001,** 35, (11), 2207-2213.

51. Behrens, S. H.; Borkovec, M. *J. Chem. Phys.* **1999,** 111, (1), 382.

52. Behrens, S. H.; Borkovec, M. *J. Phys. Chem. B* **1999,** 103, 2918-2928.

53. Behrens, S. H.; Borkovec, M. *Phys. Rev. E* **1999,** 60, (6), 7040.

54. Hiemstra, T.; de Wit, J. C. M.; van Riemsdijk, W. H. *J. Colloid Interface Sci.* **1989,** 133, 105.

55. Borkovec, M.; Jonsson, B.; Koper, G. J. M. *Colloid Surface Sci.* **2001,** 16, 99-339.

56. Biesheuvel, P. M. *J. Colloid Interface Sci.* **2004,** 275, 514-522.

57. Zhmud, B. V.; Meurk, A.; Bergstrom, L. *J. Colloid Interface Sci.* **1998,** 207, 332–343.

58. Ninham, B. W.; Parsegian, V. A. *J. Theor. Biol.* **1971,** 31, (3), 405-408.

59. Reiner, E. S.; Radke, C. J. *Adv. Colloid Interface Sci.* **1993,** 47, 59.

60. Carnie, S.; Chan, D. Y. C. *J. Colloid Interface Sci.* **1993,** 161, 260-264.

61. Numerical Algorithm Group, Fortran Library, Mark 19, Routine D02RAF.

62. Healy, T. W.; White, L. R. *Adv. Colloid Interface Sci.* **1978,** 9, (4), 303-345.

63. Westall, J.; Hohl, H. *Adv. Colloid Interface Sci.* **1980,** 12, 265.

64. McCormack, D.; Carnie, S. L.; Chan, D. Y. C. *J. Colloid Interface Sci.* **1995,** 169, 177-196.

65. Horn, D., Polyethylenimine: Physicochemical properties and applications. In *Polymeric Amines and Ammonium Salts*, Goethals, E. J., Ed. Pergamon Press: Oxford, New York, 1980; pp 333-355.

66. Lindquist, G. M.; Stratton, R. A. *J. Colloid Interface Sci.* **1976,** 55, 45.

67. Decher, G. *Science* **1997,** 277, (5330), 1232-1237.

68. Schonhoff, M. *J. Phys.: Condens. Matter* **2003,** 15, R1781–R1808.

69. Decher, G.; Hong, J. D.; Schmitt, J. *Thin Solid Films* **1992,** 210-211, (2), 831-835.

70. Sukhorukov, G. B.; Donath, E.; Lichtenfeld, H.; Knippel, E.; Knippel, M.; Budde, A.; Mohwald, H. *Colloids Surf. A* **1998,** 137, (1-3), 253-266.

71. Dietrich, A.; Neubrand, A. *J. Am. Ceram. Soc.* **2001,** 84, (4), 806-812.

72. Meszaros, R.; Thompson, L.; Bos, M.; de Groot, P. *Langmuir* **2002,** 18, 6164-6169.

73. Meszaros, R.; Varga, I.; Gilanyi, T. *Langmuir* **2004,** 20, 5026-5029.

74. Nnebe, I. M.; Tilton, R. D.; Schneider, J. W. *J. Colloid Interface Sci.* **2004,** 276, 306-316.

75. Claesson, P. M.; Paulson, O. E. H.; Blomberg, E.; Burns, N. L. *Colloids Surf., A* **1997,** 123-124, 341-353.

76. Poptoshev, E.; Claesson, P. M. *Langmuir* **2002,** 18, 2590-2594.

77. Lowack, K.; Helm, C. A. *Macromolecules* **1998,** 31, (3), 823-833.

78. Senden, T. J.; di Meglio, J. M.; Auroy, P. *Eur. Phys. J. B* **1998,** 3, (2), 211-216.

79. Sun, G.; Butt, H.-J. *Macromolecules* **2004,** 37, 6086-6089.

80. Sukhorukov, G. B.; Mohwald, H.; Decher, G.; Lvov, Y. M. *Thin Solid Films* **1996,** 284-285, 220.

81. Buscher, K.; Graf, K.; Ahrens, H.; Helm, C. A. *Langmuir* **2002,** 18, (9), 3585-3591.

82. Wang, L.; Schonhoff, M.; Mohwald, H. *J. Phys. Chem. B* **2004,** 108, (15), 4767-4774.

83. Borkovec, M.; Koper, G. J. M. *Macromolecules* **1997,** 30, (7), 2151-2158.

84. Kern, W.; Puotinen, D. A. *RCA Rev.* **1970,** 31, (2), 187-206.

85. Butt, H. J.; Jaschke, M. *Nanotechnology* **1995,** 6, (1), 1.

86. Sader, J. E.; Larson, I.; Mulvaney, P.; White, L. R. *Rev. Sci. Instrum.* **1995,** 66, (7), 3789-98.

87. Cappella, B.; Dietler, G. *Surface Science Reports* **1999,** 34, (1-3), 1.

88. Butt, H. J., Analyzing electric double layers with the atomic force microscope. In *Encyclopedia of electrochemistry*, Bard, A. J.; Stratmann, M., Eds. Wiley-VCH: Weinheim, 2003; Vol. 1, pp 225-252.

89. Hartley, P. G.; Scales, P. J. *Langmuir* **1998,** 14, 6948-6955.

90. Gergely, C.; Senger, B.; Voegel, J. C.; Horber, J. K. H.; Schaaf, P.; Hemmerle, J. *Ultramicroscopy* **2000,** 87, (1-2), 67.

91. Pfau, A.; Schrepp, W.; Horn, D. *Langmuir* **1999,** 15, 3219-3225.

92. Ortiz, C.; Hadziioannou, G. *Macromolecules* **1999,** 32, (3), 780-787.

93. Hugel, T.; Grosholz, M.; Clausen-Schaumann, H.; Pfau, A.; Gaub, H.; Seitz, M. *Macromolecules* **2001,** 34, (4), 1039-1047.

94. Rief, M.; Oesterhelt, F.; Heymann, B.; Gaub, H. E. *Science* **1997,** 275, (5304), 1295-1297.

95. Zhang, W. K.; Zou, S.; Wang, C.; Zhang, X. *J. Phys. Chem. B* **2000,** 104, (44), 10258-10264.

96. Weast, R. C.; Astle, M. J., *Crc handbook of chemistry and physics*. 60th ed.; CRC Press: Boca Raton, FL, 1980.

97. Chen, Y. L.; Helm, C. A.; Israelachvili, J. N. *J. Phys. Chem.* **1991,** 95, 10736.

98. Chen, Y. L.; Helm, C. A.; Israelachvili, J. N. *Langmuir* **1991,** 7, 2694-2699.

99. Richert, L.; Engler, A. J.; Discher, D. E.; Picart, C. *Biomacromolecules* **2004,** 5, 1908-1916.

100. Domke, J.; Radmacher, M. *Langmuir* **1998,** 14, 3320-3325.

101. Feder, J. *J. Theor. Biol.* **1980,** 87, 237.

102. Feder, J.; Giaever, I. *J. Colloid Interface Sci.* **1980,** 78, (1), 144-154.

103. Schaaf, P.; Talbot, J. *J. Chem. Phys.* **1989,** 91, 4401.

104. Adamczyk, Z.; Zembala, M.; Siwek, B.; Warszynski, P. *J. Colloid Interface Sci.* **1990,** 140, (1), 123-137.

105. Adamczyk, Z.; Warszynsky, P. *Adv. Colloid Interface Sci.* **1996,** 63, 41-149.

106. Senger, B.; Voegel, J. C.; Schaaf, P. *Colloids Surf., A* **2000,** 165, 255–285.

107. Schaaf, P.; Voegel, J.-C.; Senger, B. *J. Phys. Chem. B* **2000,** 104, 2204-2214.

108. Adamczyk, Z. *Adv. Colloid Interface Sci.* **2003,** 100, 267–347.

109. Johnson, P. R.; Elimelech, M. *Langmuir* **1995,** 11, (3), 801-812.

110. Semmler, M.; Ricka, J.; Borkovec, M. *Colloids Surf.* **2000,** 165, 79-93.

111. Johnson, C. A.; Lenhoff, A. M. *J. Colloid Interface Sci.* **1996,** 179, (2), 587-599.

112. Semmler, M.; Mann, E. K.; Ricka, J.; Borkovec, M. *Langmuir* **1998,** 14, 5127-5132.

113. Adamczyk, Z.; Szyk, L. *Langmuir* **2000,** 16, 5730-5737.

114. Kooij, E. S.; Brouwer, E. A. M.; Wormeester, H.; Poelsema, B. *Langmuir* **2002,** 18, 7677-7682.

115. Brouwer, E. A. M.; Kooij, E. S.; Wormeester, H.; Poelsema, B. *Langmuir* **2003,** 19, (19), 8102-8108.

116. Yuan, Y.; Oberholzer, M. R.; Lenhoff, A. M. *Colloids and Surfaces. A: Physicochemical and Engineering Aspects* **2000,** 165, 125-141.

117. Talbot, J.; Tarjus, G.; Van Tassel, P. R.; Viot, P. *Colloids Surf., A* **2000,** 165, 287–324.

118. Van Duijvenbode, R. C.; Koper, G. J. M.; Bohmer, M. R. *Langmuir* **2000,** 16, 7713-7719.

119. Wojtaszczyk, P.; Mann, E. K.; Senger, B.; Voegel, J. C.; Schaaf, P. *J. Chem. Phys.* **1995,** 103, (18), 8285-8295.

120. Bosman, A. W.; Janssen, H. M.; Meijer, E. W. *Chemical Review* **1999,** 99, 1665-1688.

121. Vogtle, F.; Gestermann, S.; Hesse, R.; Schwierz, H.; Windisch, B. *Progress in Polymer Science* **2000,** 25, 987–1041.

122. Tully, D. C.; Fréchet, J. M. J. *Chemical Communications* **2001,** 14, 1229-1239.

123. Tomalia, D. A.; Baker, H.; Dewald, J.; Hall, M.; Kallos, G.; Martin, S.; Roeck, J.; Ryder, J.; Smith, P. *Macromolecules* **1986,** 19, (9), 2466-2468.

124. Sheiko, S. S.; Moller, M. *Chem. Rev.* **2001,** 101, (12), 4099-4124.

125. Bliznyuk, V. N.; Rinderspachera, F.; Tsukruk, V. V. *Polymer Communications* **1998,** 39, (21), 5249-5252.

126. Hierlemann, A.; Campbell, J. K.; Baker, L. A.; Crooks, R. M.; Ricco, A. J. *J. Am. Chem. Soc.* **1998,** 120, 5323-5324.

127. Li, J.; Piehler, L. T.; Qin, D.; Jr., J. R. B.; Tomalia, D. A. *Langmuir* **2000,** 16, 5613-5616.

128. Betley, T. A.; Holl, M. M. B.; Orr, B. G.; Swanson, D. R.; Tomalia, D. A.; Baker Jr., J. R. *Langmuir* **2001,** 17, 2768-2773.

129. Betley, T. A.; Hessler, J. A.; Mecke, A.; Holl, M. M. B.; Orr, B. G.; Uppuluri, S.; Tomalia, D. A.; James R. Baker, J. *Langmuir* **2002,** 18, 3127-3133.

130. Mueller, T.; Yablon, D. G.; Karchner, R.; Knapp, D.; Kleinman, M. H.; Fang, H.; Durning, C. J.; Tomalia, D. A.; Turro, N. J.; Flynn, G. W. *Langmuir* **2002,** 18(20), 7452-7455.

131. Crooks, R. M.; Ricco, A. J. *Acc. Chem. Res.* **1998,** 31, 219-227.

132. Arrington, D.; Curry, M.; Street, S. C. *Langmuir* **2002,** 18, 7788-7791.

133. Xu, F. T.; Street, S. C.; Barnard, J. A. *J. Phys. Chem. B* **2003,** 107, 12762-12767.

134. Sano, M.; Okamura, J.; Ikeda, A.; Shinkai, S. *Langmuir* **2001,** 17, 1807-1810.

135. Van Duijvenbode, R. C.; Rietveld, I. B.; Koper, G. J. M. *Langmuir* **2000,** 16, 7720-7725.

136. Van Duijvenbode, R. C.; Koper, G. J. M.-. *J. Phys. Chem. B* **2001,** 105, (47), 11729-11736.

137. Raviv, U.; Laurata, P.; Klein, J. *J. Chem. Phys.* **2002,** 116, (12), 5167.

138. Pashley, R. M. *J. Colloid Interface Sci.* **1981,** 83, (2), 531-546.

139. Cakara, D.; Kleimann, J.; Borkovec, M. *Macromolecules* **2003,** 36, 4201-4207.

140. Barrett, S.; Bickmore, B. R.; Rufe, E.; Hochella, M. F.; Torzo, G.; Cerolini, D. *J. Comput. Assist. Microsc.* **1998,** 10, (2), 77-82.

141. Tsukruk, V. V.; Rinderspacher, F.; Bliznyuk, V. N. *Langmuir* **1997,** 13, 2171-2176.

142. Mansfield, M. *Polymer* **1996,** 37, 3835-3841.

143. Uppuluri, S.; Keinath, S. E.; Tomalia, D. A.; Dvornic*, P. R. *Macromolecules* **1998,** 31, 4498-4510.

144. Russell, W. B.; Saville, D. A.; Schowalter, W. R., *Colloidal dispersions*. Cambridge University: Cambridge, 1989.

145. Gisler, T.; Schulz, S. F.; Borkovec, M.; Sticher, H.; Schurtenberger, P.; D'Aguanno, B.; Klein, R. *J. Chem. Phys.* **1994,** 101, (11), 9924-9936.

146. Chew, W. C.; Sen, P. N. *J. Chem. Phys.* **1982,** 77, (4), 2042-2044.

147. Crank, J., *The mathematics of diffusion*. Oxford Univ. Press: London, 1975; p 414.

148. Rathgeber, S.; Monkenbusch, M.; Kreitschmann, M.; Urban, V.; Brulet, A. *J. Chem. Phys.* **2002,** 117, (8), 4047-4062.

149. Topp, A.; Bauer, B. J.; Tomalia, D. A.; Amis, E. J. *Macromolecules* **1999,** 32, 7232-7237.

150. Micheletto, R.; Fukuda, H.; Ohtsu, M. *Langmuir* **1995,** 11, (9), 3333-3336.

151. Oberholzer, M. R.; Stankovich, J. M.; Carnie, S. L.; Chan, D. Y. C.; Lenhoff, A. M. *J. Colloid Interface Sci.* **1997,** 194, (2), 138-153.

152. Scales, P. J.; Grieser, F.; Healy, T. W.; White, L. R.; Chan, D. Y. C. *Langmuir* **1992,** 8, 965-974.

153. Adamczyk, Z.; Weronski, P. *J. Colloid Interface Sci.* **1997,** 189, 348–360.

154. Sader, J. E. *J. Colloid Interface Sci.* **1997,** 188, 508–510.

155. Behrens, S. H.; Grier, D. G. *J. Chem. Phys.* **2001,** 115, (14), 6716-6721.

156. Hanarp, P.; Sutherland, D. S.; Gold, J.; Kasemo, B. *Colloids Surf., A* **2003,** 214, 23-36.

157. Michel, R.; Reviakine, I.; Sutherland, D.; Fokas, C.; Csucs, G.; Danuser, G.; Spencer, N. D.; Textor, M. *Langmuir* **2002,** 18, 8580-8586.

158. Jackson, C. L.; Chanzy, H. D.; Booy, F. P.; Drake, B. J.; Tomalia, D. A.; Bauer, B. J.; Amis, E. J. *Macromolecules* **1998,** 31, 6259-6265.

159. Prosa, T. J.; Bauer, B. J.; Amis, E. J. *Macromolecules* **2001,** 34, 4897-4906.

160. Ferretti, R.; Zhang, J. W.; Buffle, J. *Colloids Surf. A* **1997,** 121, (2-3), 203-215.

161. Kuin, A. J. *Faraday Discussions of the Chemical Society* **1990,** 90, 235 - 244.

162. Villarrubia, J. S. *J. Res. Natl. Inst. Stand. Technol.* **1997,** 102, (4), 425.

163. Derjaguin, B. V. *Kolloid Zeits.* **1934,** 69, 155-164.

164. Böhmer, M. R.; Van der Zeeuw, E. A.; Koper, G. J. M. *J. Colloid Interface Sci.* **1998,** 197, (2), 242-250.

165. Kobayashi, M.; Juillerat, F.; Galletto, P.; Bowen, P.; Borkovec, M. *Langmuir* **2005,** 21, 5761-5769.

166. Lin, W.; Galletto, P.; Borkovec, M. *Langmuir* **2004,** 20, 7465-7473.

167. Sader, J. E.; Gunning, J. S.; Chan, D. Y. C. *J. Colloid Interface Sci.* **1996,** 182, 516-525.

168. Quesada-Perez, M.; Callejas-Fernandez, J.; Hidalgo-Alvarez, R. *Adv. Colloid Interface Sci.* **2002,** 95, (2-3), 295-315.